4.2.2 Microscopic structures

S_m foliation is defined in thin section by the parallel alignment of subhedral to euhedral, medium to coarsely crystalline, plagioclase, K-feldspar, hornblende, and, less commonly, biotite grains (Plate 4.11). All grains appear to be primary igneous crystals. Feldspar grains are commonly euhedral. Plagioclase twins parallel the long axis of the plagioclase grains. Plagioclase grains exhibit mild, oscillatory zoning. Poikilitic textures, consisting of concentric growth rings marked by fine grained minerals including hornblende, are observed in K-feldspar megacrysts. Isolated hornblende grains and, more rarely, biotite grains, are aligned parallel with foliation, and are surrounded by feldspar grains which exhibit igneous microstructures.

Quartz occurs as anhedral eyes, interstitial to other grains, which display little or no preferred orientation. Locally, quartz exhibits mild undulatory extinction and the development of elongate subgrains. This suggests that mild solid-state flow, accommodated largely by the deformation of quartz, has occurred.

In samples characterized by S_t, a significantly different microstructural character was observed. S_t is irregular, and consists of isolated, anhedral, fine- to coarsely-crystalline feldspar grains which float in a fine-grained quartzo-feldspathic matrix (Plate 4.12).

Feldspar grains are rounded and equidimensional to oblong. Kink folding, fracturing, and boudinage of feldspar grains is common. Boudin necks and fractures are filled by recrystallized strained and unstrained quartz and mica (Plate 4.13). Plagioclase twins are oriented at a high angle to the long axis of feldspar grains, suggesting that thorough recrystallization has occurred (Plate 4.13).

Quartz occurs as finely crystalline aggregates of equidimensional grains which meet in 120^{o} triple junctions. These aggregates commonly include fine grained feldspar and mica (Plate 4.12). Larger quartz grains are elongate, exhibit undulose extinction and commonly consist of quartz ribbons.

Hornblende is rare to absent in rocks in which the S_t foliation is well developed. Biotite is more common than it is elsewhere and occurs as fine-grained fish with undulose extinction. Biotite also occurs as fine- to medium-grained booklets which are sub-parallel to foliation. These grains are undeformed to mildly strained and often occur in strain shadows adjacent to large feldspar augen (Plate 4.14).

Unannealed mylonitic or cataclastic textures were not observed. All samples are blastomylonitic and recrystallized.

Plate 4.11 A photomicrograph, taken under crossed nicols, of typical, coarsely crystalline foliated hornblende granodiorite of the Aishihik Batholith (sample no. 141). Foliation parallels the top and bottom margins of the photograph and is defined by the parallel alignment of primary magmatic grains p - plagioclase; h - hornblende; q - quartz; b - biotite. The scale bar represents 1 mm.

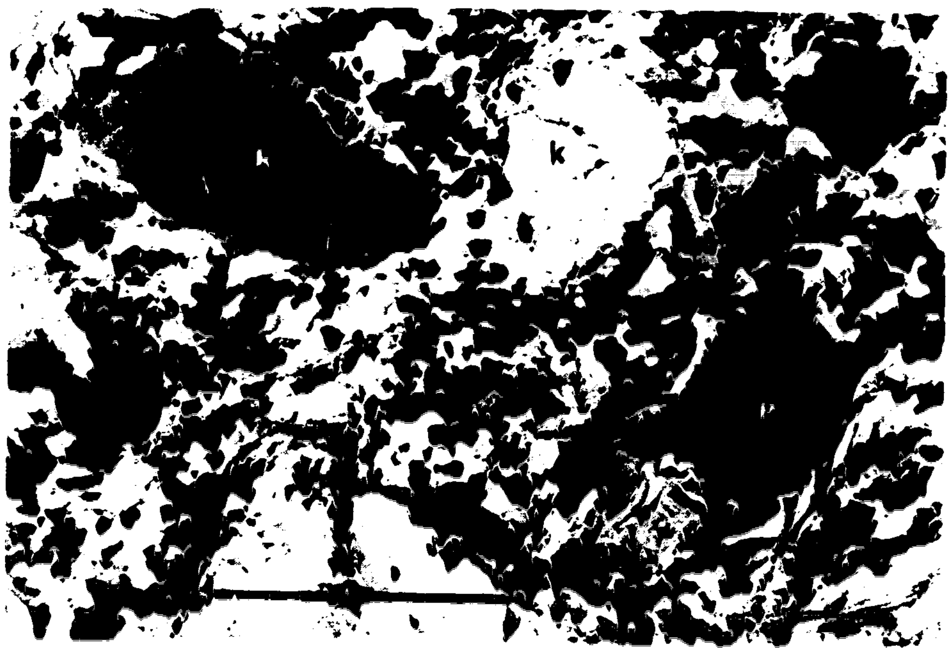

Plate 4.12 A photomicrograph, taken under crossed nicols, of a thermally annealed augen mylonite from near the west margin of the Aishihik Batholith (sample no. 60). Feldspar augen (k - K - feldspar; p - plagioclase) are rounded and anhedral. The augen float in a finely crystalline matrix of recrystallized quartz and mica. The scale bar represents 1 mm.

Plate 4.13 A photomicrograph, taken under crossed nicols of sheared hornblende quartz diorite of the Aishihik Batholith (sample no. 6). Twin planes in plagioclase (p) are oriented at a high angle to the long axis of grains, suggesting thorough recrystallization during deformation. Arrows indicate where a fractured feldspar grain has been annealed by undeformed quartz (q) and biotite (b). The scale bar represents 1 mm.

Plate 4.14 A photomicrograph, taken under crossed nicols, of thermally annealed augen mylonite from near the west margin of the Aishihik Batholith (sample no. 60). Biotite (b) has preferentially recrystallized in a strain shadow adjacent to a plagioclase augen (p). The scale bar represents 1 mm.

4.2.3 The nature of S_m and S_t

S_m is interpreted to be the result of magmatic flow during the emplacement of the batholith. This is strongly suggested by the presence of euhedral, primary igneous grains, including feldspar and hornblende, that lie within and define the planar fabric. Other observations that are consistent with a syn-magmatic origin for S_m include: the lack of deformation and fracturing of primary igneous grains; the lack of a preferred orientation of quartz grains; that foliation passes around and not through microgranitoid and microdiorite enclaves and micaschist inclusions; and that foliation is everywhere parallel to the margins of the batholith (*cf.* Paterson *et al.*, 1989).

S_t overprints S_m and is interpreted to be the result of solid-state deformation of the batholith. This is suggested by: folding of aplite veins and, locally, of foliation; the association of folds of foliation with shear zones; the heterogeneous nature of S_t; the development of mesoscopic shear zones; the plastic deformation of mineral grains; grain size reduction; and the recrystallization of minerals into fine-grained aggregates. Locally, recrystallization of biotite has produced a weakly developed schistosity.

S_t is thought to have formed at elevated temperatures, possibly near the granite solvus. This is suggested by: 1) annealing of mylonitic fabrics; and 2) the association of S_t with migmatite. This suggests that shearing took place at high enough temperatures that local pressure variations, possibly associated with bends in the shear zones, were enough to result in partial melting. Alternatively, shearing may have preferentially developed where pockets of melt were still present, resulting in the development of the compositionally heterogeneous migmatites.

The timing and tectonic significance of the S_t fabric is discussed below.

4.3 Structure of the Nisling Assemblage

4.3.1 Mesoscopic structures

Planar elements

Nisling Assemblage is characterized by a planar fabric (S_o) defined by colour and compositional banding (Plate 4.15). The light and dark coloured bands vary in width from 1 mm to 1 cm and together define a well developed lamination. S_o is only visible in quartzose rocks where it has not been overgrown and obliterated by younger mica. In addition S_o can only be distinguished from S_1 where fold hinges affecting S_o are observed. No orientation data were collected for S_o.

Plate 4.15 Deformed quartzite observed in the Upper Nisling River area. A photograph is shown at top and a labeled line drawing of the photograph below. Two phases of folds are evident. Rootless isoclinal folds of compositional banding are labeled F_1. An L_1 lineation represents the traces of the thickened F_1 fold hinges. Compositional bands and F_1 folds are deformed and define an open fold (F_2). A hammer, evident at lower left, is shown for scale.

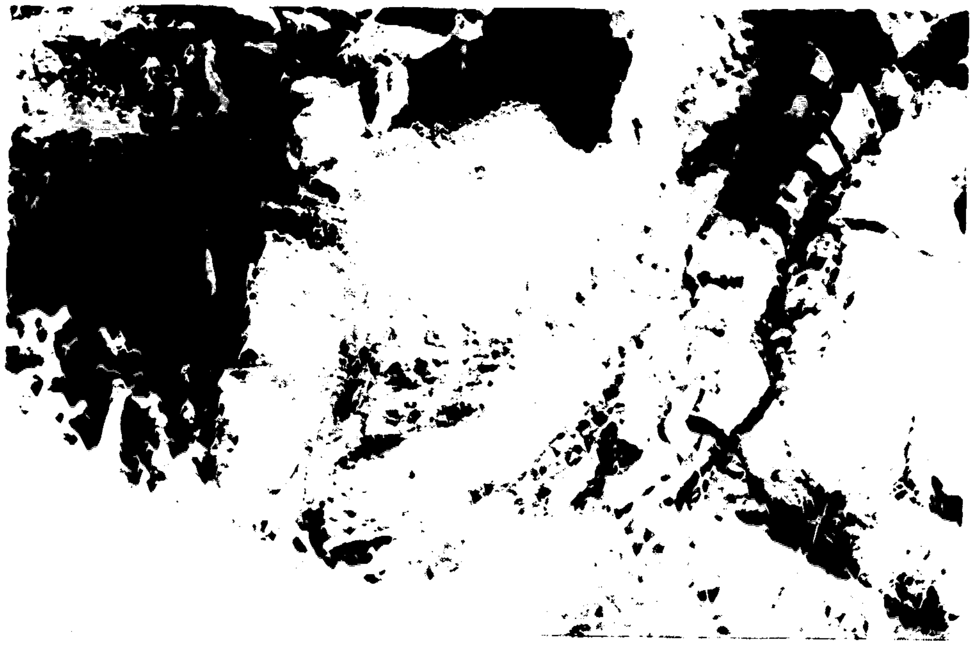


F1
F2
L1

A second planar fabric (S_1) is present in quartzose rocks and is defined by colour and compositional banding identical to that described for S_o (Plates 4.15 and 2.6). A well developed parting, with a spacing of 1 to 50 cm, which parallels S_1 and along which the rocks can be pulled apart is locally developed. Rarely, mica flakes parallel and lie along the plane of parting. Like S_o, S_1 is not preserved in micaceous rocks where it has been overgrown and obliterated by younger mica.

S_1 is also evident in amphibolite (Plate 2.4) and in marble (Plate 2.5). In amphibolite, S_1 is defined by a plane of parting along which the rock fractures into slabs 10 to 20 cm in width. The plane of parting parallels and is coincident with thin (less than 5 mm) compositional bands which consist largely of epidote. In marble, S_1 consists of fine colour and compositional banding. The colour variations consist of dark grey to brown laminae less than 1 cm thick and spaced at 1 to 20 cm intervals in white marble. Compositional layering consists of alternating bands of coarsely crystalline white calcite 1 cm to greater than 1 m in width, and thin (1 to 2 cm in width) bands of brown weathering, boudinaged chert lenses that extend parallel to the colour banding and which occur at irregular intervals. S_1 can only be distinguished from S_2 in marble where fold hinges affecting S_1 are observed.

Orientation data collected in the Upper Nisling River area in the brown quartzite unit (PPbq) reflects the orientation of the S_1 fabric (Figures 4.2 c and 4.4). Although deformed and folded, the general trend of the foliation parallels S_m and the contact with the Aishihik Batholith (Figures 4.2 c and 4.3). S_1 also parallels and is concordant with the margins of the largest of the intrusions of pink quartz monzonite of the Long Lake Suite, but is discordant with smaller related intrusions (Figure 4.2 c). Dykes of pink quartz monzonite intersect and truncate the S_1 fabric.

Orientation data recorded from the North and South Aishihik Lake areas only locally reflects the orientation of the S_1 fabric as quartzite is less commonly exposed. S_1 was not measured in marble or amphibolite.

A third planar fabric (S_2) is best developed in metapelitic rocks and consists of a coarse and irregular schistosity (Plate 2.1). The schistosity is defined by the subparallel alignment of biotite and muscovite. Migmatite occurs as irregularly shaped lenses that are characterized by corrugated contacts (Plate 2.1). The long axes of the migmatite lenses usually lies within and extends along the plane of foliation. Pinching and swelling of migmatite lenses gives the schistosity a wavy appearance. Rarely, large migmatite lenses are characterized by a planar fabric defined by compositional and colour banding which parallels and is continuous with S_2 in the adjacent schist. In quartzose rocks that are intimately interfoliated with metapelitic rocks, compositional banding, defined by grey and white gneissic bands 1 to 5 cm in width, parallels the schistosity.

In the Upper Nisling River area, where thick and continuous quartzose rocks of the brown quartzite unit crop out, S_2 is poorly developed to absent. In micaceous laminae, mica locally occurs at an angle to S_1 compositional banding and parallel to the axial plane of folds of S_1. In amphibolite, S_2 is heterogeneous. In the Upper Nisling River area amphibolite is locally characterized by significant amounts of quartz, and is interfoliated with quartzose rocks. In these areas S_2 is poorly developed. Where amphibolite is quartz-poor and where it occurs in close proximity to marble, the S_2 fabric is generally well developed and is defined by parallelism of hornblende grains and by thin and discontinuous (1 to 5 cm in width) light green and white colour and compositional bands. The light green bands are usually associated with the nearby presence of marble and consist of calc-silicate minerals including diopside and epidote. White bands represent feldspathic horizons. In marble colour and compositional banding, including brown weathering chert bands, parallel the contacts with, and schistosity in, adjacent mica-schist.

Throughout the North and South Aishihik Lake areas S_2 generally dips homoclinally to the east to northeast, and parallels the contact with, and foliation developed within Aishihik Batholith (Figures 4.2 a and b, 4.3, and 4.4).

A fourth planar fabric (S_3), defined by the parallel alignment of finely crystalline mica, overprints the main schistosity (S_2). S_3 is only locally developed and is restricted to micaceous, metapelitic horizons. It is not penetrative, but occurs at intervals of 1 to 5 cm and is associated with crenulations of the S_2 schistosity. The S_3 fabric is not developed in marble, amphibolite, or in quartzose rocks.

An additional planar fabric is defined by: 1) the parallel alignment of mica in schistose bands; 2) compositional banding consisting of alternating bands of fine grained amphibolite up to 20 cm thick and felsic quartzite and felsic metapelite bands from 5 cm to more than 1 m thick (Plate 4.16); 3) anastamosing gneissic bands which appear to represent fully recrystallized shear bands (Plate 4.17); 4) elongate marble boudins up to 50 cm thick and more than 2 m in length; 5) tight to isoclinal overthickened fold hinges. Hinge regions of folds of thin amphibolite horizons (2 cm thick measured along the limbs of the fold) are up to 60 cm thick, measured along the trace of the axial planar surface of the fold (Plate 4.16); 6) discontinuous feldspathic migmatite lenses; 7) the parallel alignment of aplite veins; and 8) the local development of shear bands (Plate 4.18) defined by distinct discrete shears spaced at regular intervals of 5 to 35 cm measured along schistosity and which cut across schistosity at an angle of less than 20^{o}. The shears often

Plate 4.16 Sheared and deformed rocks of the Nisling Assemblage observed immediately beneath the contact with the overlying Aishihik Batholith in the South Aishihik Lake area. Hornblende amphibolite (ha) and migmatitic (white lenses) feldspathic micaschist and quartzite are intimately interfoliated. White and black arrows at lower right indicate the inside and outside edges, respectively, of the hinge zone of a fold. The hinge zone consists of hornblende amphibolite and is 60 cm thick measured along the axial plane of the fold. Hornblende amphibolite in the limbs of the fold is 2 to 3 cm thick.

Plate 4.17 Anastamosing gneissic banding observed immediately beneath the contact with the overlying Aishihik Batholith in the southeast corner of the North Aishihik Lake area. The arrow points to where the anastamosing fabric has truncated earlier developed gneissic bands. The lense cap is 6.5 cm wide.

Plate 4.18 Macroscopic shear bands developed in migmatitic (white lenses) feldspathic micaschist and quartzite of the Nisling Assemblage observed immediately beneath the contact with the overlying Aishihik Batholith in the South Aishihik Lake area. Thin hornblende amphibolite horizons (ha) and aplite veins (indicated by arrows) are also indicated. The photograph was taken looking to the north. Spaced shear planes are highlighted and dip shallowly to the west. Foliation and gneissic banding are offset down-dip towards the west across the shear planes, consistent with a top-to-the-west sense of shear. The field note book at lower right is 12 cm wide.

appear to flatten into micaceous or amphibolitic horizons, while cutting across more feldspathic bands. Rocks above the shears are consistently displaced down-dip towards the west, consistent with their having developed during top-to-the-west shearing.

This fabric is only developed within 30 m of the west margin of the Aishihik Batholith. It was not observed along the north margin of the batholith. The fabric ends up against the overlying contact with granodiorite of the batholith, and is transitional into typical micaschist of the Nisling Assemblage.

The orientation of the fabric, although quite irregular and anastomosing, is subhorizontal to moderately east to northeast dipping, parallel with the overlying contact with the batholith and with the S_2 schistosity in the underlying Nisling Assemblage schists.

Folds

Deformation of compositional banding (S_o) has produced small isoclinal folds (F_1) (Plate 4.15). F_1 folds are characterized by elongate, thin (less than 1 cm) limbs and rare, divergent fold closures which are characterized by thickened hinge zones. Locally, hinge zones are boudinaged and detached. No antiform - synform pairs were observed. S_1 parallels, and is defined by, the elongate limbs of the F_1 folds.

F_1 folds are rare and difficult to recognize. S_o colour banding is commonly subtle, and subsequent deformation and metamorphism has modified F_1 folds. F_1 folds are best preserved where light and dark banding is well developed in the brown quartzite unit.

F_1 folds, and the associated S_1 axial planar fabric are deformed by isoclinal to open, recumbent to moderately inclined, horizontal to gently plunging folds (F_2). In the majority of the F_2 folds the limbs approach parallelism (isoclinal folds), although not for 1 to 3 m from the hinge line (measured along the axial planar surface). Fold amplitudes vary from less than 1 cm to more than 1 m. Antiform - synform pairs are rare.

Both symmetric (Plate 4.15) and asymmetric folds (Plate 2.6) were observed. In the Upper Nisling River area F_2 folds are weakly to strongly asymmetric, are characterized by gently to moderately north-dipping axial planar surfaces, by subhorizontal north - south to northeast - southwest trending hinge lines, and verge to the east to southeast (Figure 4.2 c). Along Aishihik Lake F_2 folds are less well preserved. Where present they are characterized by subhorizontal to gently northeast- to southeast-dipping axial planar surfaces, and by subhorizontal to gently north- to northeast-plunging hinge lines. No dominant sense of vergence was observed.

F_2 folds are best preserved in quartzose rocks. In micaceous rocks a coarse schistosity (S_2) lies in the axial surface of F_2 folds. Generally, the development of the schistosity has obliterated the associated folds. In amphibolite open folds of thin compositional bands (S_1) are rare and are generally obliterated by the development of the axial planar gneissosity or schistosity (Plate 2.4). Rare isoclinal folds in marble are characterized by axial planes which parallel the margins of the marble lenses and the schistosity in the adjacent micaschist (Plate 2.5).

S_2 is deformed by small (amplitudes of less than 10 cm, and commonly less than 1 cm) open, moderately inclined, subhorizontal to gently north-plunging kink, or chevron shaped folds (F_3). F_3 folds are asymmetric, characterized by vertical to gently east-dipping axial surfaces, and verge towards the west. The weakly developed S_3 schistosity lies in the axial surface of F_3 folds.

Larger F_3 folds are also developed and are characteristically more rounded. In quartzite F_3 folds are rare, are characteristically outcrop-scale with amplitudes and wavelengths of greater than 5 m (Plate 4.19). Upright, open F_3 folds of marble horizons with amplitudes of 20 m to more than 50 m were observed (Plate 4.20). Upright to steeply inclined, sub-horizontal to gently north-plunging, map-scale folds deform schists of the Nisling Assemblage, and the contact with, and granodiorite of, the Aishihik Batholith (Figures 4.3 a and 4.4). The folds are characterized by rounded to flattened hinge zones, amplitudes and wavelengths of 200 m to 500 m, vertical to moderately east-dipping axial surfaces, and weak westward vergence. F_3 folds are best developed in the South Aishihik Lake area in micaceous rocks. Poles to foliation for the South Aishihik Lake area, when plotted on an equal-area stereonet, define a well developed girdle pattern (Figure 4.4). The girdle pattern is characterized by a pole, reflecting the approximate average orientation of the F_3 fold axis, that plunges gently to the north.

Linear elements

A linear fabric element (L_1), defined by a rippled or wavy appearance apparent on S_1 partings, is weakly developed and is restricted to quartzose rocks in which S_o and S_1 are present (Plate 4.15). The lineation reflects the thickened and detached hinges of isoclinal F_1 folds which affect S_o.

A second lineation (L_2) is well developed in quartzose rocks and consists of the penetrative development of parallel quartz rods less than a 5 mm in width (Plate 4.21). The lineation appears to reflect the thickened hinges of small, tight, F_2 folds (Plate 2.3). An intersection lineation is developed in amphibolite where the S_1 and S_2 planar fabrics intersect (Plate 2.4). The lineation is best viewed on the surface of S_1 and consists of the surface trace of a poorly developed parting or jointing. The lineation is non-penetrative

Plate 4.19 Deformed quartzite observed in the Upper Nisling River area. The photograph is taken looking to the north. The arrow indicates the hinge of an F_2 fold, a close up of which was shown in Plate 4.16. The surface traces of a synform - antiform pair of open, asymmetric F_3 folds, which deform the F_2 fold, is also shown. The F_3 folds are characterized by moderately east-dipping axial planes and verge to the west. The outcrop is approximately 7 m high.

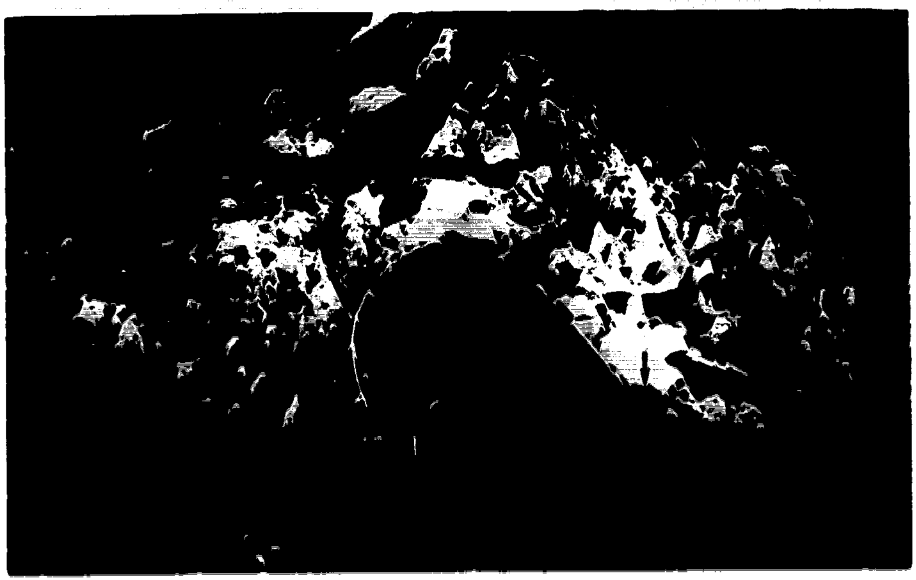

Plate 4.20 An F_3 antiform observed in the southern part of the South Aishihik Lake area. The antiform is cored by micaceous quartzite (dark grey) which is overlain by white marble (m). The arrow indicates a back-pack for scale.

Plate 4.21 Grey quartz gneiss from the South Aishihik Lake area. A photograph is shown at top and a line drawing of the photograph below. A well developed quartz rodding lineation (L_2) is deformed and folded about an F_3 fold. A brunton compass is shown for scale.

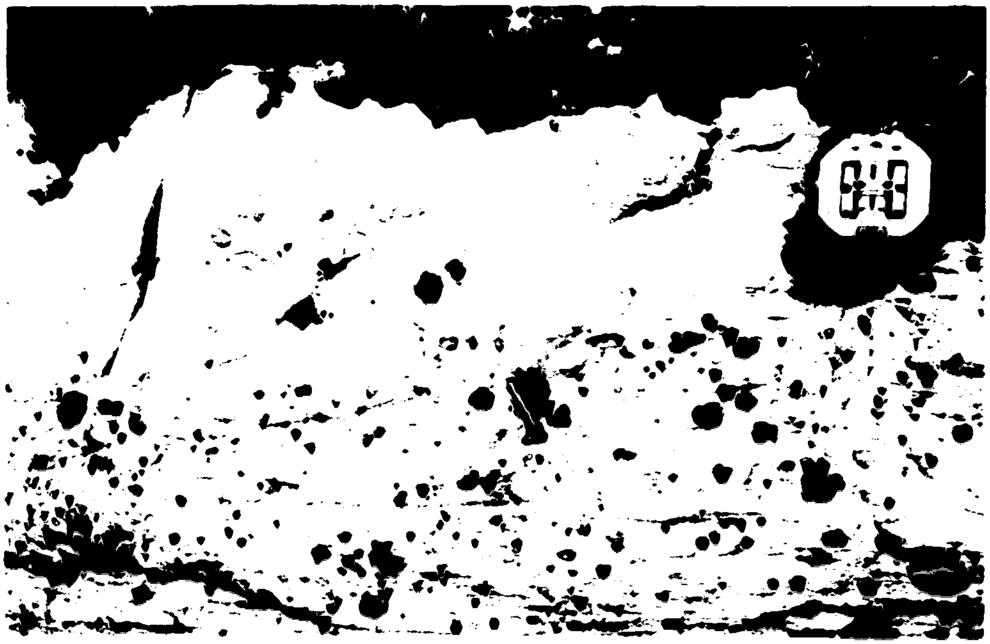

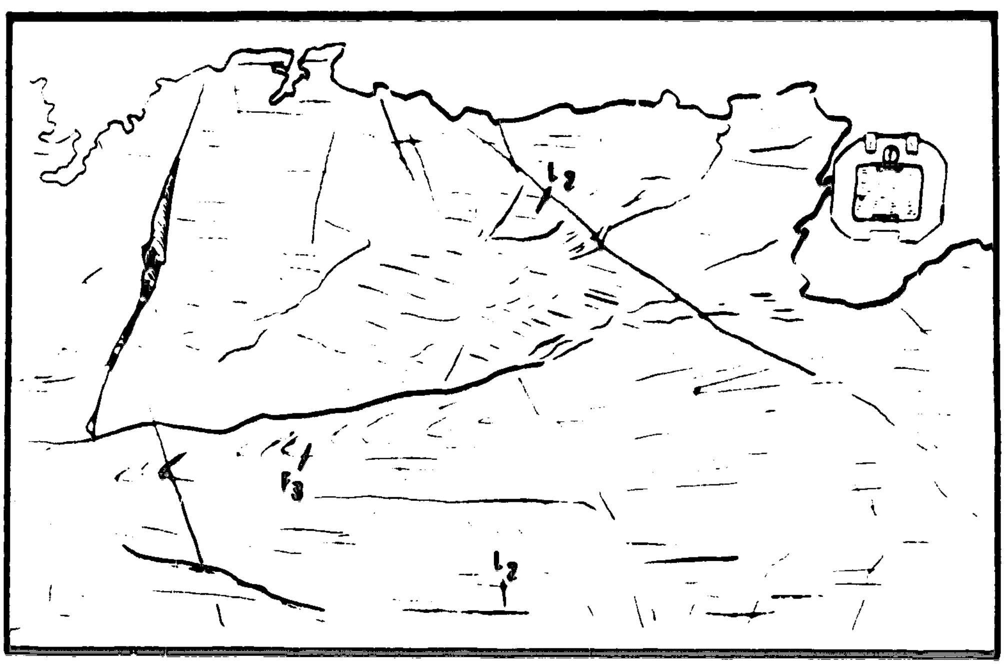
L2
F3
L2

and is not associated with the alignment of any mineral grains. L_2 is not well developed in either of marble or schistose rocks.

In the Upper Nisling River area, L_2 is subhorizontal to moderately plunging and trends northeast - southwest (Figures 4.2 c and 4.4). Along Aishihik Lake, the lineation is poorly developed but appears to be oriented parallel to subparallel with the L_3 crenulation lineation.

L_3 is developed in micaceous rocks and results from small open folds (amplitudes of less than 1 cm) that affect the main schistosity (S_2). L_3 is not well developed in amphibolite, marble, or quartzite. In micaceous quartzites it is weakly developed.

In the South Aishihik Lake area L_3 plunges gently to the north parallel with the hinge lines of F_3 folds and with the pole to the girdle pattern defined by poles to foliation (Figures 4.2 a and 4.4).

4.3.2 Microstructure

Planar fabrics and folds evident at mesoscopic scales, are also visible in thin-section. S_o, which is indistinguishable from S_1 in the absence of F_1 folds, was only identified in one thin-section (Figure 4.5) cut from a sample collected west of the Aishihik Lake in the North Aishihik Lake area. S_o consists of thin, finely crystalline, micaceous, quartzofeldspathic bands that are characterized by slightly darker colour than the surrounding quartzitic matrix.

S_o is deformed and defines an isoclinal fold (F_1) characterized by parallel limbs separated by about 2 mm. Mica grains are not, however, folded, indicating recrystallization during more recent metamorphism.

S_1, like S_o, consists of quartzofeldspathic bands. The S_1 bands are up to 1 cm in width and are also defined by micaceous laminae and by subtle colour and grain size banding. In schistose rocks (in which S_2 is pervasive) S_1 is preserved as thin (0.1 mm) iron stained laminae (Plate 4.22) and by discontinuous, quartzite boudins, eyes, and rootless fold hinges.

S_1 is deformed and defines open to tight folds (F_2). Generally, the folds are more open in quartzose rocks and become tighter as the mica content of the rocks increases. Detached tight to isoclinal fold hinges, consisting of medium grained quartz, characterize micaschist. In quartzite, micaceous laminae define tight, parasitic folds which verge towards the hinge of the larger folds.

Traces of S_1 are also preserved in younger mica, garnet, and staurolite porphyroblasts. Mica grains which define the S_2 schistosity are locally characterized by

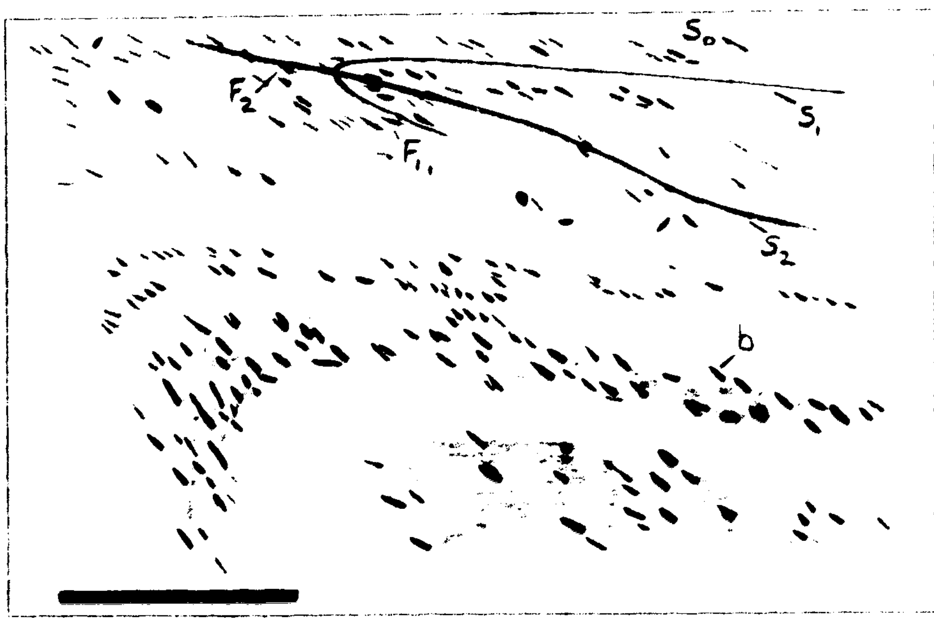

Figure 4.5 A line drawing made from a thin section cut from sample number 211 collected along the west side of Aishihik Lake in the North Aishihik Lake area. The scale bar represents 1 cm. Shaded grey and white bands indicate grain size and compositional banding (grey bands are more micaceous and feldspathic; white bands are clean quartzite; b - biotite porphyroblasts). Also indicated are S_0 - compositional banding;, S_1 - the axial plane of folds (F_1) of S_0; and S_2, the axial plane of folds (F_2) of S_1. Note that biotite porphyroblasts preferentially extend parallel to, and define the S_2 axial planar schistosity.

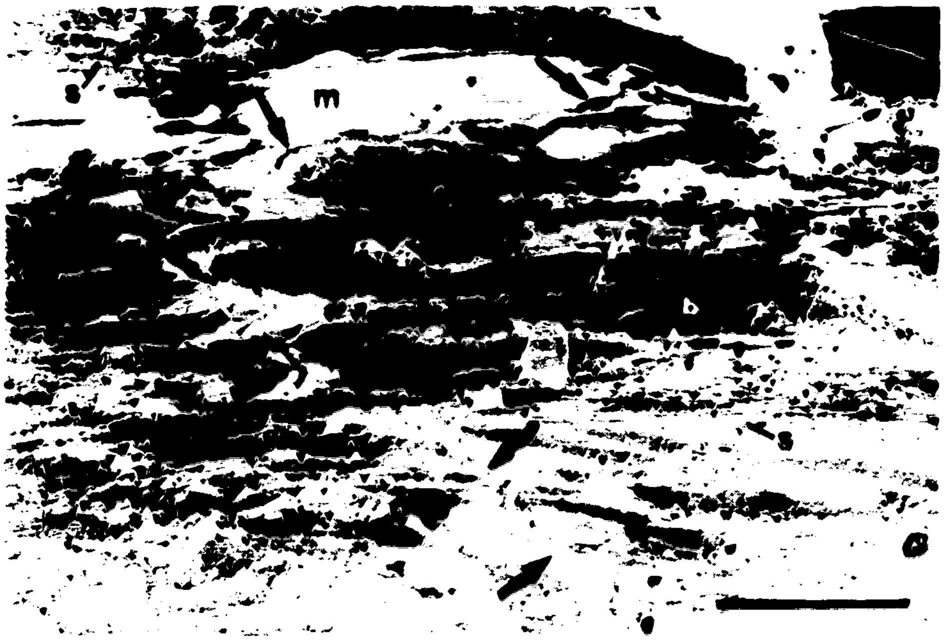

Plate 4.22 A photomicrograph, taken with plane polarized light, of sillimanite schist of the Nisling Assemblage from a sample (no. 87) collected near the contact with the Aishihik Batholith in the South Aishihik Lake area; s - sillimanite, m - muscovite, b - biotite. The arrows point to a thin, deformed horizon, defined by iron staining, which appears to represent an early, now transposed planar fabric (S_1). Mica that define the schistosity (S_2) are axial planar to folds of S_1. The scale bar represents 250 um.

fine opaque inclusions thought to be graphite (Plate 4.23). The inclusions define a finely laminated planar fabric that has been deformed and folded. Garnets include grains of quartz, feldspar, mica (usually biotite), fine opaque material (thought to be graphite), and pyrite (Plate 4.24). Inclusions trails define isoclinal to open, symmetric and asymmetric folds. Staurolite exhibits a branching habit extending both subparallel to, and at a high angle to the main schistosity (S_2). Fine opaque inclusions, thought to be graphite, define a planar fabric element (S_1) which is isoclinally folded. The limbs of the isoclinal folds parallels the staurolite branches (Plate 4.25).

Fibrolitic sillimanite defines thin (less than 1 mm in width) and continuous laminae which appear to represent aluminum-rich compositional bands (S_1) (Plate 4.26). The laminae define tight to isoclinal folds which are characterized by narrow, angular hinge zones and by foliation-parallel (S_2) axial planes. Fibrolite needles grow parallel with the lamination. Near the fold hinges fibrolite needles bend gently towards the hinge and exhibit mild undulose extinction. Needles are not, however, continuous around the fold hinges. Fibrolite needles also grow parallel to the trace of the axial planar surfaces of the folds.

S_2 parallels the axial surfaces of F_2 folds. In micaceous quartzite isolated mica grains parallel with the trace of the axial planes of folds of S_1 (Figure 4.5). In schistose rocks, the crystallization of axial planar mica defines a schistosity that has obliterated the associated folds. The schistosity is irregular with multiple generations of mica growing at a slight angle to one another (Plate 4.23). Locally two distinct planar elements, thought to represent a relic S and C fabric, are present (Plate 4.27). The S (flattening) planes consist of stacked, parallel, mica grains. The mica grains are fish-shaped, bend into, and pinch out against the C (shear) planes. The C planes oriented at an angle of about 20^o to the S planes. Isolated mica grains locally grow along the C planes. The S and C fabric is rare and poorly preserved.

As indicated above, metamorphic porphyroblasts preserve, primarily in the form of inclusion trails, traces of deformed S_1. The preservation of pervasively deformed S_1 suggests that the nucleation of porphyroblasts largely post-dated deformation of S_1. Porphyroblasts are intimately intergrown with mica oriented parallel to the axial planes of folds of S_1 (Plate 4.22; Figure 4.5). The distribution of sillimanite, kyanite, and staurolite defines a series of isograd bound metamorphic zones which extend along the west margin of the Aishihik Batholith and which parallel the S_2 schistosity (Chapter V). These observations indicate that metamorphic porphyroblasts nucleated and grew at the same time as the development of the S_2 schistosity.

Plate 4.23 A photomicrograph, taken with plane polarized light, of micaschist of the Nisling Assemblage from a sample (no. 82) collected in the South Aishihik Lake area; m - mica, b - biotite. A poorly defined foliation parallels the top and bottom margins of the photograph. Several generations of mica, each oriented at a slightly different angle, are evident. Graphitic inclusion trails are interpreted to represent an older, deformed planar fabric which was deformed and overgrown by mica. The scale bar represents 1 mm.

Plate 4.24 A photomicrograph, taken with plane polarized light, of garnet micaschist from a sample (no. 146) collected in the South Aishihik Lake area; g - garnet, m - mica. The garnet porphyroblast is characterized by graphitic inclusion trails which define a tight to isoclinal fold, indicated by the arrow. The scale bar represents 250 um.

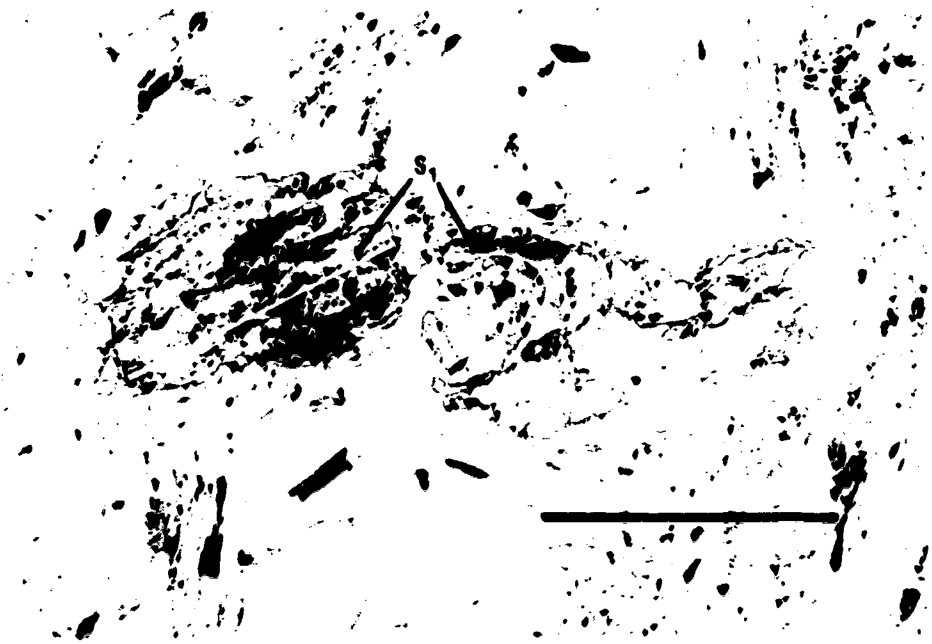

Plate 4.25 A photomicrograph, taken with plane polarized light, of staurolite micaschist from a sample (no. 17) collected in the South Aishihik Lake area. A staurolite porphyroblast, at center, is characterized by graphitic inclusion trails which define a planar fabric (S_1), highlighted in white, which is folded. The scale bar represents 1 mm.

Plate 4.26 A photomicrograph, taken with plane polarized light, of sillimanite micaschist from a sample (no. 69) collected in the Upper Nisling River area; SIL - sillimanite. A sillimanite rich laminae defines a tight, recumbent fold characterized by a schistosity parallel axial plane. Individual sillimanite needles bend gently towards, but are not continuous around, the fold hinge. Fibrolite needles and coarse sillimanite also grow parallel to the axial trace of the fold (indicated just below the SIL label). The scale bar represents 250 um.

Plate 4.27 A photomicrograph, taken under crossed nicols, of micaschist from a sample (no. 145) collected in the South Aishihik Lake area. A relic, recrystallized S and C fabric is evident. Mica define fish which extend parallel with compositional banding (S planes) and which are bound by planes oriented at about 20° to the S planes and which are thought to represent relic shear planes (C planes). The scale bar represents 250 um.

The S_2 schistosity is deformed and defines open folds (F_3) (Plate 4.28). The folds are characterized by planar limbs and by narrow, angular hinges. Both symmetric and asymmetric folds occur. When followed up and down section, fold limbs change length and pinch out, resulting in the coalescence of fold axial traces. Rarely, mica grains nucleate and grow along the axial planes of F_3 folds and define a weakly developed S_3 axial planar schistosity.

Samples of sheared micaschist collected from the contact with the Aishihik Batholith, are similar on a microscopic scale to micaschist from elsewhere in the study area (Plate 4.22). Quartzite samples are however, characterized by significant grain size reduction and recrystallization. S and C quartzite mylonites are locally developed (Plate 4.29).

4.3.3 The nature of the planar fabrics

S_o is the oldest recognized and is deformed and overprinted by the development of all subsequent fabrics. S_o is not associated with tectonism of any previous fabric, consists of colour and compositional banding, and is inferred to be bedding.

S_1, F_1, and L_1 developed during isoclinal folding of bedding (D_1). D_1 fabrics are preserved in quartzite and in younger metamorphic porphyroblasts throughout the South and North Aishihik Lake areas and the Upper Nisling River Area. The wide distribution of D_1 fabric elements suggests that the tectonic event responsible for their development was regional in extent. D_1 tectonism is older than the Aishihik Batholith (187.0 + 9.7/-0.9 Ma) which is inferred to intrude the Nisling Assemblage but which is not characterized by D_1 structures.

S_2 is best preserved in metapelitic rocks, and parallels the axial surface of open to isoclinal folds (F_2). Small- to microscopic-scale folding has produced a northeast-trending quartz rodding lineation (L_2). F_2 folds are best preserved in quartzite, are asymmetric, and are east to southeast verging. Although F_2 folds are dominantly east-vergant, the north to northeast plunging quartz rodding lineation (L_2) suggests shearing in a north - south direction.

The D_2 tectonic event was regionally extensive. D_2 tectonism resulted in deformation of D_1 fabrics throughout the study area. In quartzose rocks, most folds are attributable to D_2 tectonism. In metapelitic rocks, the schistosity and metamorphic porphyroblasts are attributable to the D_2 event.

The timing of D_2 tectonism is problematic. Regional shearing of the Nisling Assemblage did not result in deformation of the Aishihik Batholith. Except for the

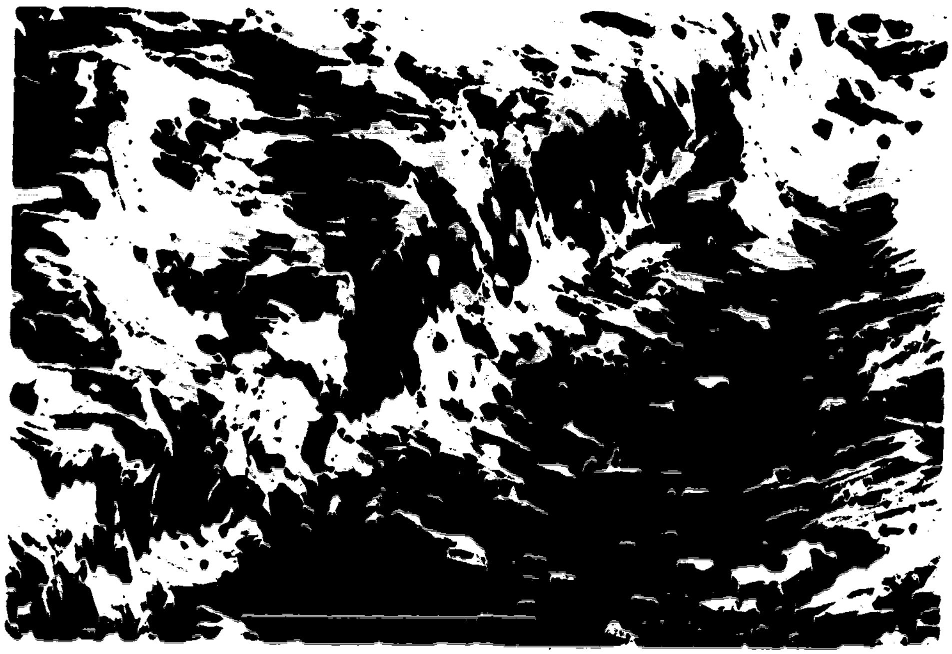

Plate 4.28 A photomicrograph, taken under crossed nicols, of crenulated micaschist from a sample (no. 131) collected in the South Aishihik Lake area. A few grains of recrystallized mica overprint the schistosity and parallel the axial plane of this F_3 fold. The scale bar represents 1 mm.

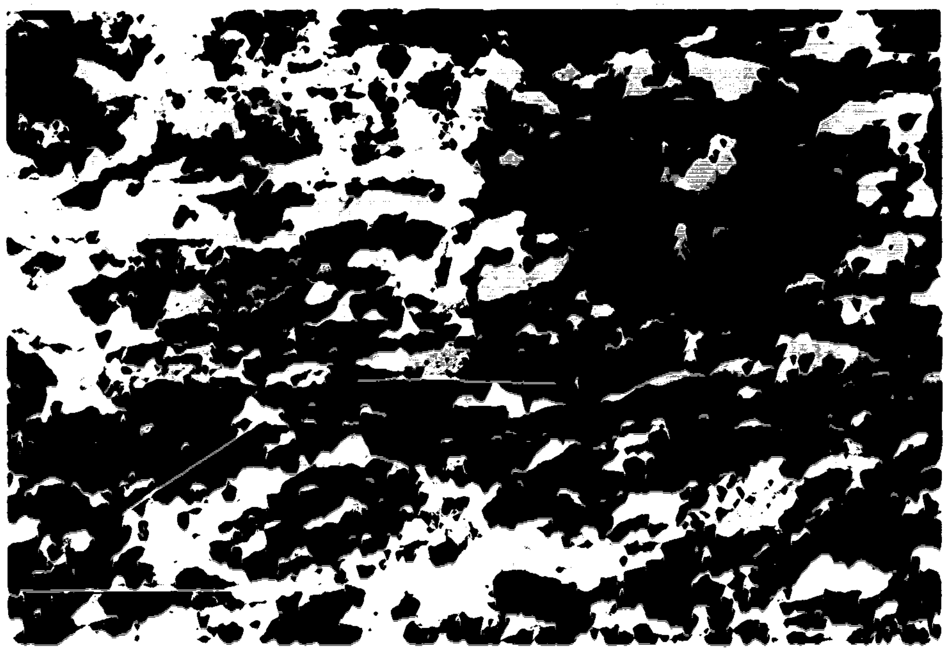

Plate 4.29 A photomicrograph, taken under crossed nicols, of thermally annealed mylonitic feldspathic quartzite from a sample (no. 62) collected immediately beneath the contact with the Aishihik Batholith in the South Aishihik Lake area. Dynamic recrystallization of quartz has resulted in the development of an S and C fabric. C planes are oriented subparallel with the top and bottom of the photograph and are defined by thin discontinuities which separate elongate composite quartz grains. S planes are oriented at about 25° to the C planes and are defined by the preferred orientation of individual quartz grains. The scale bar represents 1 mm.

restricted development of S_t, which is characterized by top-to-the-west shearing, no regionally extensive, solid-state fabric is developed in the batholith. Neither has the batholith been metamorphosed. Again, except for the restricted development of S_t, no recrystallization of biotite was observed. These observations indicate that D_2 tectonism predates the emplacement of the Aishihik Batholith (187.0 + 9.7/-0.9 Ma).

However, S_2 parallels the margins of the batholith. The distribution of metamorphic porphyroblasts that nucleated during the development of the schistosity defines a series of isograd-bound metamorphic zones. The isograds and metamorphic zones are sub-parallel to schistosity and with the margin of the batholith and record an increase in metamorphic grade towards the batholith. These observations indicate that metamorphism and the development of the S_2 axial planar schistosity developed during the emplacement of the batholith.

Together, these observations lead to the conclusion that the axial planar schistosity in part post-dates the folds with which it is associated. Several observations are consistent with this premise: 1) in metamorphic porphyroblasts that preserve earlier developed fabrics (S_1) the older fabric is invariably deformed; 2) although the S_2 schistosity is grossly axial planar, it is irregular and defined by multiple generations of mica that overprint one another and that grow at an angle to each other; 3) the margins of migmatite lenses are irregular and corrugated. In addition, migmatites do not exhibit any internal shear fabrics. 4) S_2-parallel compositional banding locally extends into and is inundated by migmatite; and 5) a relic S and C fabric is locally preserved. Thorough recrystallization and overprinting of the fabric by younger mica has, however, largely obliterated this fabric.

The following sequential geologic history is suggested: 1 - shearing of the Nisling Assemblage prior to the intrusion of the Aishihik Batholith, but after D_1 tectonism; and 2 - the emplacement of the Aishihik Batholith and the thermal enhancement of schistosity and the nucleation of metamorphic porphyroblasts. Intrusion may have occurred shortly prior to the cessation of shearing. The lack of a penetrative solid-state fabric developed throughout the batholith indicates that if intrusion of the batholith did overlap with shearing of the Nisling Assemblage, enough melt was present (greater than 30% melt (van der Molen and Peterson, 1979)) that strain was accommodated without the significant solid-state deformation.

The weakly developed S_3 crenulation schistosity and the L_3 lineation developed in response to open to tight folding of the Nisling Assemblage and the contact with the Aishihik Batholith (D_3). The F_3 folds are weakly to strongly asymmetric, verge to the west, and indicate top-to-the-west shearing of the Nisling Assemblage and the Aishihik Batholith. D_3 tectonism was regionally extensive; F_3 folds were observed through out the study area. D_3 tectonism was not, however, characterized by significant metamorphism or by the development of a penetrative planar fabric.

The timing of D_3 tectonism is only loosely constrained. F_3 folds deform and are younger than the Aishihik Batholith. The relationship of F_3 folds to the plutons of pink quartz monzonite could not be determined but they are younger than undeformed intrusions of the Ruby Range Batholith (between 90 and 58 Ma).

The planar fabric developed immediately adjacent to the west margin of the Aishihik Batholith is interpreted as the result of intense shearing. This is consistent with the preservation of: anastamosing relic mylonite; tectonically interleaved metapelite, quartzite, marble and amphibolite; and grossly overthickened, rootless fold hinges. When viewed towards the north, rocks above the subhorizontal to gently east dipping C planes are consistently displaced down-dip to the west, indicating top-to-the-west shearing. Shearing is thought to have occurred at high temperatures, as indicated by the ductile nature of deformation, and by the complete annealing of mylonitic fabrics.

The shear fabric in Nisling Assemblage is closely associated with the S_t fabric of the Aishihik Batholith. Both fabrics are developed adjacent to the west margin of the batholith, are not observed elsewhere, and provide a record of top-to-the-west shearing at elevated temperatures. Both fabrics are interpreted to have developed at the same time in response to shearing along the west margin of the batholith. The significance and timing of this shearing is discussed below.

4.4 The shape of the Aishihik Batholith and the nature of the west margin of the batholith

A cross-section, constructed perpendicular to the regional plunge and onto which the Aishihik Batholith - Nisling Assemblage contact has been projected, is shown in Figure 4.6. Intrusions of the Long Lake Suite and the Ruby Range Batholith are not shown. Assuming that the crust underlying the Aishihik Lake region behaved as a solid tabular block that has been tilted 5^{o} to the north, tilting has resulted in the exposure of an approximately 10 km thick section of the crust. Deep structural levels are exposed in the South Aishihik Lake area with progressively shallower crustal levels exposed to the north.

The Aishihik Batholith forms a large overhanging flap. The lower contact, along which the batholith overlies the Nisling Assemblage, crops out along side Aishihik Lake. An abrupt change in the orientation of the batholith - Nisling Assemblage contact occurs near the north end of Aishihik Lake (Figure 4.1). This change in orientation coincides

Figure 4.6 A regional cross-section (K - L), the location of which is indicated in Figure 4.1, showing the geometry of the Nisling Assemblage - Aishihik Batholith contact in profile. Boxes indicate the projections of the North and South Aishihik Lake map areas, and the Upper Nisling River area. Data points represent orientation data projected onto the line of section. Intrusions of the Ruby Range Batholith and the Long Lake Suite are not shown. See text for discussion.

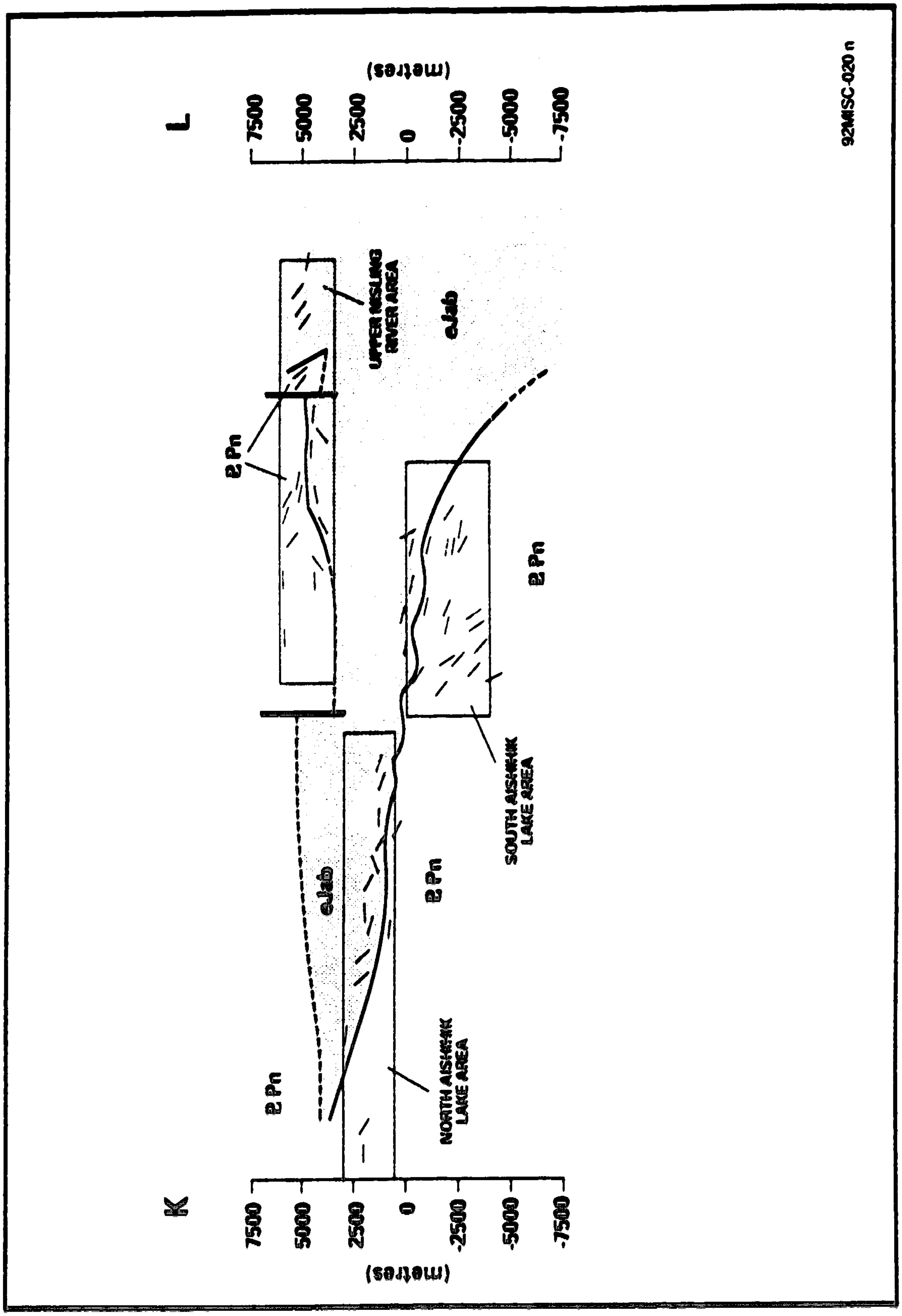
K
L
7500
5000
2500
0
-2500
-5000
-7500
(metres)
UPPER NISLING RIVER AREA
NORTH AISHIHIK LAKE AREA
SOUTH AISHIHIK LAKE AREA
eJab
92MSC-020 n

with the pinching out of the batholith to the west. To the north, the roof of the batholith, along which the Nisling Assemblage overlies the batholith, is complicated and deformed by late steeply dipping faults.

S_t is developed along the lower contact of the batholith. A similar shear fabric is developed in metamorphic rocks beneath the contact. Similar tectonic foliations have been attributed to: 1) post-intrusive tectonism (e.g. Page and Bell, 1986); 2) syn-tectonic intrusion (e.g. Gapais and Barbarin, 1986); or 3) ballooning of a diapir (e.g. Sylvester *et al.*, 1978; Bateman *et al.*, 1983). These three models are discussed here in light of the cross-section through the batholith.

1 - Post-intrusive tectonism

The batholith and Nisling Assemblage are deformed by asymmetric west-verging folds (F_3). Some shearing may have resulted from folding. However, although F_3 folds do occur along the north margin of the batholith, no associated S_t fabric development was observed. The shear fabric in the Nisling Assemblage is restricted to the immediate vicinity of the lower contact of the batholith and yet F_3 folds are evident throughout the Nisling Assemblage. Finally, F_3 folds postdate and deform rocks characterized S_t in the batholith and the shear fabric in the Nisling Assemblage. F_3 folds, therefore, post-date S_t.

With the exception of the F_3 folds, no other regionally developed, post-intrusive structures have been observed. This suggests that the S_t fabric is not the result of post-intrusive tectonism.

2 - Syn-tectonic intrusion

Criteria used for the identification of syn-tectonic intrusions include: 1) parallel or subparallel magmatic and high-temperature solid-state foliations in the intrusion; 2) continuity of the solid-state fabric with a regionally developed foliation in the wall rocks; and 3) development of synkinematic porphyroblasts with respect to foliation, in the contact aureole (Paterson *et al.*, 1989).

The fabrics developed along the west margin of the batholith satisfy all of these requirements: 1) S_t in the batholith is a high-temperature solid-state foliation which parallels the magmatic (S_m) foliation; 2) S_t and S_m are parallel to the S_2 schistosity developed in the Nisling Assemblage; and 3) metamorphic porphyroblasts developed at the same time as the schistosity.

However, this model fails to explain the distribution and nature of the tectonic fabrics. Along the north margin of the batholith, no significant shearing either of granodiorite or of the host metamorphic rocks was observed. Shearing is restricted to the west margin of the batholith even though D_2 tectonism affected rocks of the Nisling

Assemblage throughout the study area. In addition, D_2 tectonism resulted in the development of a north-trending quartz rodding lineation, consistent with shearing in a north - south direction. The tectonic fabrics developed along the west margin of the batholith in both the batholith and the adjacent metamorphic rocks is characterized by top-to-the-west shear. These observations suggest that the batholith is not a syn-tectonic intrusive.

3 - Ballooning

Ballooning occurs as a result of the continued emplacement of magma into the core of diapir, the outer portions of which have already solidified (Sylvester *et al.*, 1978; Bateman, 1985). It is however, difficult to separate solid-state foliations that developed in response to ballooning from those that developed in response to post-emplacement tectonism (Paterson *et al.*, 1989). Criteria used for the recognition of ballooning include: 1) a lack of post-emplacement regional deformation of the wall rocks; 2) evidence of high temperature solid-state deformation; 3) evidence of diapirism; 4) the development of an anastomosing foliation in the wallrocks along the contact. Foliation development results from thinning of the wall rocks during pluton expansion and is characterized by the recrystallization of quartz and biotite; and 5) the presence of discontinuities in the intensity of magmatic and solid-state foliations across internal contacts within the intrusion (Sylvester *et al.*, 1978; Bateman, 1985; Paterson *et al.*, 1989).

Post-emplacement regional deformation of the Nisling Assemblage is restricted to the development of west-verging folds (F_3) that also affect the batholith. As shown above, F_3 folds, and an associated axial planar, crenulation schistosity (S_3), deform, overprint, and clearly post-date the development of earlier tectonic fabrics. S_t in the batholith developed at elevated temperatures as indicated by its association with migmatites and by the thorough recrystallization of the shear fabrics. Strong evidence that Aishihik Batholith constitutes a diapir is its profile, shown in Figure 4.6. In addition, a well developed magmatic foliation parallels the margins of the batholith. The shear fabric developed in the wallrock schists is characterized by anastamosing shear zones defined by thorough recrystallization of all mineral grains. Significant thinning of the wall rocks is suggested by the preservation of numerous rootless, thickened fold hinges whose limbs have been thinned and boudinaged. No internal contacts have been identified within the Aishihik Batholith. It remains to be seen whether late stage magmatic pulses can be identified within the core of the Aishihik Batholith.

The development of the tectonic fabrics along the lower contact of the Aishihik Batholith appears to be best explained by ballooning of a diapir. The lack of significant solid state deformation along the roof of the diapir suggests that ballooning resulted largely in sideways expansion of the intrusion. An analogue for sideways expansion during ballooning of an intrusion, albeit on a smaller scale, may be the Papoose Flats pluton of California (Sylvester *et al.*, 1978). Like the Aishihik Batholith, only one margin of the Papoose Flats intrusion is characterized by a well developed solid-state foliation. Adjacent wallrocks are thinned by up to 90%. Deformation resulted from the sideways expansion of the pluton during the final stages of intrusion in which massive quartz monzonite was emplaced in the core of the intrusion. Paterson *et al.* (1991) have, however, shown that at least some fabric development in the Papoose Flats intrusion is attributable to post-emplacement tectonism.

This model implies that the batholith is largely post-tectonic: metamorphism associated with the emplacement of the Aishihik Batholith is predicted to post-date tectonism responsible for the development of the F_2 folds preserved in the Nisling Assemblage. This is consistent with observations outlined above that suggest that D_2 tectonism is divisible into two stages: 1) shearing of the Nisling Assemblage prior to the intrusion of the Aishihik Batholith but after D_1 tectonism; and 2 - the late to post-tectonic emplacement of the Aishihik Batholith and the development of the schistosity and the metamorphic porphyroblasts at about 187.0 + 9.7/0.9 Ma.

4.5 Steep faults

Late, steep to vertical faults that truncate older structures and fabrics affect the Nisling Assemblage, the Aishihik Batholith, and plutons of pink quartz monzonite of the Long Lake Suite. Faults are poorly exposed and are rarely observed. They are commonly recognized as linear features evident on the ground and on aerial photographs

In the Upper Nisling River area, the displacement of the steeply-dipping margins of an intrusion of pink quartz monzonite across a series of north - south trending lineaments suggests that faulting was characterized by a component of strike-slip motion (Figure 4.2 c). The margins of the pluton are sinistrally offset 100 to 1500 m. A north-northwest trending set of faults is also observed (Figure 4.2 c). The sense of displacement along these faults could not be directly determined. However, mapping immediately to the west of the Upper Nisling River area by Tempelman-Kluit (1974) indicates that the north margin of the Aishihik Batholith is dextrally offset by about 10 km along a north-northwest trending topographic depression (Figure 4.1).

In the North Aishihik Lake area, west of the Aishihik Lake, a linear, north-northwest trending fault zone truncates quartzite, amphibolite and marble of the

Nisling Assemblage (Figure 4.2 b). Foliation in quartzite is deflected in a dextral sense adjacent to the fault, and suggests that faulting was characterized by a component of dextral strike-slip motion (Plate 4.30). Marble in the fault zone is mylonitized (Plate 4.31).

North-northwest trending faults are subparallel to, and appear to be characterized by the same dextral sense of offset as the Denali fault, present 100 km to the southwest (Figure 1.1). 340 km of dextral slip occurred across the Denali fault between 57 Ma and 54 Ma (Eisbacher, 1976). The parallelism of the fault trends, and the matching sense of displacement (dextral strike-slip) suggests that faulting is Eocene and is related to displacement along the Denali fault. North trending faults, which are characterized by a component of sinistral strike-slip offset, probably developed at the same time and would represent a conjugate fault set.

In the South Aishihik Lake area, the Nisling Assemblage - Aishihik Batholith contact is faulted (Figure 4.2 a). The faults strike north to north-northwest. In foliated granodiorite of the batholith individual faults are defined by discrete planar surfaces (Plate 4.32). There is usually some discordance in the orientation of foliation across the faults. In schistose rocks of the Nisling Assemblage, the faults are defined by narrow, recessive zones up to 1 m in width, which are characterized by fault gouge (Plate 4.32). The faults are characterized by predominantly dip-slip displacement. Foliation in rocks in the immediate footwall of one well exposed fault deflects down into the fault. In the hangingwall of faults that cut the Nisling Assemblage - Aishihik Batholith contact, the contact is displaced down-dip 1 to 100 m (Figure 4.3 - cross-section E - F). Both down-dip to the east and down-dip to the west faults were observed.

The timing and tectonic significance of faults characterized by primarily dip-slip motion is not known. There is no evidence to suggest that these faults developed in response to significant extension of the region. Only three faults of minor displacement were identified. No penetrative fabric development is associated with the faults and no fault-related volcanic rocks were observed.

4.6 Discussion

Hornblende granodiorite intrusions of the Klotassin Suite, including the Aishihik Batholith, are characteristically foliated (Tempelman-Kluit, 1974; Woodsworth *et al.*, 1991). It has generally been assumed that the foliation resulted from syn- or post-intrusive deformation and tectonism (Tempelman-Kluit, 1974; 1979; Erdmer, 1989; Currie, 1992). Deformation has been attributed to: 1) Middle Jurassic overthrusting of the North

Plate 4.30 Brown graphitic quartzite next to a steeply dipping, brittle fault zone observed in the North Aishihik Lake area. The fault gouge consists of shattered and broken fragments of brown graphitic quartzite. The knife, which sits atop the fault gouge, is 4 cm long.

Plate 4.31 A photomicrograph, taken under crossed nicols, of mylonitized marble with characteristic quartz eyes (q). The scale bar represents 1 mm.

Plate 4.32 A steep fault that offsets the contact of the Aishihik Batholith with underlying schist of the Nisling Assemblage (highlighted with a white line) observed in the South Aishihik Lake area. The fault, indicated by the arrows, consists of a discrete plane in granodiorite (gd) and a narrow, fault gouge zone (fg) in schist (sch). The deflection of foliation in strata adjacent to the fault is consistent with the dip-slip offset of the contact. A hammer is shown for scale.

American continental margin by the Stikine terrane, including the Nisling Assemblage (Tempelman-Kluit, 1979); and 2) the Early to Middle Jurassic tectonic juxtaposition of the Nisling Assemblage with the Stikine terrane (Currie, 1992).

The foliation that characterizes the Aishihik Batholith is inferred largely magmatic and to have developed in response to magmatic flow during the diapiric emplacement of the batholith. A solid-state fabric that characterizes the lower contact of the batholith developed in response to late stage ballooning of the diapir. These relationships indicate that the batholith is post-tectonic and does not provide a record of either of Middle Jurassic overthrusting of the North American continental margin or of Early to Middle Jurassic tectonic juxtaposition of the Nisling Assemblage and the Stikine terrane.

The Nisling Assemblage has been variously interpreted as being: 1) continuous with, and representative of, semi-autochthonous North American continental margin (Hansen, 1990); 2) the basement of the Stikine terrane (Tempelman-Kluit, 1979); or 3) part of the Yukon - Tanana terrane (Mortensen, 1990; in press).

The Nisling Assemblage is inferred to be intruded by the Aishihik Batholith. The batholith constitutes part of the Early Jurassic Klotassin Suite (Tempelman-Kluit, 1974; Woodsworth *et al.*, 1991), which is characteristic of suspect terranes including the Yukon - Tanana and Stikine terranes. Similar plutons are not found intruding the North America continental margin. This suggests that the Nisling Assemblage does not constitute part of, and is not continuous with, the North American continental margin.

Correlation of the Nisling Assemblage with the North American continental margin led Hansen (1990) to suggest that North American rocks are characterized by structural fabrics that developed in response to Early Jurassic top-to-the-east shearing. While the Nisling Assemblage is characterized by east verging folds thought to have developed in the Early Jurassic (F_2), Early Jurassic structures characteristic of top-to-the-east shearing have not been documented for North American rocks and should not be used as a criterion for the recognition of North American strata.

Intrusion of the Nisling Assemblage by the Aishihik Batholith indicates that the Nisling Assemblage was part of Stikinia terrane by 186 Ma. However, pre-Aishihik Batholith, Early Jurassic, shearing in the Nisling Assemblage is not characteristic of Late Triassic and older strata of the Stikine terrane. Late Triassic Lewes River Group strata of the Stikine terrane are relatively undeformed and unmetamorphosed (Tempelman-Kluit, 1974; Wheeler, 1961). The Aishihik Batholith is, therefore, the oldest geologic element that is common to both the Stikine terrane and the Nisling Assemblage. The lack of any significant pre-Aishihik Batholith, shearing of Late Triassic strata suggests that the Stikine terrane and the Nisling Assemblage constituted separate and distinct tectonic elements prior to the Early Jurassic.

In both the Yukon - Tanana terrane and the Nisling Assemblage the oldest preserved structural fabrics provide a record of ductile deformation of primary bedding (D_1). In the Early Jurassic the Yukon - Tanana terrane was imbricated with ophiolitic strata of the Slide Mountain terrane along regional thrust faults (Mortensen, 1990; in press; Mortensen and Jilson, 1985). Ductile top-to-the-east shearing followed by the intrusion of the Aishihik Batholith characterizes the Nisling Assemblage in the Early Jurassic. Structural fabrics preserved in the Yukon - Tanana terrane and the Nisling Assemblage do not, therefore, preclude the inclusion of the Nisling Assemblage as part of the Yukon - Tanana terrane. They do suggest, however, that the Nisling Assemblage in the Aishihik Lake region was at a deeper structural level in the Early Jurassic than much of the rest of the Yukon - Tanana terrane.

4.7 Conclusions

1 - The Aishihik Batholith is inferred to be an asymmetric, post-tectonic diapir which intrudes the Nisling Assemblage.

2 - The foliation that characterizes the Aishihik Batholith is largely magmatic and to have developed in response to flow during the emplacement of the batholith.

3 - A solid-state fabric that characterizes the lower contact of the Aishihik Batholith developed in response to late stage sideways ballooning of the diapir.

4 - The Aishihik Batholith does not provide a record of either of Middle Jurassic overthrusting of North America by the Stikine terrane, or of Early to Middle Jurassic tectonic juxtaposition of the Nisling Assemblage and the Stikine terrane.

5 - The Nisling Assemblage records at least three episodes of regional deformation including: D_1 - pre-Early Jurassic isoclinal folding of primary bedding; D_2 - Early Jurassic deformation characterized by the development of asymmetric, east-verging folds; and D_3 - post-Early Jurassic, pre-Late Cretaceous folding. The folds are asymmetric and verge to the west and affect both the Nisling Assemblage and the contact with the Aishihik Batholith.

6 - D_2 tectonism is divisible into pre-Aishihik Batholith and syn-Aishihik Batholith phases. Folding and shearing of the Nisling Assemblage preceded the emplacement, and did not result in deformation, of the Aishihik Batholith. The S_2 axial planar schistosity and metamorphic porphyroblasts developed, and provide a record of metamorphism, during the emplacement of the batholith.

7 - The Klotassin Suite plutonic assemblage intrudes Nisling Assemblage, but does not intrude North American strata, suggesting that Nisling Assemblage does not constitute part of, and is not continuous with, the North American continental margin.
8 - The structural evolution of the Nisling Assemblage is similar to and compatible with the structural evolution of the Yukon - Tanana terrane. The Nisling Assemblage in the Aishihik Lake region was, however, at a deeper structural level in the Early Jurassic than much of the rest of the Yukon - Tanana terrane.
9 - Two types of steep faults that are characterized by a component of strike-slip displacement affect rocks in the study area. These include a set of north-northwest trending faults characterized by dextral strike-slip offset and a set of north trending faults characterized by sinistral strike-slip offset. These two sets of faults are inferred to be a conjugate pair that developed in the Eocene at the same time as the Denali fault.
10 - Steeply dipping faults characterized by dip-slip displacement are rare and trend to the north or north-northwest. Both down-dip to the west faults and down-dip to the east faults are developed. Dip-slip faulting is not regionally significant and does not provide a record of significant extension of the Aishihik Lake region.
11 - The crust in the Aishihik Lake region has been regionally tilted more than 5^{o} to the north. Tilting, and subsequent erosion, has resulted in the exposure of an approximately 10 km thick section of the crust. Deep structural levels are exposed near the south end of Aishihik Lake, and progressively shallower structural levels to the north.

V. METAMORPHIC PETROLOGY

5.1 Introduction

The Nisling Assemblage, a heterogeneous package of continental clastic, carbonate, and amphibolitic rocks, that crops out west of the Stikine terrane in southwest Yukon and northwest British Columbia (Figures 1.1 and 1.2), is regionally metamorphosed to upper greenschist to amphibolite grade (Tempelman-Kluit, 1976; Wheeler, 1961; Currie, 1991; Kindle, 1952; Muller, 1967; Way, 1977; Werner, 1977; 1978). Near Aishihik Lake in southwest Yukon metamorphism of the Nisling assemblage is indicated by the schistosity; the presence, in pelitic rocks, of aluminosilicate porphyroblasts including kyanite and sillimanite; and by horizons of amphibolite and marble (Erdmer, 1989; 1990; 1991; Gordey, 1973; Tempelman-Kluit, 1974).

The timing and tectonic significance of metamorphism is, however, poorly understood. Pre-Late Triassic metamorphism is indicated by: 1 - the truncation of metamorphic foliation by undeformed Late Triassic intrusions (Tempelman-Kluit, 1976); 2 - the incorporation of clasts of schistose rocks of the Nisling Assemblage in the Tally Ho Shear Zone, a strike slip fault thought to be active prior to 220 Ma (Hart and Radloff, 1990); 3 - unmetamorphosed sedimentary rocks which include Early Jurassic fossils and which unconformably overlap metamorphosed rocks of the Boundary Ranges Metamorphic Suite, thought to be at least in part correlative with the Nisling Assemblage (Mihalynuk and Rouse, 1988 a and b); and 4 - the incorporation of clasts of schist and gneiss similar to that of the Nisling Assemblage in unmetamorphosed sediments of the Late Triassic Stuhini Group (Currie, 1990). Regional metamorphism may also have occurred as recently as the Early Jurassic, and may have resulted from the intrusion of the Aishihik Batholith at 187.0 +9.7/-0.9 Ma (this study) as indicated by the regional decrease in metamorphic grade from amphibolite facies in the vicinity of the batholith, to greenschist facies along strike to the south (Tempelman-Kluit, 1974; Wheeler, 1961).

Because so little is known about the nature, timing, and tectonic significance of metamorphism of the Nisling Assemblage, it is difficult to determine the relationship of the assemblage with adjacent terranes. Tempelman-Kluit (1979) interpreted Nisling Assemblage as basement of the Stikine terrane. Hansen (1990) interprets the assemblage as part of the North American continental margin which is exposed in a window through the overlying accreted terranes. Mortensen (1992) has suggested that the Nisling Assemblage is correlative with the Yukon-Tanana terrane. Erdmer (1991) observed that the style and grade of metamorphism recorded in Nisling Assemblage is similar to that of the Kluane Schist and suggested that the two may be related.

This chapter reports on the metamorphic history of the Nisling Assemblage including an estimate of the pressure and temperature conditions of metamorphism. The timing and tectonic significance of metamorphism and possible terrane correlations of the Nisling Assemblage are examined in light of these data.

5.2 The distribution and morphology of metamorphic minerals and migmatite in pelitic rocks

The distribution of metamorphic indicator minerals is shown in Figures 5.1 a, b, and c, as are the locations of cross-sections included in Figure 5.2. Sample location coordinates and descriptions for each sample are listed in Appendices 5.1. and 5.2, respectively.

Mica

Mica occurs as medium-sized, anhedral grains that define a schistosity (S_2) which is evident throughout much of the study area and which parallels the contact with the Aishihik Batholith. In the hinges of folds of compositional banding mica occurs at an angle to compositional banding and defines an axial planar fabric (Plate 4.24). S_2 is defined by the parallel alignment of both biotite and muscovite. Within mica grains graphitic inclusion trails are locally evident, as are fine rutile needles. Euhedral zircon and tourmaline grains are also included within mica.

A second schistosity (S_1), defined by fine, anhedral biotite and muscovite grains, is locally evident. S_1 is preserved in a variety of habits including: 1 - within pelitic laminae, where it is characteristically folded and overgrown by foliation-parallel (S_2) mica. These folds are locally well preserved in strain shadows developed adjacent to garnet (Plate 5.1) and have S_2 as its axial planar fabric; 2 - as folded and variably oriented mica within quartz microlithons; 3 - within and adjacent to isolated fold hinges defined by discontinuous quartz horizons; and 4 - parallel to tightly folded compositional banding in micaceous quartzite.

Mica occurs in three other habits: 1 - Biotite overprints and grows at the expense of garnet. Both randomly oriented biotite and foliation subparallel biotite grains are observed, suggesting that garnet replacement occurred late in, and in part postdates, the foliation-forming event. Biotite is, however, affected by, and predates open folding of foliation; 2 - Within pelitic horizons S_2 is locally overgrown by fine-grained mica, usually muscovite, which is axial planar to open folds and crenulations of the main schistosity.

Figure 5.1 Detailed maps showing the distribution of map units, sample locations, the metamorphic mineral paragenesis for metapelitic samples characterized by porphyroblast development, and mineral isograds for each of: a) the South Aishihik Lake area; b) the North Aishihik Lake area; and c) the Upper Nisling River area. The location of these maps is shown in Figure 1.2. See text for explanation and discussion.

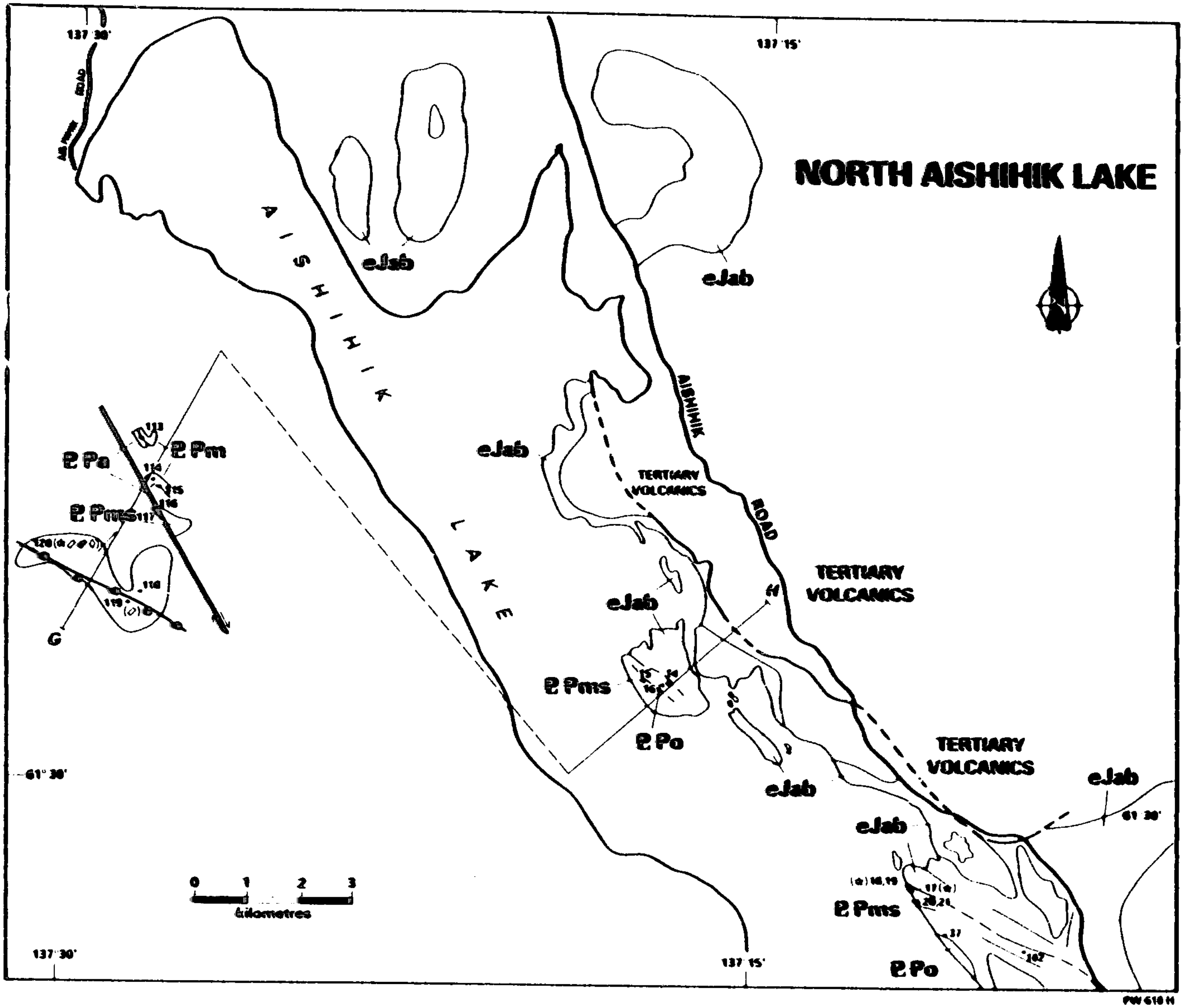
NORTH AISHIHIK LAKE
AISHIHIK LAKE
AISHIHIK ROAD
TERTIARY VOLCANICS
TERTIARY VOLCANICS
TERTIARY VOLCANICS
eJab
ЄPms
ЄPo
ЄPm
137°30'
137°15'
61°30'
kilometres
0 1 2 3
G
H
PW 610 H

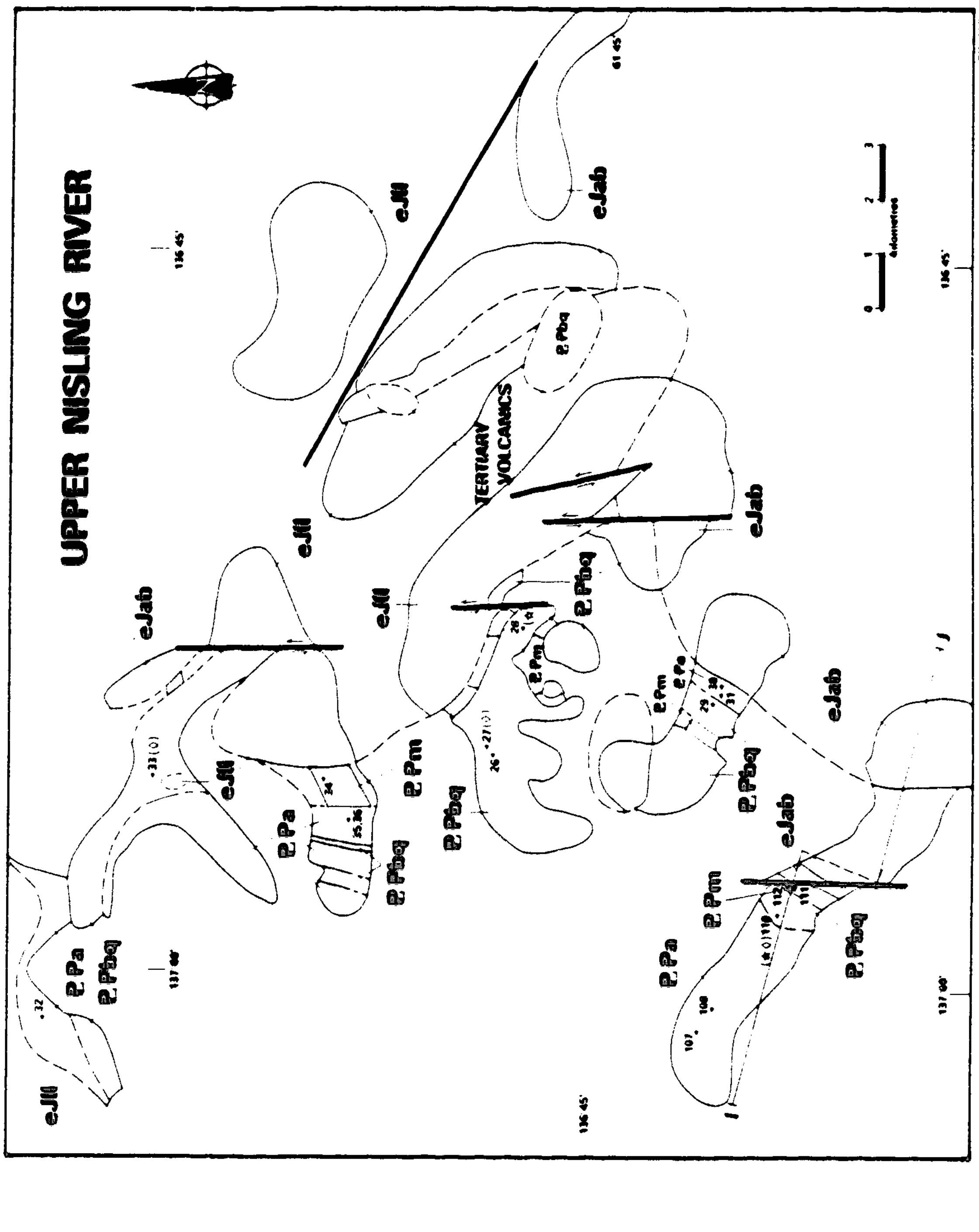
UPPER NISLING RIVER
TERTIARY VOLCANICS
eJab
eJll
P Pa
P Pbq
P Pm
136 45'
137 00'
61 45'
kilometres

LEGEND

PLUTONIC ROCKS

TERTIARY

T_{fp}

FELDSPAR PORPHYRY
heterogeneous igneous suite which includes plugs and small plutons of orange and pink weathering, flesh colored, miarolitic, massive, felspar and quartz - feldspar porphyry; and dykes of brown and dark green weathering, green to buff colored, feldspar and hornblende feldspar porphyry.

CRETACEOUS & TERTIARY

KT_{rr}

RUBY RANGE BATHOLITH
grey to tan weathering, grey to dark grey, medium to coarsely crystalline, massive to mildly foliated, hornblende and biotite hornblende diorite and granodiorite to nebulitic hornblende biotite granite.

EARLY JURASSIC

eJll

LONG LAKE PLUTONIC SUITE
orange weathering, orange and pink colored, coarsely crystalline to porphyritic, massive, miarolitic, quartz and biotite quartz monzonite.

STIKINE TERRANE

eJab

AISHIHIK BATHOLITH
grey to light grey weathering, grey to dark grey colored, coarsely crystalline, equigranular to K-feldspar megacrystic, hornblende and biotite hornblende granodiorite to quartz diorite. A foliation, defined by the alignment of mineral grains, is commonly developed. A second foliation, defined by protomylonitic, and gneissic banding, is locally developed and overprints the mineral foliation.

METAMORPHIC ROCKS

METAMORPHIC SYMBOLS

- ● Sample Location
- (★◊) Mineral Assemblage
- ★ Garnet
- ✦ Andalusite (M_2)
- ⊕ Andalusite (M_4)
- ◊ Staurolite
- ◆ Kyanite
- ◇ Sillimanite (M_2)
- ◎ Sillimanite (M_4)
- △ Cordierite (M_2)
- ◉ Cordierite (M_4)

ISOGRADS (M_2)

- Sillimanite In - Kyanite Out
- Staurolite Out
- Kyanite In

NISLING ASSEMBLAGE

DEVONO-MISSISSIPPIAN

P Po

ORTHOGNEISS
tan weathering, light grey colored, medium to coarsely crystalline, feldspar augan, muscovite and biotite muscovite orthogneiss; and dark grey weathering, dark grey colored, medium grained, hornblende and biotite hornblende diorite and quartz diorite orthogneiss.

- outcrop
- contact (defined, assumed)
- steeply dipping faults,
- displacement: unknown, strike-slip,
- dip-slip (U-up, D-down)
- cross section (A – B)
- road

PALEOZOIC & OLDER

P Pbq

BROWN QTZITE
dark to light brown weathering, brown to buff colored, medium to fine grained, locally graphitic, micaceous and feldspathic quartzite. Includes thin and discontinuous marble, amphibolite and micaschist lenses.

P Pm

MARBLE
light grey to light brown weathering, white to grey colored, fetid, coarsely crystalline, laminated calcite marble. Includes minor skarn, amphibolite, and calc-silicate

P Pa

AMPHIBOLITE
dark green to black weathering, green colored, fine to coarsely crystalline, gneissic to well foliated, hornblende and biotite hornblende quartzite, micaschist and marble, and significant amounts of pistachio green, epidote hornblende diopside calc-silicate

P Pms

MICASCHIST
Brown weathering, dark to light grey colored, medium to coarsely crystalline, well foliated to gneissic, migmatitic, muscovite biotite schist with minor grey quartz gneiss and brown weathering, tan colored, medium grained, foliated, micaceous & feldspathic quartzite. Includes minor amphibolite and marble.

Figure 5.2 Cross-sections, the locations of which are indicated on the maps in Figure 5.1. Symbols are defined in the legend to Figure 5.1. Marble is colored black; amphibolite is indicated by a striped pattern. The apparent dip of foliation is indicated. Sample locations and mineral isograds are also indicated.

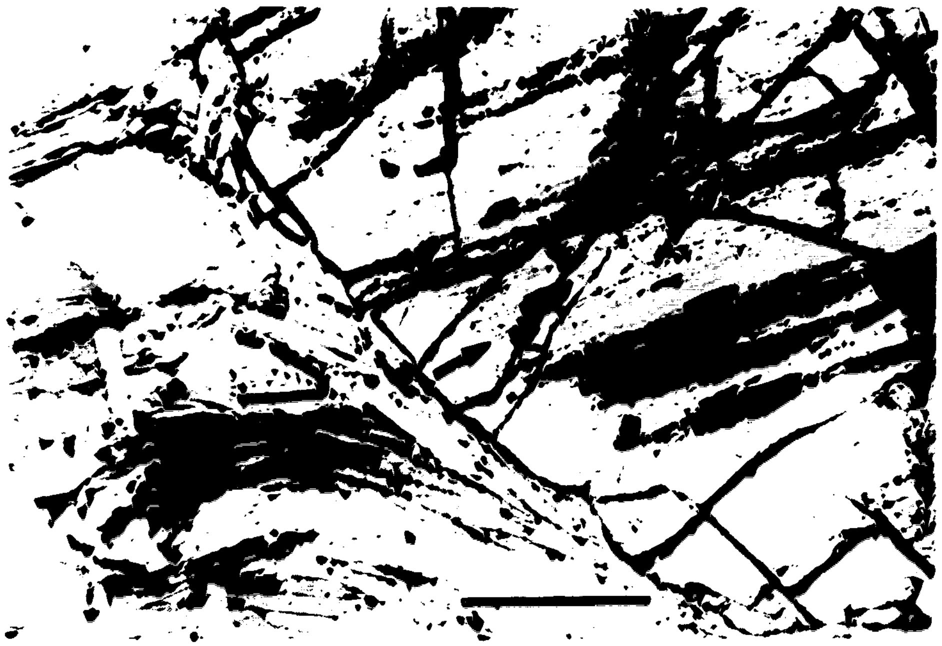

Plate 5.1 A photomicrograph, taken with plane polarized light, of a garnet porphyroblast hosted in micaschist (sample no. 79). The core of the garnet is characterized by a planar fabric (S_1) defined by numerous, fine graphite inclusions. The rim of the garnet is inclusion free. The arrow indicates the abrupt core - rim contact. To the left of the garnet, highlighted by a black line, are fine-grained micas which define a small, tight fold, thought to represent an F2 fold preserved in a pressure shadow adjacent to the garnet. The scale bar represents 250 um.

These mica define a weakly developed crenulation schistosity (S_3); 3 - In the southern part of the South Aishihik Lake area S_2 is locally overgrown by randomly oriented, anhedral to subhedral, fine- to medium-grained muscovite and biotite porphyroblasts. These mica are most abundant adjacent to the Ruby Range Batholith.

Migmatite

Migmatite, defined as schist hosting an aplitic phase, is common and is present throughout the study area. Aplite occurs as elongate lenses and boudins which extend along foliation, and which are 1 to 20 cm thick and up to 2 m in length. Aplite lenses increase in size and number towards the Aishihik Batholith, but are evident throughout the study area. Foliaform mica and compositional banding wraps about and, rarely is truncated against aplite lenses. Where aplite lenses are abundant, foliation is wavy and irregular, primarily as a result of pinching and swelling of aplite lenses (Plate 2.1). Thin (< 2 mm) fine-grained, aphanitic, mafic selvages which mantle aplite lenses are locally evident. Large aplite lenses locally exhibit an internal curviplanar fabric, defined by coarsely crystalline horizons characterized by abundant K-feldspar augen, which merge with and parallel foliation in the adjacent schist. Larger aplite lenses also locally display a textural asymmetry. The basal surfaces of these asymmetric lenses are planar and define a sharp contact with the adjacent schist. The upper surfaces are, however, diffuse and irregular (Plate 5.2). These 'cauliflower structures' (Burg, 1991) are interpreted as geopetal features that develope in response to the upward migration metamorphic fluid. Upward migration results from a density contrast between the relatively light metamorphic fluid and the relatively heavy melanosome and schist. The presence of cauliflower structures on the top surfaces of aplite lenses suggest that these rocks are, at present, the same way-up as they were during metamorphism and migmatization.

Veins of aplite and granite are also common. Aplite veins are associated with migmatite, locally root in aplite lenses, and trend both along and across foliation. Locally, in metapelitic schist which is interfoliated with thin amphibolite horizons, aplite veins exhibit an asymmetric geometry, preferentially developing along the underside of the thin amphibolite horizons (Plate 4.20). This asymmetric geometry is interpreted as a geopetal feature. Amphibolite horizons are thought to act as impermeable barriers that prevent the upward migration of relatively light metamorpnic fluids resulting in their along the undersides of the amphibolite horizons (Burg, 1991a; 1991b). This suggests that these rocks are currently the same way-up as they were during metamorphism and aplite vein development. Lenses of mildly foliated granite that root in migmatitic schist are locally evident close to the Aishihik Batholith. Elsewhere intrusions of massive granite truncate schistosity and include rafts of variably oriented schist.

Because aplite occurs as schistosity-parallel lenses and as boudins which are intimately interleaved with and wrapped by foliaform mica migmatite, it is interpreted to have developed contemporaneously with the development of the schistosity (S_2). Although some aplite and granite veins and intrusions are related to syn-schistosity migmatization, the presence of unfoliated granite which truncates the schistosity and which includes variably oriented schist rafts suggests at least one episode of post-schistosity granite intrusion. Unfoliated, cross-cutting granite intrusions are most abundant in the southern part of the South Aishihik Lake area adjacent to the intrusions of the Ruby Range Batholith and is inferred to be directly related to the Ruby Range Batholith (Figure 5.1 a).

Garnet

Garnet, though rare, is found throughout the study area, and occur as pink to dark red, subhedral to anhedral porphyroblasts <1 to 10 mm in diameter, and as fine, disseminated, anhedral grains which extend along the plane of schistosity. Subhedral "spongy" grains of garnet, which consist largely of inclusions within a garnet frame, are common (Plate 5.3). Garnet grains are usually located within pelitic horizons although they do occur in quartz and feldspar. Mica which lies within and defines S_2 wraps around garnet porphyroblasts (Plate 5.3). In almost all samples some replacement of garnet by biotite is evident (see above). Locally garnet porphyroblasts have been entirely replaced by biotite.

Garnets include grains of quartz, feldspar, mica (usually biotite), fine opaque material (thought to be graphite), and pyrite. Inclusions trails generally define a planar fabric that is tightly to isoclinally folded (Plate 4.26) and which is thought to represent an earlier fabric (S_1) which was deformed and subsequently overgrown by garnet. Garnets sometimes exhibit inclusion-free rims (Plate 5.1). Inclusion-free cores were also observed (Plate 5.4).

Garnets are interpreted to have nucleated and grown during the development of the S_2 schistosity as indicated by their preservation, in the form of inclusion trails of an older, deformed planar fabric (S_1) and by their relationship to mica which defines the S_2 schistosity. The presence of inclusion free rims and cores suggests that garnet growth may have resulted from several different reaction mechanisms and that garnet growth was episodic.

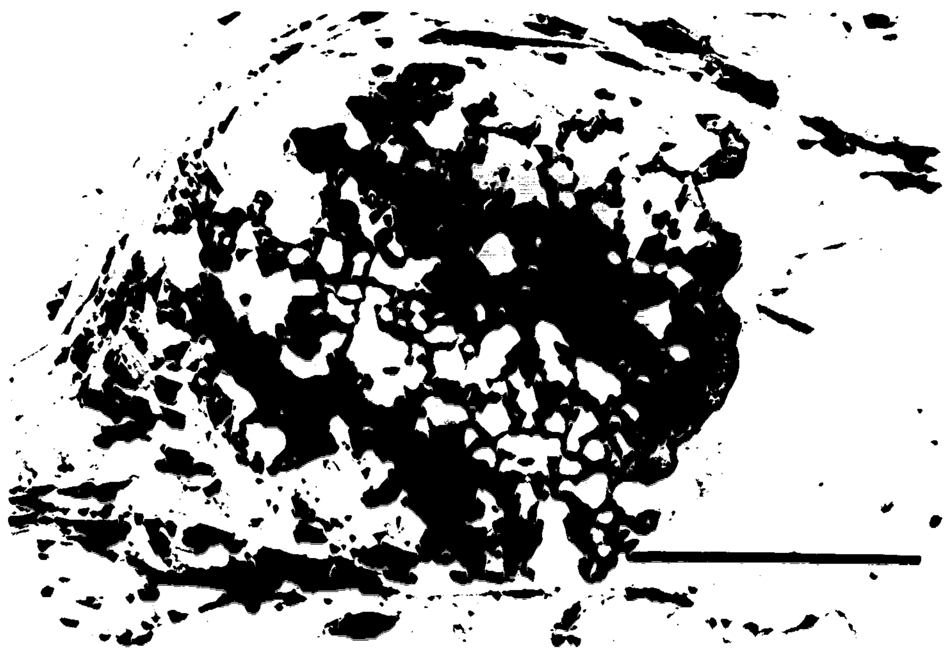

Plate 5.3 A photomicrograph, taken with plane polarized light, of an inclusion rich, spongy garnet in micaceous quartzite of the Nisling Assemblage (sample no. 93). Micas wrap around the garnet porphyroblast at upper left. The scale bar represents 1 mm.

Plate 5.4 A photomicrograph, taken with plane polarized light, of a garnet porphyroblast from a sample of garnet micaschist of the Nisling Assemblage (sample no. 91). The garnet core is characterized by coarse pyrite inclusions but is devoid of graphite inclusions. The outer part of the porphyroblast is characterized by abundant, fine graphite inclusions. The arrow indicates the abrupt core - rim contact. The scale bar represents 1 mm.

Sillimanite

Schistosity-parallel fibrolite and finely crystalline sillimanite occurs intimately intergrown with biotite, and, less commonly, surrounded by quartz and feldspar (Plate 4.24). Locally fibrolitic sillimanite defines thin (less than 1 mm in width) and continuous laminae which define aluminum rich-compositional bands (S_1) (Plate 4.28). The laminae outline tight to isoclinal folds characterized by narrow, angular hinge zones and with S_2 along their axial surface. Fibrolite needles lie parallel to the lamination. Near the fold hinges fibrolite needles bend gently towards the hinge and exhibit mild undulose extinction. Needles are not, however, continuous around the fold hinges. Fibrolite needles also lie parallel to the trace of the axial planar surfaces of the folds. Upright open folds which affect schistosity also affect sillimanite (Plate 5.5).

Sillimanite is restricted to a zone approximately 2 km thick, measured perpendicular to schistosity, which extends out from, and parallels both the contact with the Aishihik Batholith and the S_2 schistosity (Figures 5.1 and 5.2).

As sillimanite is intimately intergrown with foliaform biotite, defines a schistosity-parallel zone, and is most commonly oriented parallel with schistosity, it is interpreted to have developed contemporaneously with the development of schistosity (S_2). However, because sillimanite locally exhibits undulose extinction where it is associated with tight to isoclinally folded S_1 aluminous laminae, it may have, at least in part, developed early during the schistosity-forming event.

A second generation of sillimanite occurs in a variety of habits including: 1 - thin fibrolite veins which parallel and cut across schistosity (Plate 5.6); 2 - randomly oriented fibrolite needles which nucleate in muscovite and along grain boundaries in quartz and feldspar; 3 - fibrolitic clots which pseudomorph and replace staurolite and andalusite; and 4 - fine crystalline sillimanite which fringes and mantles andalusite porphyroblasts. Sillimanite of this variety is not affected by upright open folds of schistosity; clearly post-dates the development of schistosity; is restricted to the South Aishihik Lake area (Figure 5.1 a) and is most abundant adjacent to the Ruby Range Batholith.

Kyanite

Kyanite is evident in five samples and occurs as elongate subhedral to anhedral porphyroblasts 1 to 7 mm in length which are usually oriented subparallel with schistosity (Plate 5.7), and as fine anhedral grains. Kyanite porphyroblasts characteristically include quartz along cleavage planes. Opaque grains and euhedral tourmaline grains also occur as

Plate 5.5 A photomicrograph, taken with plane polarized light, of sillimanite (SIL) staurolite (ST) kyanite (KY) schist of the Nisling Assemblage (sample no. 120). A well defined synformal crenulation of schistosy that also affects sillimanite is apparent in the upper left corner of the photograph. The scale bar represents 250 um.

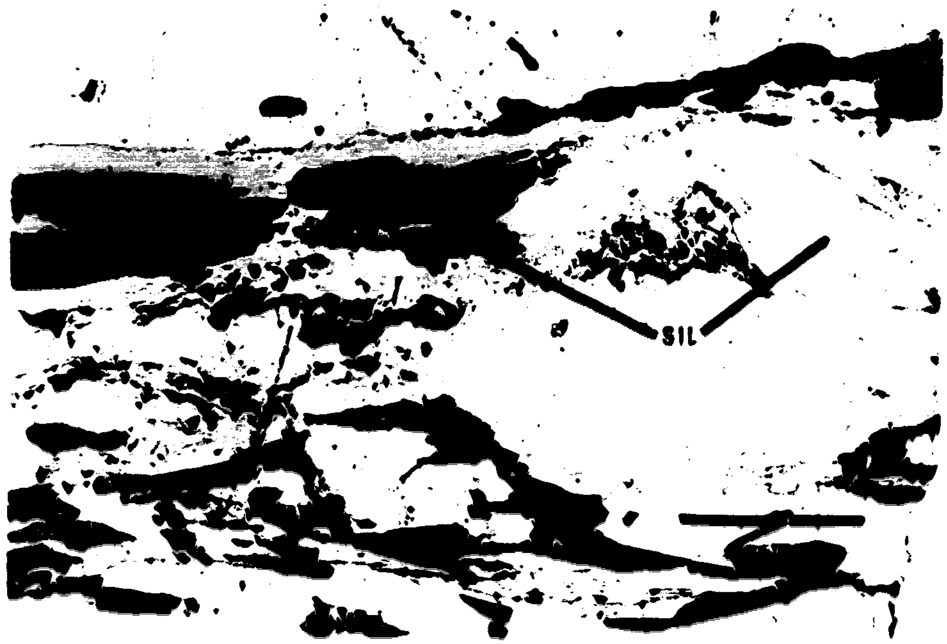

Plate 5.6 A photomicrograph, taken with plane polarized light, of micaceous orthogneiss of the Nisling Assemblage (sample no. 55). A fibrolite vein (SIL) cuts across foliation. Randomly oriented fibrolite needles root in the vein and grow out into the quartz feldspar matrix. The scale bar represents 250 um.

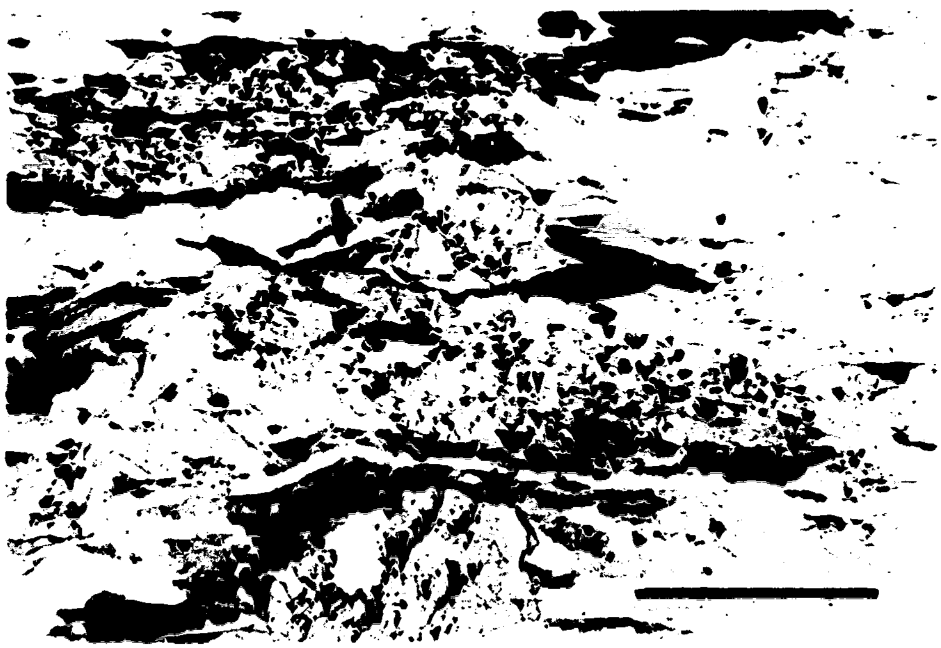

Plate 5.7 A photomicrograph, taken with plane polarized light, of garnet (GA) kyanite (KY) micaschist of the Nisling Assemblage (sample no. 48). The kyanite porphyroblasts lie along the plane of schistosity which parallels the top and bottom of the pho ›graph. The scale bar represents 1 mm.

inclusions. No deflection of schistosity around kyanite porphyroblasts is evident. Where kyanite porphyroblasts are developed adjacent to garnet they are rarely bent, together with foliaform mica, around the garnet. Locally kyanite grains are embayed by and appear to be overgrown and replaced by muscovite. Upright open folds which affect schistosity also affect kyanite (Plate 5.5). Kyanite grains locally exhibit undulose extinction and are visibly folded, rarely resulting in the development of kink bands.

Kyanite is restricted to a 1.5 to 2.5 km thick zone, measured perpendicular to schistosity, which extends the entire length of the Aishihik Lake (Figures 5.1 a, b; and 5.2). The kyanite zone is subparallel with schistosity and with the contact with the Aishihik Batholith, and lies west of and subparallel to the zone in which foliaform sillimanite is developed. In the southern part of the study area the contact between the kyanite and foliaform sillimanite zones is sharp and no overlap is evident. Samples 47 and 48 are located about 200 m apart, measured perpendicular to schistosity, and exhibit well developed fibrolitic sillimanite and kyanite porphyroblasts, respectively (Figure 5.2, cross-section A - B). At the north end of Aishihik Lake, however, some overlap of the kyanite and sillimanite zones exists. Sample no. 120 is characterized by coexisting stable fibrolitic sillimanite and kyanite porphyroblasts (Plate 5.5).

As kyanite coexists with foliaform sillimanite and garnet, as it defines a foliaform zone which trends subparallel with the sillimanite zone, and as it predates the development of upright folds of schistosity, it is interpreted to be contemporaneous with the development of schistosity (S_2).

Staurolite

Staurolite occurs as elongate, anhedral to subhedral porphyroblasts less than 5 mm in length. Staurolite rarely exhibits a branching habit extending both subparallel to, and at a high angle to the S_2 schistosity (Plate 4.27). It also occurs as sigmoidal porphyroblasts which merge with plane of schistosity. Fine opaque inclusions, thought to be graphite, define a planar fabric (S_1) which is tight to isoclinally folded. Staurolite also includes tourmaline grains. Foliaform mica usually exhibits some mild deflection around staurolite porphyroblasts. Open folds of schistosity also affect staurolite grains (Plate 5.5).

Staurolite occurs in an elongate zone which, like the kyanite zone, extends the length of the Aishihik Lake and parallels both schistosity and the contact with the Aishihik Batholith (Figures 5.1 a, b; and 5.2). The staurolite zone lies west of and overlaps with the kyanite zone. Two samples, one collected at the south end of the South Aishihik Lake area (no. 96) and one collected near the north end of Aishihik Lake (no. 120), are characterized by coexisting staurolite and kyanite. Sample no. 8, in which staurolite is present, was collected about 500 m, measured perpendicular to schistosity, east of sample no. 79, in which kyanite is present, suggesting that the zone of kyanite - staurolite overlap is at least 500 m thick. Sample no. 120, collected in the North Aishihik Lake area (Figure 5.1 b), also contains sillimanite (see above) (Plate 5.5), indicating that, in the North Aishihik Lake area the staurolite zone overlaps with the sillimanite zone. In the south end of the study area the staurolite and sillimanite zones are about 1.5 km apart, measured perpendicular to schistosity. The staurolite zone appears to extend west outside the limit of the study area and is thought to be at least 2 km thick.

As staurolite occurs as porphyroblasts which extend along and preserve an older, deformed fabric (S_1); as schistosity is mildly deflected by staurolite porphyroblasts; as open folds which affect schistosity also affect staurolite grains; and as the zone of staurolite stability extends subparallel to, and overlaps with the kyanite and sillimanite zones; staurolite is interpreted to have developed contemporaneously with the development of schistosity (S_2).

Andalusite

Andalusite occurs as subhedral chiastolitic porphyroblasts 3 - 7 mm in length that extend subparallel to schistosity and include quartz and opaque grains (Plate 5.8). Under crossed polars andalusite porphyroblasts have a felted appearance, consisting of individual "leaves" that extend subparallel to the long axis of the grains. Some deflection of foliaform mica around andalusite porphyroblasts is usually evident. Andalusite also mantles staurolite porphyroblasts. Andalusite appears to postdate and grow at the expense of staurolite as indicated by the presence of isolated, optically continuous staurolite grains within andalusite porphyroblasts (Plate 5.9). Andalusite mantles extend parallel with the long axes of enclosed staurolite grains and are locally sigmoidal, and merge with schistosity. Some deflection of foliaform mica around these composite porphyroblasts is usually evident. Open upright folds affect schistosity in andalusite-bearing rocks, although it is not possible to point to a folded andalusite grain. However, foliaform andalusite porphyroblasts are evident on the planar limbs of open folds of schistosity suggesting that andalusite developed prior to folding.

The area over which andalusite is present is coincident with the staurolite zone (Figure 5.1 a). Both staurolite-mantling andalusite and andalusite porphyroblasts (some of which may represent staurolite porphyroblasts which have been totally replaced by andalusite) are inferred to have developed late in the development of schistosity. This is

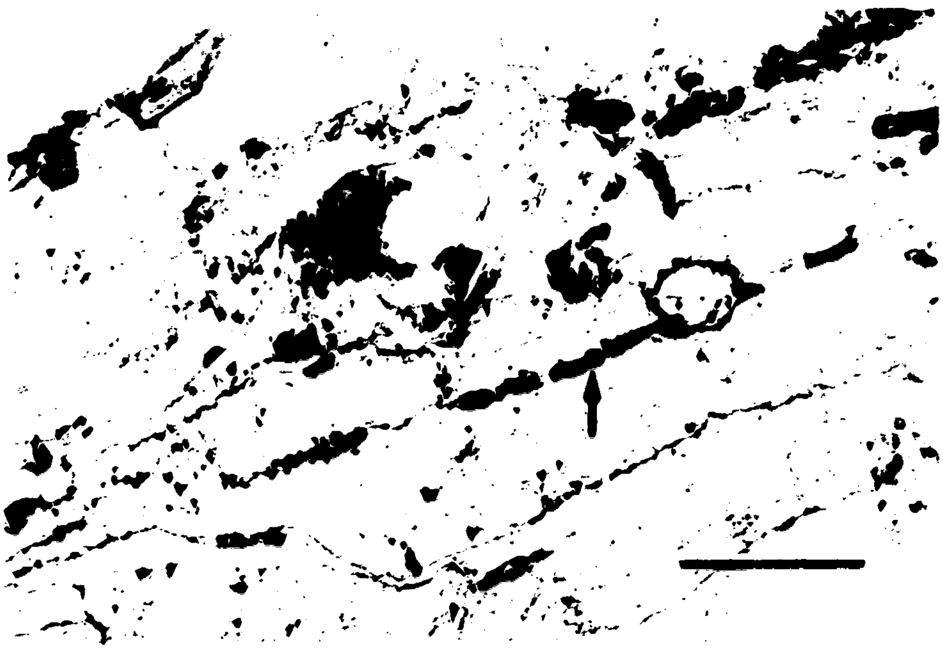

Plate 5.8 A photomicrograph, taken with plane polarized light, of andalusite schist of the Nisling Assemblage (sample no. 43). The arrow indicates the medial inclusion train in a chiastolitic andalusite porphyroblast. The scale bar represents 250 um.

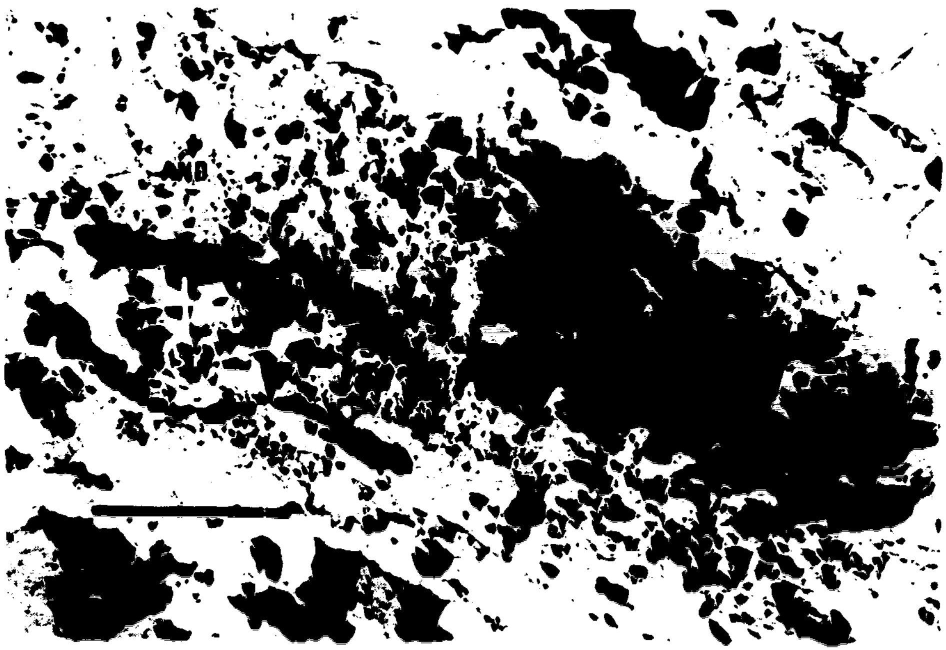

Plate 5.9 A photomicrograph, taken with crossed nicols, of andalusite (AND) staurolite (ST) schist of the Nisling Assemblage (sample no. 8). The andalusite mantles and encloses optically continuous staurolite grains. The scale bar represents 250 um.

consistent with the alignment of andalusite porphyroblasts along schistosity, with the foliaform geometry of andalusite mantles, with the mild deflection of foliaform mica around both andalusite porphyroblasts and mantles, with the parallelism and overlap of the andalusite zone with the staurolite zone, and with the development of andalusite prior to open folding of schistosity. However, andalusite developed after, and grew at the expense of staurolite.

Andalusite also occurs as subhedral to euhedral (square in cross-section) grains, <<1 to 10 mm in diameter, that preferentially nucleate on and grow at the expense of biotite, and that grow across and disrupt foliaform mica (Plate 5.10). This variety of andalusite also includes and grows at the expense of kyanite, garnet, and staurolite. Under crossed polars a few of the larger andalusite porphyroblasts have a felted appearance, consisting of individual "leaves" that radiate out from nucleation points and grain boundaries. Andalusite grows across and postdates open folds of schistosity.

Andalusite of this variety clearly post-dates the development of the S_2 schistosity. It is only observed in a thin zone immediately adjacent to intrusions of the Ruby Range Batholith.

Cordierite

Cordierite occurrence mimics that of andalusite. Cordierite occurs both as small (<5 mm in diameter) porphyroblasts which include graphite and mica grains and which is characterized by intersecting sets of multiple lamellar twins and by yellow, pinitic alteration (Plate 5.11). Inclusions define a planar fabric oriented at a slight angle to schistosity. Some mild deflection of foliaform mica around cordierite porphyroblasts is usually evident. Cordierite also occurs as a thin (<2 mm thick) mantle on foliaform mica and around garnet, kyanite, staurolite, andalusite, and andalusite-mantled staurolite porphyroblasts. Like the andalusite mantles, cordierite mantles extend parallel with the long axes of enclosed porphyroblasts, are characterized by a sigmoidal geometry, and merge with schistosity. Open upright folds affect schistosity in cordierite-bearing rocks, although it is not possible to point to a folded cordierite grain. However, foliaform cordierite porphyroblasts are evident on the planar limbs of open folds of schistosity suggesting that cordierite developed prior to folding.

The area over which cordierite is present is coincident with the andalusite zone (Figure 5.1 a). Both cordierite mantles and cordierite porphyroblasts are inferred to have developed late in the development of schistosity. This is consistent with the inclusion of a planar fabric, defined by graphite and mica grains, oriented at a slight angle to schistosity,

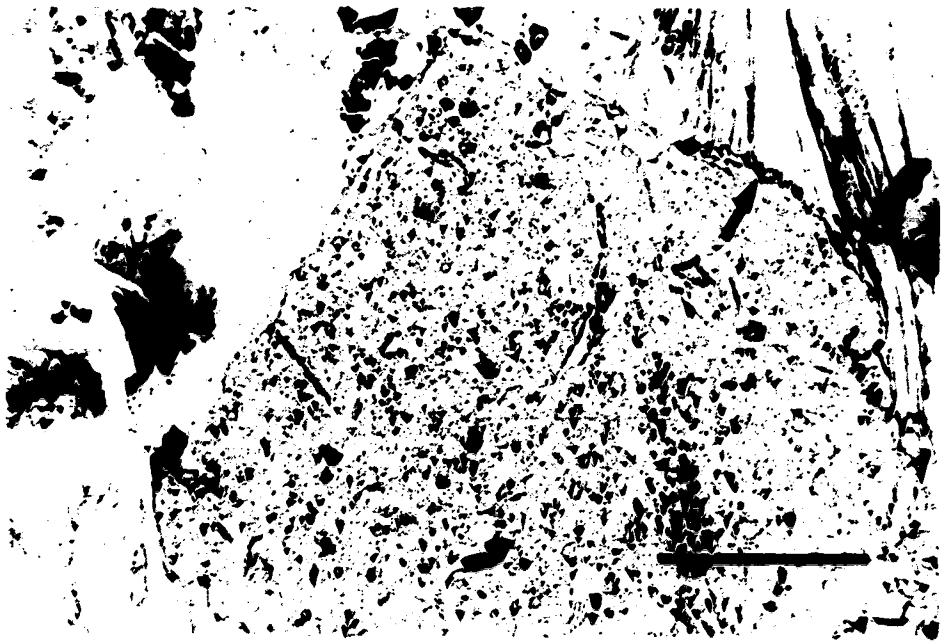

Plate 5.10 A photomicrograph, taken with plane polarized light, of andalusite micaschist of the Nisling Assemblage (sample no. 97). The arrow indicates where a euhedral (square outline) andalusite porphyroblast has overgrown and truncated schistosity parallel mica. The scale bar represents 250 um.

Plate 5.11 A photomicrograph, taken with plane polarized light, of cordierite micaschist of the Nisling Assemblage (sample no. 8). The arrow indicates the abrupt contact between the core, characterized by abundant fine graphite inclusions, and the inclusion free rim, of a cordierite porphyroblast. The scale bar represents 250 um.

and with the similarity between cordierite and andalusite morphology and distribution.

Cordierite also occurs as round, anhedral, inclusion free grains that most commonly occur in aggregates of 5 to 10 grains and that exhibit yellow pinitic alteration (Plate 5.12). Locally cordierite is altered to a yellow-brown, amorphous, isotropic substance (pinnite). Cordierite nucleates on and grows across both micaceous and quartzofeldspathic laminae.

Cordierite of this variety post-dates the development of the S_2 schistosity. Like post-schistosity andalusite, cordierite of this variety is only observed in a thin zone immediately adjacent to intrusions of the Ruby Range Batholith.

Feldspar

Potassium and plagioclase feldspar are present throughout the study area. Plagioclase occurs as anhedral to subhedral grains that are intimately intergrown with quartz and K-feldspar and which are locally characterized by curviplanar inclusion trails, consisting of quartz and graphite particles, oriented at a high angle to schistosity. Plagioclase also occurs as subhedral to euhedral porphyroblasts which extend along schistosity, and which include quartz grains and foliaform mica. Quartz lamella accounting for 35% of individual grains, is locally evident. K-feldspar occurs as anhedral to subhedral grains intimately intergrown with plagioclase and quartz and as subhedral porphyroblasts. K-feldspar porphyroblasts extend along schistosity, include quartz grains and foliaform mica, and locally are cored by plagioclase porphyroblasts with quartz exsolution features (Plate 5.13). Upright open folds which affect schistosity also affect plagioclase and K-feldspar grains.

Feldspar development spans the entire schistosity-forming event as indicated by; the preservation of an earlier developed schistosity (S_1) in plagioclase grains; the inclusion of foliaform mica (S_2) in both plagioclase and K-feldspar grains; and by the schistosity-parallel alignment of feldspar porphyroblasts. K-feldspar porphyroblasts are cored by plagioclase porphyroblasts, include mica which parallels the S_2 schistosity, and probably developed late relative to the peak metamorphic paragenesis.

Sericite - Chlorite

Minor sericitic alteration of feldspar is evident throughout the study area. Significant alteration, characterized by the development of dense mats of randomly oriented, anhedral muscovite and sericite grains that preferentially overgrow and replace aluminosilicate porphyroblasts, including kyanite, staurolite, and andalusite (Plate 5.14), is

Plate 5.12 A photomicrograph, taken with plane polarized light, of cordierite (CD) micaschist of the Nisling Assemblage (sample no. 42). A cordierite porphyroblast, at center, consists of an agregate of anhedral, inclusion free grains that overgrow and replace schistosity-parallel biotite. The scale bar represents 250 um.

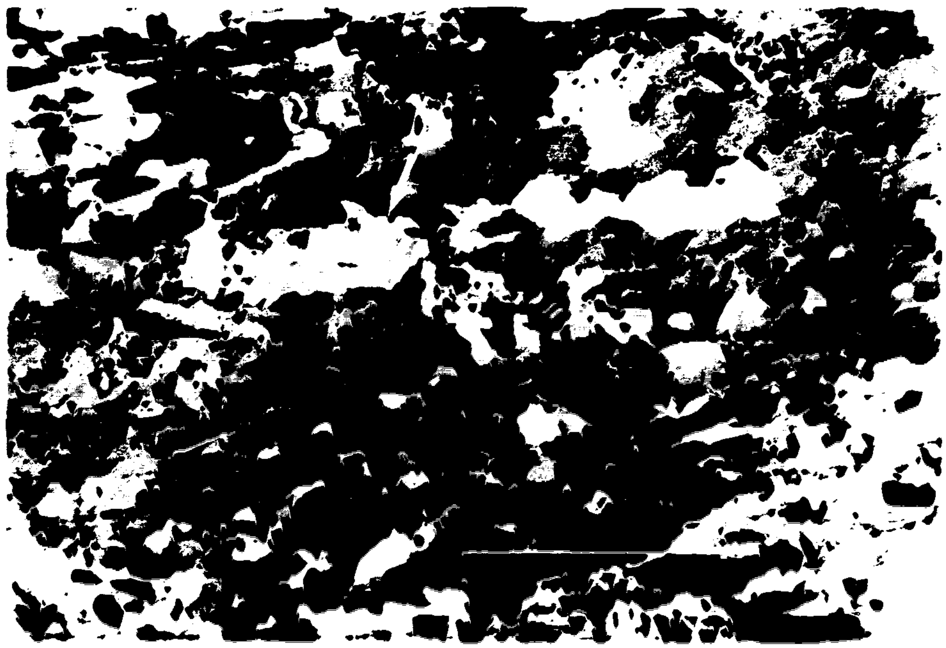

Plate 5.13 A photomicrograph, taken with crossed nicols, of micaschist of the Nisling Assemblage (sample no. 42). A large inclusions rich K-feldspar porphyroblast occupies much of the field of view. Both the feldspar grain and the inclusions are oriented parallel to the enclosing schistosity. Inclusions include opaque grains, mica, quartz lenses, and (indicated by the arrow) a plagioclase grain that is characterized by quartz lamella. The scale bar represents 1 mm.

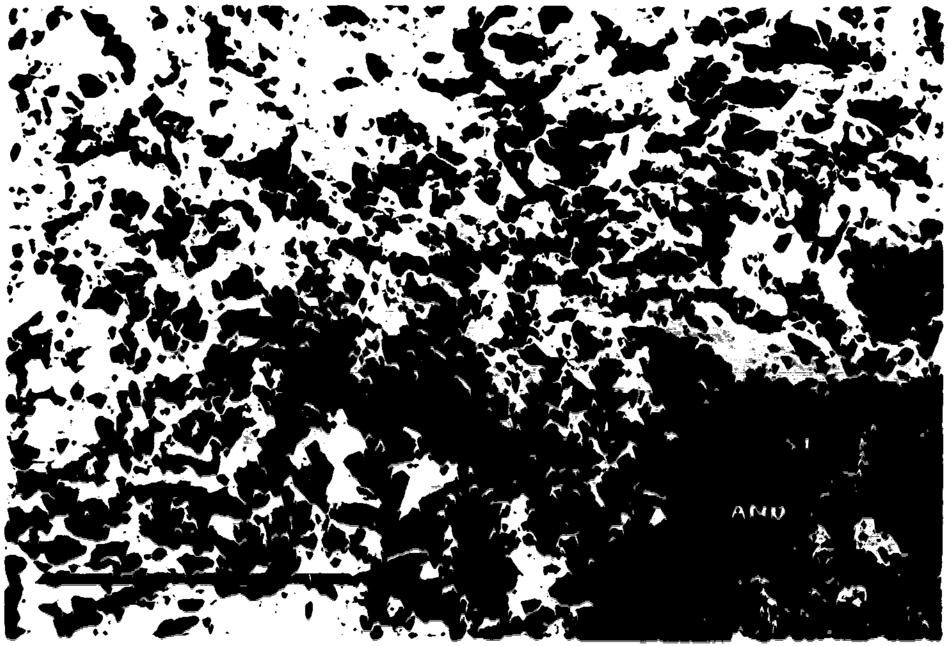

Plate 5.14 A photomicrograph, taken with crossed nicols, of sericitized andalusite (AND) staurolite (ST) micaschist of the Nisling Assemblage (sample no. 5). Intense sericitization has resulted in the almost total replacement of a composite andalusite - staurolite porphyroblast, some of which is evident at lower right, by fine-grained, randomly oriented, mica. The scale bar represents 1 mm.

only observed in the South Aishihik Lake area (Figure 5.1 a) adjacent to the Ruby Range Batholith. Sericitic alteration postdates and is not affected by open folds of schistosity.

Chlorite is widely distributed in the study area and occurs as randomly oriented anhedral to subhedral grains and preferentially replaces mica and garnet. Chlorite is also present along fractures and locally overgrows and totally replaces schistosity. Chlorite grains postdate and are not affected by open folds of schistosity.

Like sericite, chlorite alteration is most significant in the southern part of the study area adjacent to the Ruby Range Batholith.

5.3 Mineral isograds

Textural relationships and the areal distribution of metamorphic indicator minerals (Figure 5.1 a, b, and c) suggests that rocks of the Nisling Assemblage have been subjected to four metamorphic events (Figure 5.3). Evidence of the earliest metamorphic event (M_1) consists of a locally preserved micaceous schistosity (S_1) that has been deformed and overgrown during subsequent tectonism. This early schistosity is also preserved as inclusion trails in various porphyroblasts including mica, garnet, staurolite, and plagioclase. Staurolite porphyroblasts exhibit a branching habit that mimics an earlier developed schistosity.

Most metamorphic minerals, including mica (which defines a schistosity - S_2 - evident throughout the study area), garnet, sillimanite, kyanite, staurolite, andalusite, and cordierite, postdate and overprint S_1, and record a younger metamorphic event, M_2 (Figure 5.3). Significant amounts of migmatite developed during this event. The distribution of sillimanite, kyanite, and staurolite define a series of isograd-bound metamorphic zones (Figure 5.1). Isograds are well defined in the South Aishihik Lake area and are more loosely defined to the north. In the Upper Nisling River area (Figure 5.1 c) only sillimanite was observed. West of the Aishihik Batholith sillimanite (in), kyanite (out and in), and staurolite (out) isograds are oriented sub-parallel with the S_2 schistosity and with the contact with the Aishihik Batholith, and dip east beneath the batholith (Figure 5.2). Mineral isograds truncate to the south against the Ruby Range Batholith. The regional distribution of M_2 isograds and metamorphic zones is shown in Figure 5.4, a map of the study area. Andalusite and cordierite post-date peak M_2 metamorphism and cannot be used to define isograds. This is discussed further below.

Of the four metamorphic events, M_3 is the least significant. During folding and crenulation of the S_2 schistosity small mica grains (mostly muscovite) nucleated and grew subparallel with the axial planes of the crenulations. S_3 mica are rare and are not

Figure 5.3 The relative timing of metamorphic mineral nucleation and growth. Four metamorphic events are recognized. See text for discussion. Ga - garnet; Bi - biotite; St - staurolite; Ad - andalusite.

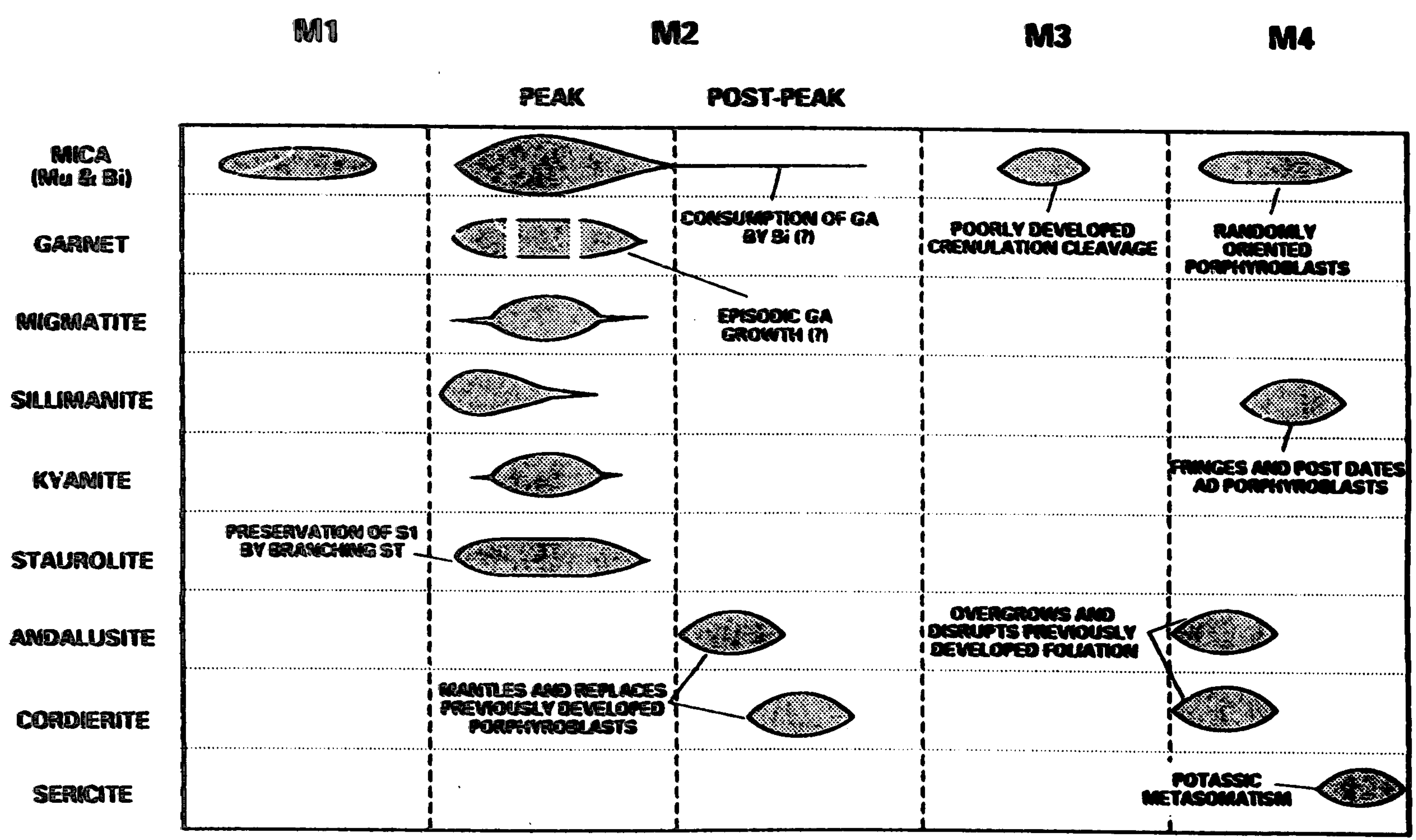

M1
M2
M3
M4
PEAK
POST-PEAK
MICA (Mu & Bi)
GARNET
MIGMATITE
SILLIMANITE
KYANITE
STAUROLITE
ANDALUSITE
CORDIERITE
SERICITE
CONSUMPTION OF GA BY Bi (?)
EPISODIC GA GROWTH (?)
PRESERVATION OF S1 BY BRANCHING ST
MANTLES AND REPLACES PREVIOUSLY DEVELOPED PORPHYROBLASTS
POORLY DEVELOPED CRENULATION CLEAVAGE
OVERGROWS AND DISRUPTS PREVIOUSLY DEVELOPED FOLIATION
RANDOMLY ORIENTED PORPHYROBLASTS
FRINGES AND POST DATES AD PORPHYROBLASTS
POTASSIC METASOMATISM

Figure 5.4 A map of the Aishihik Lake area showing the distribution of isograd-bound metamorphic mineral zones that reflect the peak M_2 metamorphic mineral paragenesis. Map units follow from Figure 1.2. Sil - sillimanite; Ky - kyanite; St - staurolite.

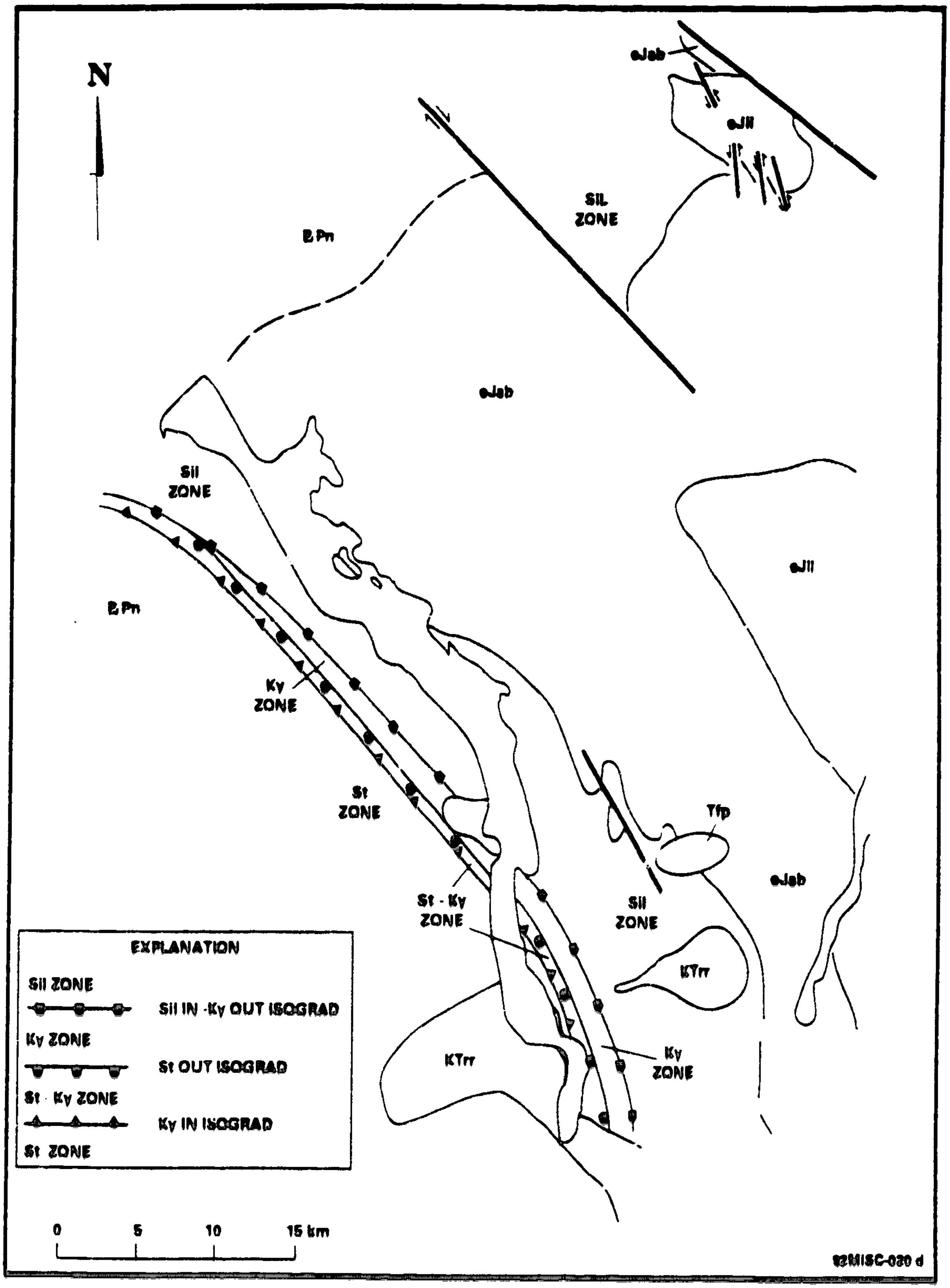
N
eJab
eJll
SIL
ZONE
Ɇ Pn
eJab
Sil
ZONE
eJll
Ɇ Pn
Ky
ZONE
St
ZONE
Tfp
eJab
St - Ky
ZONE
Sil
ZONE
KTrr
KTrr
Ky
ZONE
EXPLANATION
Sil ZONE
Sil IN -Ky OUT ISOGRAD
Ky ZONE
St OUT ISOGRAD
St - Ky ZONE
Ky IN ISOGRAD
St ZONE
0
5
10
15 km
92MISC-030 d

associated with the development of any other metamorphic porphyroblasts.

Metamorphic minerals attributable to the most recent metamorphic event, M_4, including mica, andalusite, cordierite and sillimanite, overprint all previously developed metamorphic mineral parageneses. Discordant sillimanite is evident across much of the South Aishihik Lake area. Andalusite and cordierite are evident immediately adjacent to intrusions of the Ruby Range Batholith (Figure 5.1 a).

5.4 Estimate of metamorphic conditions

5.4.1 Petrogenetic relations

Metamorphic mineral assemblages and mineral textures in pelitic rocks can be used to provide an estimate of peak metamorphic conditions. This analysis makes use of the calibrated petrogenetic grid of Spear and Cheney (1989). Too little of the M_1 metamorphic parageneses is preserved to allow any quantitative analysis of the M_1 metamorphic event. The presence of a micaceous schistosity suggests that M_1 metamorphism was characterized by, at the very least, greenschist facies conditions.

The M_2 metamorphic mineral paragenesis is divisible into a series of isograd-bound metamorphic zones. The isograds, which are based upon continuous and discontinuous reactions, and characteristic mineral assemblages for each zone, are shown in Table 5.1. Petrogenetic relationships are summarized in Figure 5.5, a petrogenetic grid. Metamorphism is restricted to pressures of 7.5 kbars; the minimum pressure at which staurolite breaksdown and is replaced by kyanite. Pressure may decrease to the north as indicated by the coexistence of staurolite, kyanite, and sillimanite in sample no. 120 from the North Aishihik Lake area (Figure 5.1 b). Temperatures are restricted to a minimum of 600 ^{o}C by the widespread occurrence of migmatite (assumes that boron, which can cause a significant decrease in temperature of the west solidus, was not present in significant quartities). Temperatures range from 600 ^{o}C to 650 ^{o}C in the staurolite zone; 650 ^{o}C to 680 ^{o}C in the zone of staurolite - kyanite coexistence; 680 ^{o}C to 720 ^{o}C in the kyanite zone; and greater than 720 ^{o}C in the sillimanite zone. These mineral zones dip east beneath the batholith and define a hot side up metamorphic sequence - the highest grade rocks (sillimanite zone) are present at the shallowest structural levels (immediately beneath the batholith) while lower grade rocks (the kyanite and staurolite zone, respectively) are present at deeper structural levels away from the batholith (Figure 5.2).

The mantling of staurolite by andalusite and cordierite and the presence of andalusite and cordierite porphyroblasts in the staurolite zone presents a significant dilemma. The andalusite - cordierite paragenesis suggests temperatures of between 550

TABLE 5.1. Characteristic mineral paragenesis for M2 mineral zones.
See text for discussion.

Zone	Bounding isograds and/or related mineral equilibria
M_2 peak metamorphic mineral paragenesis	
1) Sillimanite zone	
	Kyanite out - sillimanite in isograd reflecting the discontinuous equilibria KY = SIL
2) Kyanite zone	
	Staurolite out isograd reflecting the discontinuous equilibria ST + QT = KY + BI + H_2O
3) Kyanite - Staurolite zone	
	Kyanite in isograd reflecting the continuous equilibria represented by shifting of the ST - GA - ALSI sub-triangle to the right on a Thompson projection
4) Staurolite zone	
Note that migmatite, quartz, biotite, muscovite, feldspar, and garnet are present throughout each of these zones.	
M_2 post-peak metamorphic mineral paragenesis	
5) Andalusite - Cordierite zone	
	AD reflects the continuous equilibria represented by shifting of the ST - GA - ALSI sub-triangle to the right on a Thompson projection. CD reflects the continuous equilibria represented by shifting of the BI - CD - ALSI subtriangle to the left on a Thompson projection.

TABLE 5.1. (continued)

Zone	Bounding isograds and/or related mineral equilibria
M_4 metamorphism	
6) Sillimanite zone	
	Reflects the discontinuous equilibria $MU + QT = SIL + KF + H_2O$
7) Andalusite - Cordierite zone	
	Continuous reactions (?) reflecting breakdown of the pre-existing metamorphic mineral paragenesis

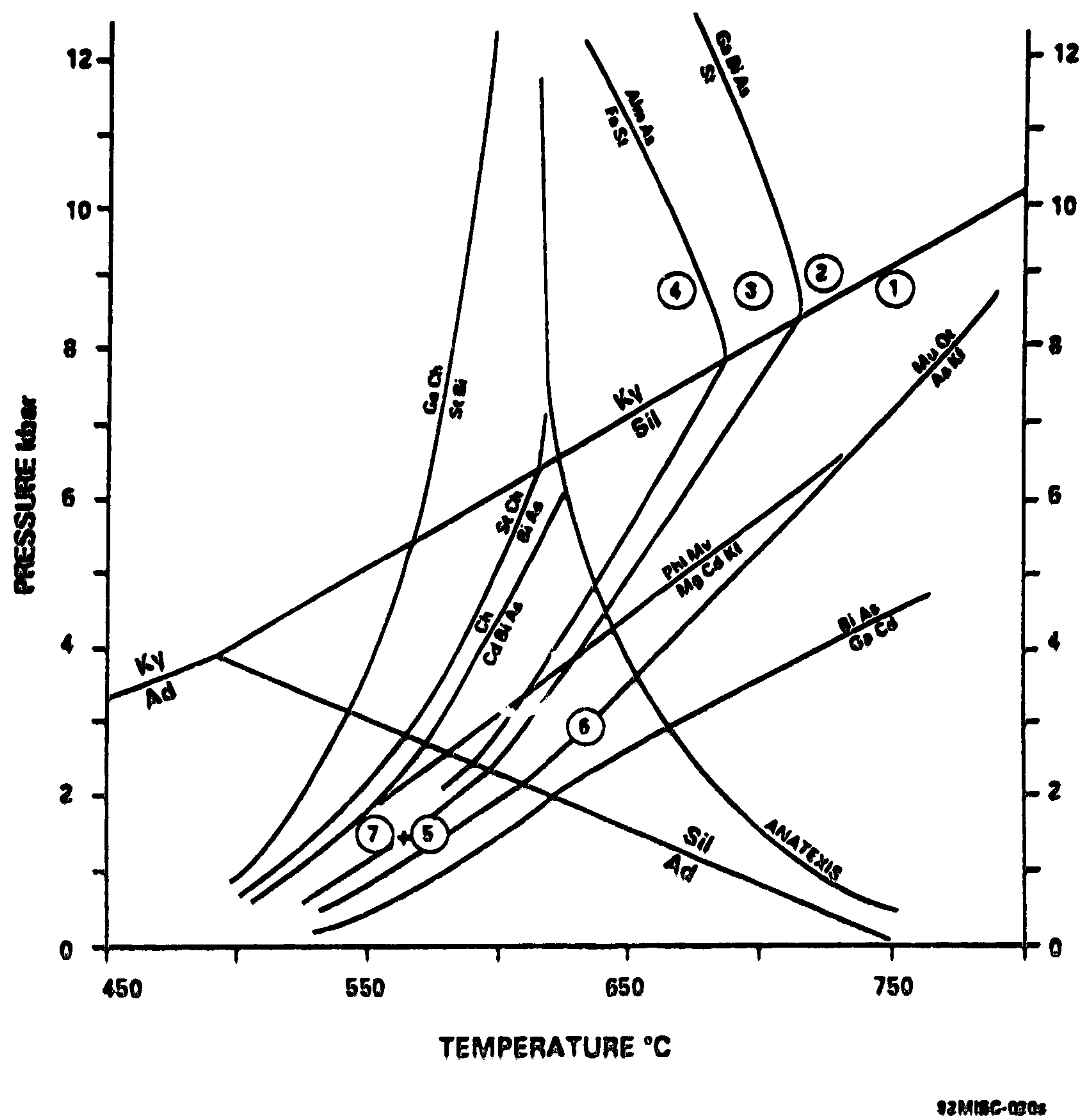

Figure 5.5 A calibrated petrogenetic Pressure - Temperature grid after Spear and Cheney (1989) showing metamorphic reactions in metapelitic rocks of the Nisling Assemblage. The numbers refer to metamorphic zones as defined in Table 5.1. Alm - almandine garnet; As - Aluminosilicate (And - andalusite; Ky - kyanite; Sil - sillimanite); Bi - biotite; Cd - cordierite (MgCd - Magnesium end member cordierite); Ch - chlorite; Kf - potassium feldspar; Mu - muscovite; Phl - phlogopite; Qt - quartz; St - staurolite (FeSt - iron end member staurolite).

^{o}C and 600 ^{o}C and pressures of 2 kbar or less, and point to a significant change in metamorphic conditions relative to the pressures indicated by the peak metamorphic mineral paragenesis. This calls into question the interpretation of andalusite and cordierite as having developed late during the M_2 metamorphic event. This will be further discussed later in this chapter.

The nucleation of a negligible number of mica grains, and the lack of the nucleation of any other porphyroblasts during the M_3 metamorphic event suggests that M_3 metamorphism was characterized by sub-greenschist temperatures and by relatively low pressures.

The metamorphic mineral paragenesis that developed in response to M_4 metamorphism are consistent with a thermal metamorphic event. The development of narrow andalusite and cordierite aureoles, present immediately adjacent to intrusions of the Ruby Range Batholith, restricts pressure to 2 kbar or less. The widespread development of sillimanite indicates that peak temperatures exceeded 550 ^{o}C.

5.4.2 Geothermometry and geobarometry

Methods

Analyses of grains of garnet, biotite, and plagioclase, thought to represent part of the M_2 mineral paragenesis, were obtained using an eight-channel ARL SEMQ electron microprobe at the University of Calgary (operating conditions are described in Nichols and Stout, 1988), using silicate standards. Characteristic mineral assemblages for samples used in geothermobarometry studies are shown in Table 5.2. Data reduction, using the method of Bence and Albee (1968), was accomplished using online computer programs modified from Nicholls *et al.*(1977). Analytical data are shown in Table 5.3.

Mineral Chemistry

garnet - All analyzed garnets are almandine rich and exhibit an increase in grossular content in grain cores. Almandine content increases from core to rim in garnets obtained from samples collected in the foliaform sillimanite zone. Most samples show some spessartine enrichment in the rims suggesting some retrogressive re-equilibration of garnets with matrix minerals.

biotite - Mild zonation is evident in most of the analyzed biotite grains. All but one of the biotite grains analyzed are characterized by a phlogopite enriched core relative to rim compositions. This is consistent with retrogressive enrichment of biotite in Fe.

plagioclase - Analyzed plagioclase grains range from 65 mole% to 80 mole% albite

Table 5.2. Characteristic mineral assemblage for samples used in geothermobarometry studies.

SAMPLE	QT	PL	KF	BI	MU	GT	AS	ST	OP[a]	AM	EP	CA	CL[b]	SC[b]
48	x	x	x	x	x	x	KY	-	x	-	-	-	x	x
77	x	x	x	x	x	x	SI	-	x	-	-	-	x	-
79	x	x	x	x	x	x	KY	-	x	-	-	-	x	-
81	x	x	x	x	x	x	-	-	x	-	-	-	x	x
91	x	x	x	x	x	x	-	-	x	-	-	-	x	x
93	x	x	x	x	x	x	SI	-	x	-	-	-	x	x
101	x	x	x	x	x	x	SI,AD[c]	x	x	-	-	x	x	
104	x	x	x	x	x	x	SI	-	x	-	-	-	x	x
110	x	x	x	x	x	x	SI	-	x	-	-	-	x	x
120	x	x	x	x	x	x	SI,KY	x	x	-	-	-	x	x

Notes:

x - present in the sample. Mineral abbreviations QT - quartz, PL - plagioclase, KF - potassium feldspar, BI - biotite, MU - muscovite, GT - garnet, AS - aluminosilicate, ST - staurolite, OP - opaques, AM - amphibolite, EP - epidote, CC - calcite, CL - chlorite, SC - sericite, KY - kyanite, SI - sillimanite, AD - andalusite.

a - opaque minerals include graphite, pyrite, and ilmenite.

b - both chlorite and sericite are retrogressive phases.

c - andalusite postdates, and is not part of, the peak metamorphic mineral paragenesis. See text for discussion.

Table 5.3. Data used in the calculation of paleotemperatures and paleopressures.

Sample[a]	garnet			biotite				garnet			plagioclase				AS[b]
	Mg	Fe	Fe/(Mg+Fe)	Mg	Fe	Fe/(Mg+Fe)	K_t	Ca	Mn	X_{Ca}	Ca	Na	K	X_{Ca}	
48-C	0.34	4.68	0.93	2.04	3.04	0.60	-2.22	1.12	0.06	0.18	0.99	2.01	0.03	0.33	KY
48-R	0.52	4.74	0.90	2.00	3.13	0.61	-1.76	0.86	0.12	0.14	1.02	1.98	0.03	0.34	KY
77-C	0.84	4.32	0.84	1.96	2.80	0.59	-1.29	0.34	0.64	0.05	0.87	2.10	0.03	0.29	SI
77-R	0.48	4.10	0.89	1.93	2.77	0.59	-1.78	0.30	1.24	0.05	0.72	2.19	0.03	0.24	SI
79-C	0.36	4.16	0.92	2.47	2.53	0.51	-2.44	0.94	0.78	0.15	0.57	2.37	0.03	0.19	KY
79-R	0.58	4.46	0.88	2.45	2.65	0.52	-1.96	0.86	0.30	0.14	0.72	2.22	0.03	0.24	KY
81-C	0.58	4.46	0.88	2.44	3.10	0.56	-1.71	0.86	0.30	0.14					
81-R	0.80	4.88	0.86	2.33	3.10	0.57	-1.53	0.46	0.02	0.08					
91-C	0.22	4.50	0.95	1.77	3.25	0.65	-2.41	0.98	0.38	0.16					
91-R	0.50	4.96	0.91	1.90	3.63	0.66	-1.63	0.54	0.06	0.09					
93-C	0.50	4.54	0.90	1.81	3.21	0.64	-1.64	0.78	0.28	0.13	0.96	2.04	0.03	0.32	SI
93-R	0.54	4.78	0.90	1.77	3.15	0.64	-1.60	0.52	0.24	0.08	0.93	2.04	0.03	0.31	SI
101-C	0.56	4.76	0.89	2.00	3.08	0.61	-1.70	0.90	0.02	0.14	0.81	2.19	0.00	0.27	SI,AD[c]
101-R	0.58	4.64	0.89	1.97	3.07	0.61	-1.63	0.68	0.22	0.11	0.81	2.19	0.00	0.27	SI,AD[c]
104-C	0.60	4.66	0.89	1.85	3.16	0.63	-1.51	0.32	0.50	0.05	0.90	2.07	0.03	0.30	SI
104-R	0.50	4.72	0.90	1.80	3.31	0.65	-1.63	0.32	0.52	0.05	0.63	2.01	0.21	0.22	SI
110-C	0.64	4.60	0.88	1.88	3.07	0.62	-1.48	0.40	0.48	0.07	1.02	1.98	0.03	0.34	SI
110-R	0.42	4.66	0.92	1.88	3.16	0.63	-1.87	0.36	0.68	0.06	1.02	1.98	0.03	0.34	SI
120-C	0.26	4.54	0.95	1.87	3.12	0.63	-2.37	1.12	0.16	0.18	0.60	2.34	0.03	0.21	SI,KY[d]
120-R	0.46	4.68	0.91	1.57	3.31	0.68	-1.56	0.74	0.20	0.12	0.60	2.34	0.03	0.21	SI,KY[d]

Notes:

a) C - grain core analysis; R - grain rim analysis.

b) Mineral abbreviations; KY - kyanite; SI - sillimanite; AD - andalusite.

c) Andalusite is post-peak metamorphism. See text for discussion.

d) Sillimanite and kyanite are both stable.

(oligoclase - andesine). Mild zonation (both normal and reverse) is common. No systematic variation in plagioclase composition is apparent either on the scale of individual grains or on a map scale.

Garnet - biotite geothermometry

The applicability of garnet - biotite geothermometry to analysis of the M_2 metamorphic event is severely restricted by the paucity of garnet; by complex zonation of the garnets; by the uncertain relationship of some andalusite and cordierite to the peak M_2 metamorphic mineral paragenesis; by alteration of the M_2 metamorphic mineral paragenesis during [illegible] thermal metamorphism including the widespread development of retrogressive chloritic alteration of both biotite and garnet. Retrogressive alteration is also indicated by the presence of spessartine enriched garnet rims and phlogopite enriched biotite cores.

Garnet - biotite pairs from ten samples, in which only minor retrogressive alteration was apparent, were analyzed. Only biotite grains in contact with garnet were analyzed. Core (garnet and biotite grain cores) and rim (rims of adjacent garnet and biotite grains) temperatures were calculated for each sample. Core temperatures are suspect as there is no way to show that the garnet core and the biotite core were ever in equilibrium with one another. Rim temperatures are assumed to provide minimum estimates of peak temperature as retrogressive re-equilibration of garnet - biotite pairs is common. Error bars on absolute temperatures are at least 50 ^{o}C (Ferry and Spear, 1978) and, because of microprobe analytical error, are likely larger. Because of the paucity of suitable garnet - biotite pairs it was not possible to analyze multiple garnet - biotite pairs for each sample and determine a sample specific standard deviation. Based on a review of recent papers which employed garnet - biotite geothermometry on similar rocks (i.e. McClelland *et al.*, 1991) it is assumed that there is an error of 80 ^{o}C on absolute temperatures.

Results are shown in Table 5.4. Sample 101, collected from within the staurolite - kyanite zone immediately adjacent to the Ruby Range Batholith, is characterized by relatively high garnet - biotite temperatures (678 ^{o}C to 713 ^{o}C) relative to other samples collected in the staurolite - kyanite zone. These anomalous results are thought to be attributable to thermal metamorphism (M_4) associated with the intrusion of the Ruby Range Batholith. Rim temperatures for samples 77 and 110 are low relative to core temperatures for the same samples. Both samples are characterized by chloritization of garnet rims. For these reasons core and rim temperatures for sample 101 and rim

Table 5.4. Temperature and pressure estimates.

Sample	Core Temperature (°C)	Core Pressure (kbar)	Rim temperature (°C)	Rim Pressure (kbar)
48	439	2.7	639	9.0
77	766	7.6	563	6.6
79	475	8.4	580	9.4
81	624		713	
91	502		668	
93	680	10.0	674	7.5
101	678	11.1	713	10.8
104	673	5.6	622	5.6
110	684	6.8	553	3.7
120	477	6.55	751	13.8

Notes: Pressure and temperature estimates were calculated using the PTAX function of GEOCALC (Berman *et al.*, 1987), a program for the calculation of mineral equilibria. In all cases the Berman (1988) garnet, McMullin and Berman (1988) biotite, and the Fuhrman and Lindsley (1988) plagioclase solution models were used to account for the effects of non-ideal mixing in the respective solid-solution phases. No corrections were made for the presence of additional components including Mn and Fe^{+++} in garnet and Ti in biotite. Where plagioclase grains were not present, temperatures were calculated assuming P = 8 kbar. Minimum errors on calculated temperatures and pressures are estimated to be 80 °C and 1.6 kbar, respectively.

temperatures for samples 77 and 110 are not further considered here. Core temperatures average 656 °C in the sillimanite zone, 521 °C in the kyanite zone, and 475 °C in the staurolite - kyanite zone. Rim temperatures provide slightly higher temperature estimates, averaging 682 °C in sillimanite zone, 673 °C in the kyanite zone, and 580 °C in the staurolite - kyanite zone (Figure 5.6). These results are consistent with the decrease in metamorphic grade away from the batholith suggested by the metamorphic mineral paragenesis. Temperatures are, however, lower than (although within error of) temperatures suggested by the peak metamorphic mineral paragenesis. This may reflect disequilibrium resulting from younger thermal overprinting.

Garnet - Al_2SiO_5 - plagioclase (GASP) geobarometry

Restrictions on the use of garnet - biotite geothermometry, outlined above, are also applicable to GASP geobarometry. Only six samples were suitable for GASP geobarometry. Matrix plagioclase were analyzed - plagioclase in contact with biotite and garnet was not observed. Sericitic alteration of plagioclase is common and care was taken to avoid affected grains. Core and rim pressures were calculated for each sample. Errors associated with the calculation of temperature propagate through the calculation of pressure. Error bars on absolute pressures are at least 1.6 kbar (Ghent *et al.*, 1979).

Results are shown in Table 5.4. Pressure estimates for sample 101 and rim pressure estimates for samples 77 and 110 are not considered here as their associated temperature estimates are considered unreliable (see above). Core and rim pressure estimates average 6.8 and 9.0 kbar, respectively. However, a core pressure estimate of 2.7 kbar for sample 48 is inconsistent with the presence of kyanite in that sample. A rim pressure estimate of 13.8 kbar for sample 120 is inconsistent with the absence of eclogite in mafic rocks which crop out a short distance from where sample 120 was collected. Discarding these two data points results in core and rim average pressures of 7.5 and 7.9, respectively. These results are within error of each other and are similar to the pressure suggested by the peak metamorphic mineral paragenesis.

5.5 The nature of the metamorphic events

At least four metamorphic events have affected rocks of the Nisling Assemblage (Figure 5.3).

$\underline{M_1}$ - The mineral paragenesis attributable to the M_1 metamorphic event are the most ancient preserved within the study area. As a result, these minerals have been largely obliterated, overgrown, and deformed during subsequent metamorphism and deformation.

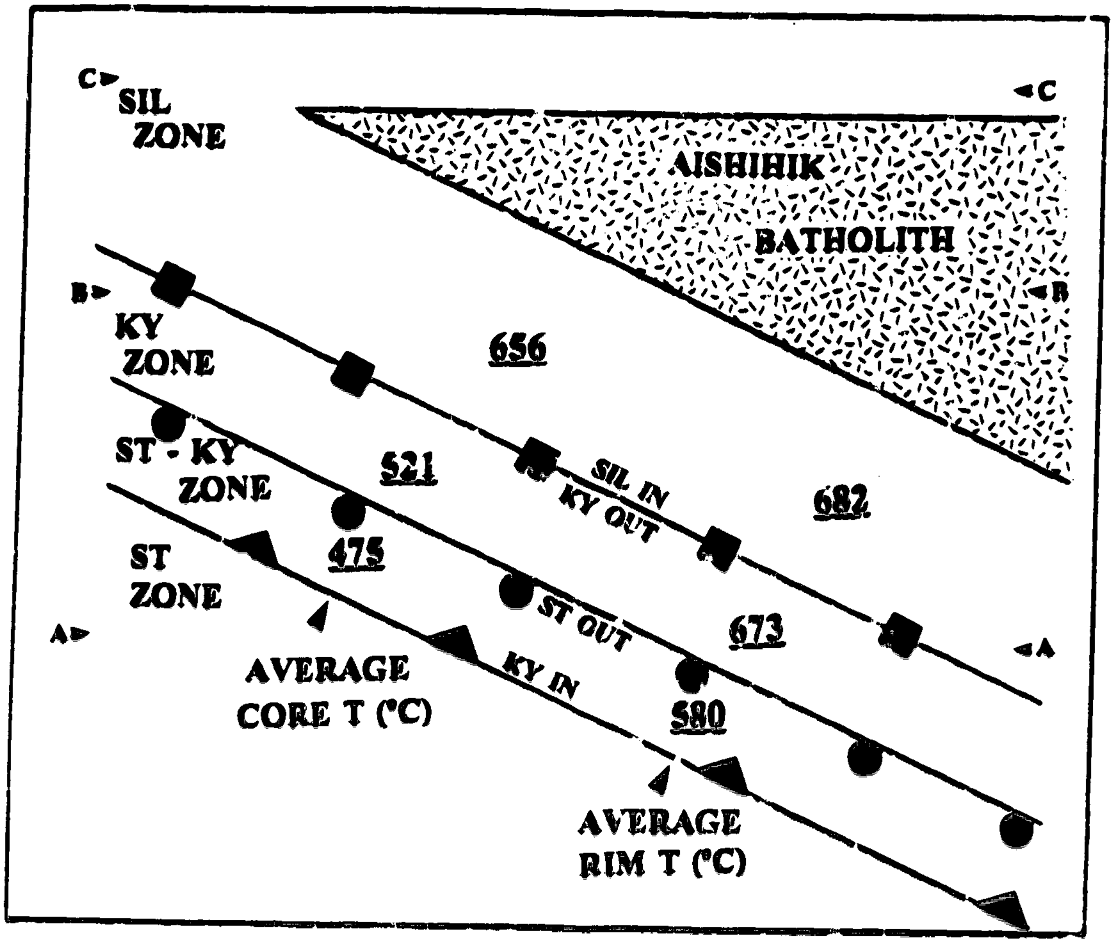

Figure 5.6 A schematic cross-section showing the geometry of the metamorphic aureole developed in Nisling Assemblage adjacent to the west margin of Aishihik Batholith. Average core and rim temperatures, based on garnet-biotite geothermometry, are shown, as are the kyanite (KY) in, staurolite (ST) out, and kyanite out - sillimanite (SIL) in isograds. A - A, B - B, and C - C indicates the approximate level of exposure in each of the South Aishihik Lake, North Aishihik Lake, and Upper Nisling River areas, respectively. See text for discussion.

M_1 appears to have been a regional event, as indicated by the widespread distribution of minerals and fabrics attributable to M_1 metamorphism. The presence of biotite and muscovite suggests that metamorphism was characterized by at least greenschist facies metamorphism.

$\underline{M_2}$ - The dominant metamorphic event to have affected the assemblage, M_2, resulted in the development of mineral paragenesis characteristic of upper amphibolite grade metamorphism. Syn-metamorphic mica define a schistosity (S_2) which parallels the margin of the Aishihik Batholith. Isograds parallel the margin of the Aishihik Batholith and define an increase in metamorphic grade (temperature) towards the batholith. Results of garnet - biotite geothermometry are also consistent with an increase in temperature towards the batholith. These observations indicate that regional metamorphism is directly related to, and resulted from, the intrusion of the Aishihik Batholith. U - Pb isotopic analyses of zircon separates from samples of the batholith indicate that the batholith crystallized at 187.0 +9.7/-0.9 Ma (this study) and restricts the timing of peak metamorphism to the Early Jurassic.

The metamorphic mineral paragenesis together with geobarometric data indicate that deep crustal levels (25 to 30 km) are exposed in the study area. This is consistent with the distribution of isograds, which define a hot-side-up metamorphic aureole beneath the Aishihik Batholith, and implies that erosion has removed much of the overlying rocks. Moderate to deep crustal levels are also suggested by the coarse-grained equigranular nature of the Aishihik Batholith; by the foliaform nature of the batholith - Nisling Assemblage contact; and by the presence of primary magmatic epidote within the batholith.

The andalusite - cordierite problem

Foliaform andalusite and cordierite mantles (on staurolite) and porphyroblasts are interpreted to have developed late during M_2, post-dating peak metamorphism. Their presence requires rapid uplift of the Nisling Assemblage and the Aishihik Batholith to shallow crustal levels ($P = 2$ kbar) during the waning stages of M_2. The development of foliaform andalusite and cordierite as a result of rapid uplift of a still hot metamorphic terrain is, however, problematic. Andalusite is not thought to be stable under rapidly changing pressure and temperature conditions. If the entire terrain was subjected to rapid uplift, why is it that andalusite and cordierite porphyroblasts appear to be restricted to the staurolite zone? Andalusite and cordierite should, according to this model, be present throughout the Nisling Assemblage.

Two possible explanations are suggested: 1) M_2 andalusite and cordierite record a metamorphic event which significantly post-dates regional (M_2) metamorphism. This hypothesis explains the juxtaposition of high and low-pressure metamorphic mineral paragenesis. However, it does not address the limited distribution of andalusite and cordierite (within the staurolite zone) or the morphology of these minerals (lying within schistosity and preserving, in the form of inclusion trails, traces of the S_1 planar fabric); 2) The high-pressure metamorphic parageneses predates the intrusion of the batholith. In this scenario a pre-intrusive, hot-side-down metamorphic package may have been dragged into a hot-side-up orientation by the diapiric emplacement of the batholith at shallow crustal depths. Andalusite and cordierite record metamorphism associated with intrusion. This model fails, however, on several counts. It does not explain why andalusite and cordierite do not overprint the kyanite and sillimanite zones. Metamorphic geopetal features, including cauliflower structures and asymmetric vein clusters, suggest that the Nisling Assemblage is, at present, the same way-up as it was during metamorphism and migmatization. Finally, the style of intrusion of the batholith, in addition to the presence of magmatic epidote, indicate that the batholith was intruded at deep crustal levels.

Three lines of evidence are consistent with the development of andalusite and cordierite as a result of rapid post-peak-metamorphism uplift of the Nisling Assemblage and the Aishihik Batholith: 1 - Plutons of the Long Lake Suite that intrude and truncate schistosity in both the Aishihik Batholith and the Nisling Terrane appear to have been emplaced at shallow crustal levels. The plutons are characterized by the presence of miarolitic cavities; by syn-intrusive brittle deformation of the wall rocks, including brecciation; and by the presence of an extensive dyke swarm (this study). U - Pb isotopic studies of zircon separates from samples of the Pink Quartz Monzonite plutons indicate that these plutons crystallized within about 1 Ma of crystallization of the Aishihik Batholith (189.0 +9.7/-0.9 Ma) (this study); 2 - K - Ar hornblende, U - Pb titanite, and U - Pb zircon isotopic studies of samples from the Aishihik Batholith yield overlapping age determinations consistent with rapid cooling of the batholith. Rapid cooling of the batholith is unexpected, given that the batholith was intruded at moderate to deep crustal levels and suggest rapid, post-crystallization uplift of the batholith; and 3 - Blocks of foliated hornblende granodiorite, similar to that of the Aishihik Batholith, and micaschist, similar to that of the Nisling Assemblage, are incorporated in unmetamorphosed conglomerates of the Early Jurassic Laberge Group. Laberge Group conglomerates crop out a short distance to the east of the study area, within the Whitehorse Trough. This stratigraphic relationship requires unroofing of the Nisling Assemblage and the Aishihik Batholith soon after metamorphism. These observations support the hypothesis that andalusite and cordierite developed in response to the rapid uplift of the still hot metamorphic terrain.

M3 - The close association of mica that nucleated during the M_3 metamorphic event with crenulations of the S_2 schistosity (M_3 mica grows along the axial planes of the crenulations) indicates that M_3 metamorphism was associated with folding of the Nisling Assemblage. The timing of folding is poorly constrained. The folds affect and are younger than the S_2 schistosity, but are older than the Late Cretaceous to Tertiary Ruby Range Batholith: crenulated micaschist is truncated by granitic intrusions of the Ruby Range Batholith.

M4 - The final metamorphic event to affect rocks of the Nisling Assemblage is characterized by thermal overprinting of the previously developed metamorphic paragenesis. Metamorphism is restricted to the South Aishihik Lake area (Figure 5.1 a). Andalusite - cordierite aureoles developed immediately adjacent to intrusions of the Ruby Range Batholith. Sillimanite is more widespread and post-dates the andalusite - cordierite aureoles: fine-grained sillimanite and fibrolitic sillimanite replaces, nucleates on, and mantles andalusite. Potassic metasomatism, characterized by sericitization, increases towards the Ruby Range Batholith and is, locally, pervasive immediately adjacent to the batholith. These observations indicate that thermal metamorphism is related to the intrusion of the Ruby Range Batholith. U - Pb zircon geochronology indicate that Ruby Range plutonism probably ranged from between 68 and 90 Ma to 58 Ma.

5.6 Pressure - temperature - time displacement

Geochronologic data, together with pressure and temperature determinations, define a pressure - temperature - time (P - T - t) evolution for the Nisling Assemblage (Figure 5.7 a and b). Only the M_2 and M_4 metamorphic events are considered here. Too little is known about the M_1 and M_3 metamorphic events to include them in this discussion.

During the M_2 event rocks of the Nisling Assemblage were metamorphosed at moderate to high P - T conditions. Metamorphism was directly attributable to the intrusion of the Aishihik Batholith and resulted in the overprinting of the folded S_1 planar fabric. The batholith and metamorphosed rocks of the Nisling Assemblage were then rapidly uplifted and unroofed prior to the intrusion of the Long Lake Suite of post-tectonic plutons. Andalusite and cordierite developed at this time. Sediments of the Early Jurassic Laberge Group, preserved within the Whitehorse Trough just east of the study area, consist of immature clastic rocks derived from the west and provide a record

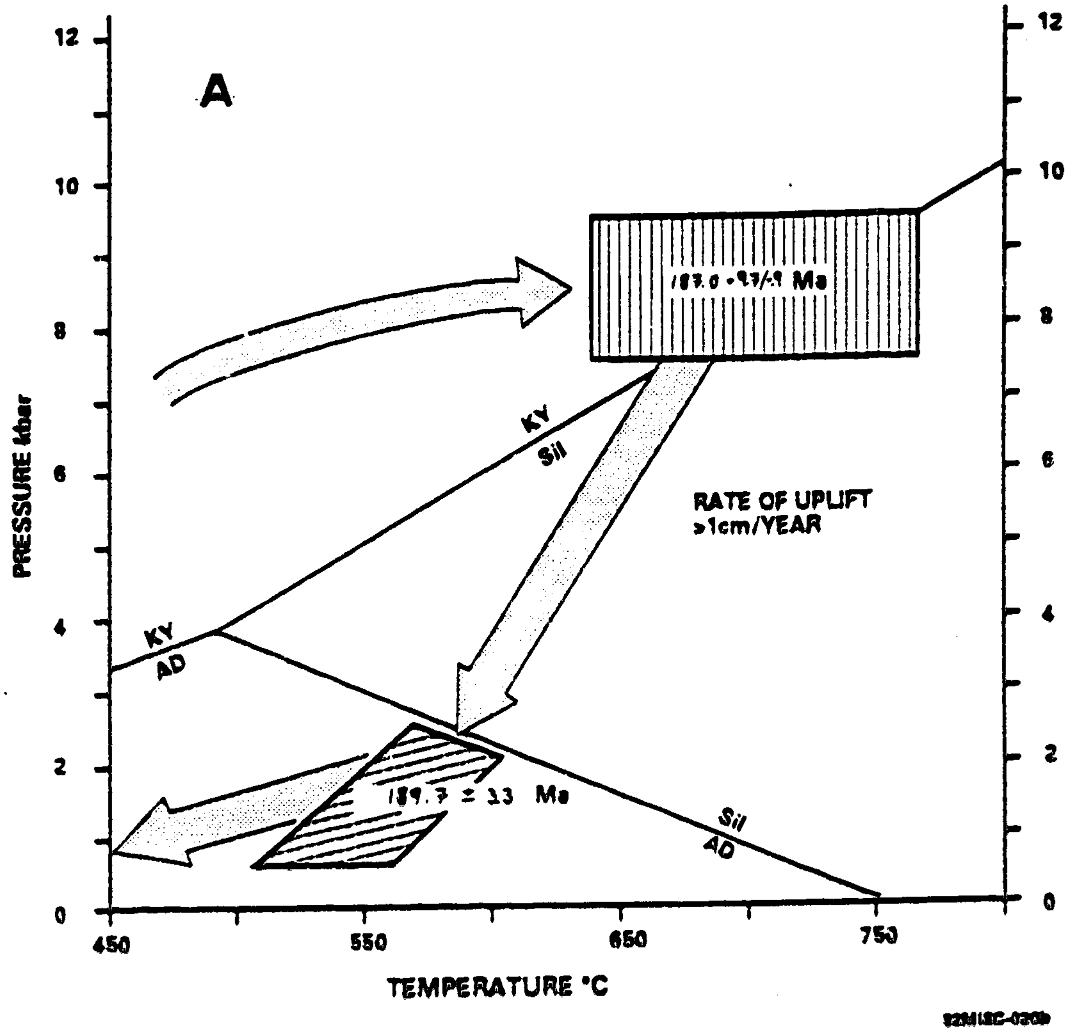

Figure 5.7 Pressure - temperature - time displacement diagrams for the Nisling Assemblage. Arrows indicate the relative order of crustal conditions experienced by the Nisling Assemblage as indicated by metamorphic mineral parageneses. A - M_2 metamorphism; B - M_4 metamorphism. See text for discussion.

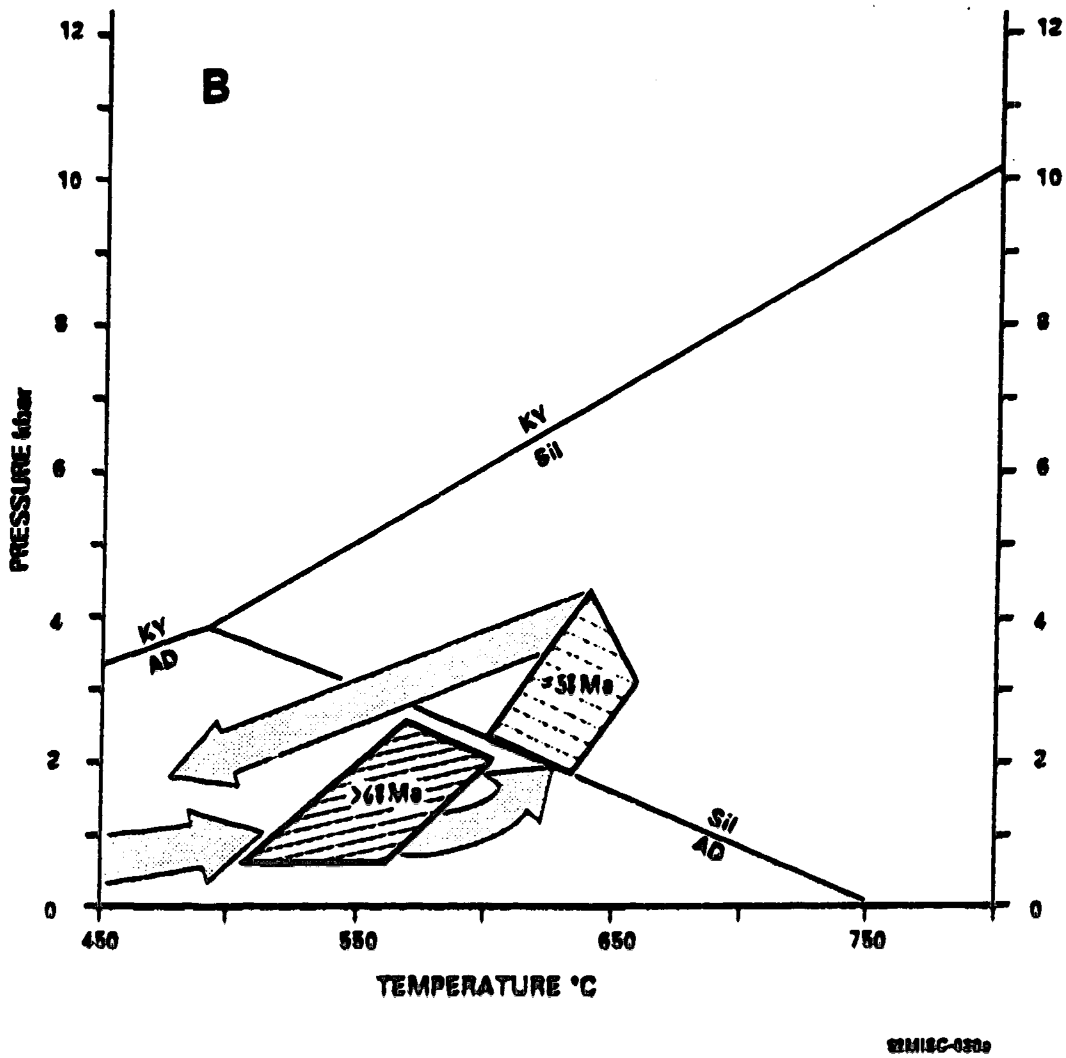
B
PRESSURE kbar
TEMPERATURE °C
KY
Sil
KY
AD
Sil
AD
>58 Ma
>68 Ma
92MISC-030a

of this uplift. K - Ar biotite age determinations from samples of the Long Lake Suite suggests that the terrain cooled through the 300 ^{o}C isotherm by 150 Ma (Tempelman-Kluit and Wanless, 1975).

These data define a clockwise P - T - t evolution which is divisible into four segments: 1) initial tectonic burial of the Nisling Assemblage to crustal depths of 25 to 30 km. The time of initiation of tectonic burial is not constrained; 2) intrusion of the Aishihik Batholith at 189.0 +9.7/-0.9 Ma and associated metamorphism of the Nisling Assemblage; 3) rapid uplift and unroofing of the batholith and the Nisling Assemblage. Geochronologic constraints suggest that more than 20 km of uplift occurred in less than 2 Ma - a rate of uplift of greater than 1 cm/year; and 4) a prolonged post-tectonic period characterized by relative tectonic stability.

During M_4 metamorphism rocks of the Nisling Assemblage were metamorphosed at low P, high T conditions. Metamorphism, potassic metasomatism, and alteration of the Nisling Assemblage was directly related to the intrusion of the Ruby Range Batholith. K - Ar mineral ages (Tempelman-Kluit and Wanless, 1975; Farrar *et al.*, 1988) and U - Pb zircon ages (this study) indicate that the Ruby Range Batholith developed during a prolonged period of plutonism extending from at least 68 Ma to about 58 Ma. Geochronologic and metamorphic studies of the Kluane Schist southwest of the Ruby Range batholith indicate that widespread sillimanite-grade metamorphism of those rocks occurred during the Eocene (Mortensen and Erdmer, 1992). This suggests that similar widespread sillimanite-grade metamorphism of the Nisling Assemblage developed late in the Ruby Range plutonic event and is consistent with the presence of mantles of fine-grained sillimanite on andalusite.

These relationships define a linear P - T - t path that is divisible into three segments: 1) initiation of Ruby Range plutonism before 68 Ma and associated development of andalusite - cordierite aureoles; 2) continued plutonism and crustal heating, culminating at about 58 Ma (?) with the widespread development of sillimanite; 3) cessation of Ruby Range plutonism and associated metamorphism. No constraints are available on the rate of post-Ruby Range cooling of the Nisling Assemblage.

5.7 Discussion

The metamorphic evolution of a package of rocks can be used to constrain the terrane affinities of those rocks. Three terrane correlations have been proposed for Nisling Assemblage. These are: 1 - North America (Hansen, 1990 a and b); 2 - Yukon-Tanana terrane (Mortensen, 1992); and 3 - Stikine terrane (Tempelman-Kluit, 1979).

North America - Hansen (1990 a and b) defined North America on the basis of structural position and time of unroofing. North American rocks are present at structurally deep levels, having been overthrust by Stikine terrane (?) in the Early Jurassic, and were not unroofed until the Middle Cretaceous when crustal extension and granite plutonism affected large areas of southwest Yukon and Alaska. Nisling Assemblage rocks were correlated with North America as they were thought to record a similar metamorphic history.

Like North American rocks, rocks of Nisling Assemblage that underlie the study area were overthrust and tectonically buried in the Early Jurassic or earlier. Nisling Assemblage rocks were, however, unroofed in the Early Jurassic. No structures attributable to Middle Cretaceous extension of the Nisling Assemblage in the vicinity of Aishihik Lake have been identified (Tempelman-Kluit, 1974; this study), although Middle Cretaceous plutons of the Whitehorse - Coffee Cr. Suite (Woodsworth *et al.*, 1991) intrude the Nisling Assemblage northwest of Aishihik Lake (Tempelman-Kluit, 1974).

North American and Nisling Assemblage rocks, therefore, share a similar Early Jurassic tectonic history. However, the post-Early Jurassic histories of these terranes are significantly different.

Yukon-Tanana terrane - Mortensen (1992), suggested that Nisling Assemblage is similar to, and should be included as part of, the Yukon-Tanana terrane. The similarities include homotaxiality of the Nisling Assemblage and strata of the Yukon-Tanana terrane; broadly similar metamorphic grade; and correlative orthogneiss suites. The Yukon-Tanana terrane is characterized by: 1) fabrics and metamorphic mineral parageneses related to pre-Late Triassic but post-Permian mylonitization and regional metamorphism (D_1); 2) regional scale thrust faulting and imbrication with ophiolitic strata of the Slide Mountain terrane in the Early Jurassic (D_2). Tectonism was not accompanied by regional metamorphism; and 3) extension and localized contact metamorphism associated with extensive Middle Cretaceous granite plutonism (D_3) (Mortensen, 1992; 1990).

The M_1 metamorphic event recorded by rocks of the Nisling Assemblage may be correlative with D_1 metamorphism of the Yukon-Tanana terrane. There is, however, little to substantiate this correlation. Early Jurassic tectonism resulted in moderate to high P - T metamorphism of Nisling Assemblage while Yukon-Tanana terrane experienced regional-scale imbrication at shallow crustal levels.

These data do not rule out correlation of Yukon-Tanana terrane and Nisling Assemblage. They do, however, indicate that Yukon-Tanana terrane and Nisling

Assemblage were at different structural levels in the Early Jurassic.

Stikine terrane - The Nisling Assemblage has been suggested as the possible basement for Stikine terrane based on the assumption that the Aishihik Batholith represented the plutonic root of the Late Triassic Lewes River volcanic arc (Tempelman-Kluit, 1979).

However, the Aishihik Batholith crystallized in the Early Jurassic (this study). Late Triassic and older strata of the Stikine terrane do not record significant regional metamorphism of Early Jurassic or pre-Early Jurassic age. This suggests that the Nisling Assemblage and the Stikine terrane constituted separate tectonic elements until at least the Early Jurassic and that the Nisling Assemblage is not basement to Late Triassic rocks of Stikine terrane.

Post-tectonic plutons of the Long Lake Suite intrude metamorphosed rocks of the Nisling Assemblage, the Aishihik Batholith and unmetamorphosed mafic volcanic rocks of the Stikine terrane (Tempelman-Kluit, 1974; Wheeler, 1961). These plutons define an overlap assemblage that stitches together the Nisling Assemblage and the Stikine terrane by 189.7 $\pm$ 3.3 Ma (this study). These relationships suggest that M_2 metamorphism of the Nisling Assemblage is closely associated with the amalgamation of the Nisling Assemblage and the Stikine terrane.

5.8 Conclusions

1. Rocks of the Nisling Assemblage record four metamorphic events. These are, in order of occurrence:

M_1 - Pre - Early Jurassic regional greenschist to amphibolite grade (?) metamorphism, signs of which have now been largely obliterated by more recent metamorphism;

M_2 - Early Jurassic region, syn- to post-kinematic, moderate to high P - T metamorphism directly attributable to the intrusion of the Aishihik Batholith;

M_3 - Post - Early Jurassic but pre - Late Cretaceous sub-greenschist facies metamorphism related to folding of the Nisling Assemblage and the development of crenulations of the S_2 schistosity;

M_4 - Late Cretaceous to Tertiary low P - high T thermal metamorphism associated with the Ruby Range Batholith.

2. Nisling Assemblage rocks that underlie the study area were tectonically buried to depths of 25 to 30 km depth (corresponding to a pressure of 8 to 9 kbar) in the Early Jurassic as indicated by the development of staurolite - migmatite schist. The exposure of

deep crustal levels at the present erosion surface is consistent with the results of geothermobarometry studies and with the distribution of mineral isograds: mineral isograds define a hot side up metamorphic aureole developed beneath the overlying Aishihik Batholith.

3. Immediately after intrusion of the Aishihik Batholith, the Nisling Assemblage and the batholith were rapidly uplifted (uplift rates of over 1 cm/year for two million years) and unroofed. Uplift is indicated by: 1 - the development of andalusite and cordierite mantles on staurolite; and 2 - by the intrusion of metamorphosed rocks of the Nisling Assemblage and the Aishihik Batholith by discordant, shallow level, miarolitic dykes and plutons of the Long Lake Suite at about 189.7 $\pm$ 3.3 Ma.

4. Thermal metamorphism associated with the Ruby Range Batholith is divisible into two distinct phases. An initial phase is characterized by the development of andalusite - cordierite aureoles in the wall rocks immediately adjacent to intrusions of the Ruby Range Batholith. A second phase, associated with the final stages of intrusion of the Ruby Range Batholith and of probable Eocene age, is characterized by the widespread development of sillimanite.

5. It is difficult to reconcile any of the terrane correlations suggested for the Nisling Assemblage, although the following can be said: The Nisling Assemblage does not constitute the basement of the Stikine terrane; rocks of the Nisling Assemblage and the Yukon-Tanana terrane both record Early Jurassic and pre-Early Jurassic tectonic events, although the Nisling Assemblage was at structurally deep levels in the Early Jurassic while the Yukon-Tanana terrane was at shallow structural levels; rocks of the Nisling Assemblage and North America were overthrust and tectonically buried in the Early Jurassic, although the Nisling Assemblage was unroofed in the Early Jurassic, while North American rocks were not unroofed until the Middle Cretaceous.

VI. DISCUSSION

6.1 Towards a tectonic model

Observations made in the Aishihik Lake map-area can be used to constrain models of the early- to mid-Mesozoic tectonic evolution of the Northern Cordillera. Presented here are: 1) criteria used to constrain the tectonic evolution of Nisling Assemblage in the Aishihik Lake area; and 2) a suggested model of terrane interaction.

Constraining criteria:

1) Nisling Assemblage consists of a structurally thickened and metamorphosed quartzose clastic shelf sequence more than 10 km thick. The nature of the basement onto which this shelf sequence was deposited remains unknown. Plutons that intrude Nisling Assemblage are characterized by initial strontium ratios in excess of .706 (LeCouteur and Tempelman-Kluit, 1976) and by the presence of a component of inherited zircon of early Proterozoic age consistent with the presence of a crystalline basement beneath Nisling Assemblage. Nisling Assemblage plunges to the north throughout the Aishihik Lake area, resulting in the exposure of the structurally deepest part of the terrane in the region south of Aishihik Lake. If basement to Nisling Assemblage is exposed in Yukon it may be in this region. Further mapping is necessary to investigate this possibility.

Interfoliated with quartzose rocks is a 4 km thick amphibolite-marble sequence and orthogneiss. These rocks provide a record of volcanism, carbonate deposition and intrusion which define an apparent volcanic arc sequence of mid-Paleozoic age. Middle Paleozoic volcanic arc sequences are present in Yukon-Tanana Terrane and Stikinia and intimates a Paleozoic link between these terranes (L Currie, pers.comm. 1992; Mortensen, 1992).

Yukon-Tanana Terrane consists of a Paleozoic and older pericratonic succession similar to that of Nisling Assemblage and an inferred volcanic arc sequence that consists of Devono-Mississippian orthogneiss (the Mink Cr. and Selwyn gneisses), metavolcanics, and marble (Mortensen, 1990; 1992). Like Nisling Assemblage, plutons that intrude Yukon-Tanana Terrane are characterized by initial strontium ratios in excess of .706 (LeCouteur and Tempelman-Kluit, 1976) and by the presence of a component of inherited zircon of early Proterozoic age (Mortensen, 1990; 1992) suggesting that the basement beneath Nisling Assemblage is continuous beneath Yukon-Tanana Terrane.

Stikinia includes the Devonian to Middle Triassic Stikine Assemblage which consists of arc-related volcanic and volcaniclastic strata, and carbonate rocks (Monger, 1977; Brown et al., 1991). The nature of the basement beneath the Stikine Assemblage remains unknown. However, younger volcanics deposited on Stikine Assemblage are characterized by juvenile Nd isotopic values and have not been significantly contaminated by evolved crystalline crust (Samson *et al.*, 1989).

Because of temporally and lithologically similar mid-Paleozoic volcanic arc sequences, Nisling Assemblage, Yukon-Tanana Terrane, and Stikinia are interpreted to have formed a coherent microcontinent through much of the Paleozoic (J. Mortensen, pers. comm, 1992; Mortensen, 1992). The apparent lack of crystalline basement beneath Stikinia suggests that crystalline basement beneath Nisling Assemblage is discontinuous to the south.

2) Nisling Assemblage was regionally deformed twice between the middle Paleozoic and the Early Jurassic. Little is known about the nature of D_1 deformation as fabrics attributable to the earlier event have been largely obliterated during younger metamorphism and deformation. D_2 deformation is characterized by tight to isoclinal folding (F_2) of a previously developed tectonic fabric (S_1), and by the development of a north-trending quartz-rodding lineation (L_2). Deformation had largely ceased by 186 Ma as Aishihik Batholith, which intrudes Nisling Assemblage, was not significantly deformed. F_2 folds in Nisling Assemblage are characterized by an axial planar schistosity which parallels the margin of the batholith, suggesting that the batholith may have intruded during the final stages of deformation.

D_2 tectonism resulted in the tectonic burial of Nisling Assemblage to moderate to deep crustal levels. Evidence for tectonic burial of Nisling Assemblage comes primarily from the metamorphic mineral paragenesis which characterizes the metamorphic aureole around the late- to post-kinematic Aishihik Batholith. The aureole includes staurolite migmatite but not eclogite, limiting pressure to between 8 kbar and 10 kbar. Sparse geobarometry data are consistent with metamorphism at pressures in excess of 8 kbar. Mineral isograds define a hot-side-up metamorphic aureole developed beneath the overlying Aishihik Batholith, consistent with the exposure of deep crustal levels at the present erosion surface. In the batholith late stage magma reacted with plagioclase and hornblende to produce epidote and biotite, a process indicative of pressures of about 8 kbar (Zen, 1989; Zen and Hammerstrom, 1984).

Yukon-Tanana Terrane is characterized by similar high-pressure-moderate-temperature metamorphism associated with post-Middle Permian but pre-Early Jurassic deformation (Mortensen, 1992; Dusel-Bacon and Douglass, 1990). This is strong evidence in favour of continued correlation of Yukon-Tanana Terrane and Nisling Assemblage (Mortensen, 1992). There is, however, no record of Triassic (?) high-pressure-moderate-temperature metamorphism in Stikinia. Instead Stikinia is characterized in the Late Triassic by the development of a volcanic arc as indicated by volcanic rocks of the Stuhini Group. Because Nisling Assemblage was buried to moderate crustal depths synchronously with the development of a volcanic arc on Stikinia, Stikinia is inferred to have been a tectonic element distinct from Nisling Assemblage by the Late Triassic.

3) The Aishihik Batholith crystallized at 187.0 +9.7/-0.9 Ma and intrudes Nisling Assemblage. The batholith is characterized by rare micaschist inclusions similar to micaschist of Nisling Assemblage, and by a margin-parallel foliation, defined by the alignment of primary magmatic grains. Solid-state deformation, characterized by top-to-the-west shearing of the west margin of the batholith, is thought to reflect late magmatic ballooning. Intrusion resulted in metamorphism of Nisling Assemblage; isograds are parallel to the margin of the batholith and define an increase in grade towards the batholith. Sparse geothermometric data are consistent with an increase in temperature towards the batholith.

The batholith is part of the Klotassin Plutonic Suite (Tempelman-Kluit, 1974; 1979) which ranges in age from 210 Ma to 185 Ma (LeCouteur and Tempelman-Kluit, 1976; Tempelman-Kluit and Wanless, 1980; this study) and which is intrusive into both Nisling Assemblage (Tempelman-Kluit, 1974; this study) and Yukon-Tanana Terrane (Mortensen, 1992). Lithologically similar intrusions of the same age are also present in Stikinia (the Texas Creek and Topley suites) and in the Slide Mountain and Cache Creek terranes (Gabrielse and Reesor, 1974; Woodsworth et al., 1991). Magmatism was synchronous with the development of the Hazelton volcanic arc in Stikinia.

4) Rapid uplift of Nisling Assemblage occurred after intrusion of Aishihik Batholith and before, or during, the intrusion of the Long Lake Suite. Plutons of the suite post-date the batholith and crystallized by about 189.7 $\pm$ 3.3 Ma at shallow crustal levels and are characterized by miarolitic cavities and discordant contacts. Dyke swarms that consist of pink quartz monzonite and that are spatially associated with plutons of the Long Lake Suite are common. Geochronological data indicate rapid cooling (between 100 ^{o}C/Ma and 45 ^{o}C/Ma) of Aishihik Batholith, consistent with rates of uplift in excess of 2 cm/year. The preservation of unaltered magmatic epidote in Aishihik Batholith requires quenching by rapid uplift and cooling (Zen, 1989; Zen and Hammarstrom, 1984). Staurolite grains in staurolite migmatite schist are mantled by andalusite and cordierite, requiring that pressure dropped from 8 kbar during peak metamorphic conditions, to less than 3 kbar. West-verging folds of Nisling Assemblage and Aishihik Batholith may have

developed at this time. Modern analogues suggest that rapid uplift of the order inferred for Nisling Assemblage and Aishihik Batholith can be associated with collision (Copeland et al., 1988; Wang and Burnett, 1990).

In Yukon-Tanana Terrane intrusion of the Klotassin Plutonic Suite was followed by imbrication of the terrane along regional scale thrust faults. Thrust faults are characterized by slices mafic and ultramafic rock thought to represent ophiolite of the Slide Mountain Terrane (Mortensen, 1990). In Stikinia Hazelton arc volcanism began to wane by about 187 Ma (Marsden and Thorkelson, 1992) although contraction, during which Cache Creek Terrane was thrust westward over Stikinia along the Nahlin and King Salmon thrust faults, did not occur until the Middle Jurassic.

A tectonic model for Nisling Assemblage :

These criteria are consistent with a tectonic model (Figure 6.1) in which Nisling Assemblage: 1) formed part of a microcontinent which included Yukon-Tanana Terrane and Stikinia through much of the Paleozoic; 2) collided with and was subducted beneath another terrane in the Late Triassic; 3) was the site of Early Jurassic magmatic arc development; and 4) collided with and was thrust above another terrane in the middle to late Early Jurassic.

The model begins with the Devono-Mississippian development of volcanic arc sequences in Nisling Assemblage, Stikinia and Yukon-Tanana Terrane, consistent with mid-Paleozoic subduction beneath a Nisling-Yukon-Tanana-Stikinia microcontinent (Figure 6.1a). Permian volcanic arc sequences occur in both Stikinia (Monger, 1977) and Yukon-Tanana Terrane (Mortensen, 1992; 1990), but have not been recognized in Nisling Assemblage. Further field mapping and geochronological studies of Nisling Assemblage are necessary to determine if this arc sequence is absent from Nisling Assemblage.

Subsequent to Permian subduction beneath part or all of the Nisling-Yukon-Tanana-Stikinia microcontinent, Nisling Assemblage and Yukon-Tanana Terrane collided with and were underthrust beneath another terrane (Figure 6.1b and c). Stikinia was characterized by volcanic arc sequence, represented by volcanic rocks of the Stuhini Group, and constituted a tectonic element distinct from Nisling Assemblage and Yukon-Tanana Terrane. Pre-Stuhini Group deformation of Stikinia - the Tahltanian Orogeny (Monger, 1977) - may provide a record of separation of Stikinia from Nisling Assemblage, although the significance of this event remains a matter of conjecture.

The landmass beneath which Nisling Assemblage was underthrust is likely to be Cache Creek Terrane. Cache Creek Terrane is characterized by a structural and

Figure 6.1 A model of the tectonic evolution of Nisling Assemblage. See text for discussion. Terranes: NYTS - Nisling Assemblage-Yukon-Tanana-Stikinia microcontinent; NYT - Nisling Assemblage-Yukon-Tanana microcontinent; CC - Cache Creek; WM; Windy-McKinley; IS - Insular SuperTerrane. Plutonic, volcanic, and sedimentary suites: SA-MCSG - Stikine Assemblage-Mink Cr. - Selwyn Gneiss; KLR - Kutcho-Lewes River groups; LI - Laberge Group-Inklin Formation (with arrow indicating sedimentary transport direction); AK - Aishihik-Klotassin Plutonic Suite; LL - Long Lake Plutonic Suite.

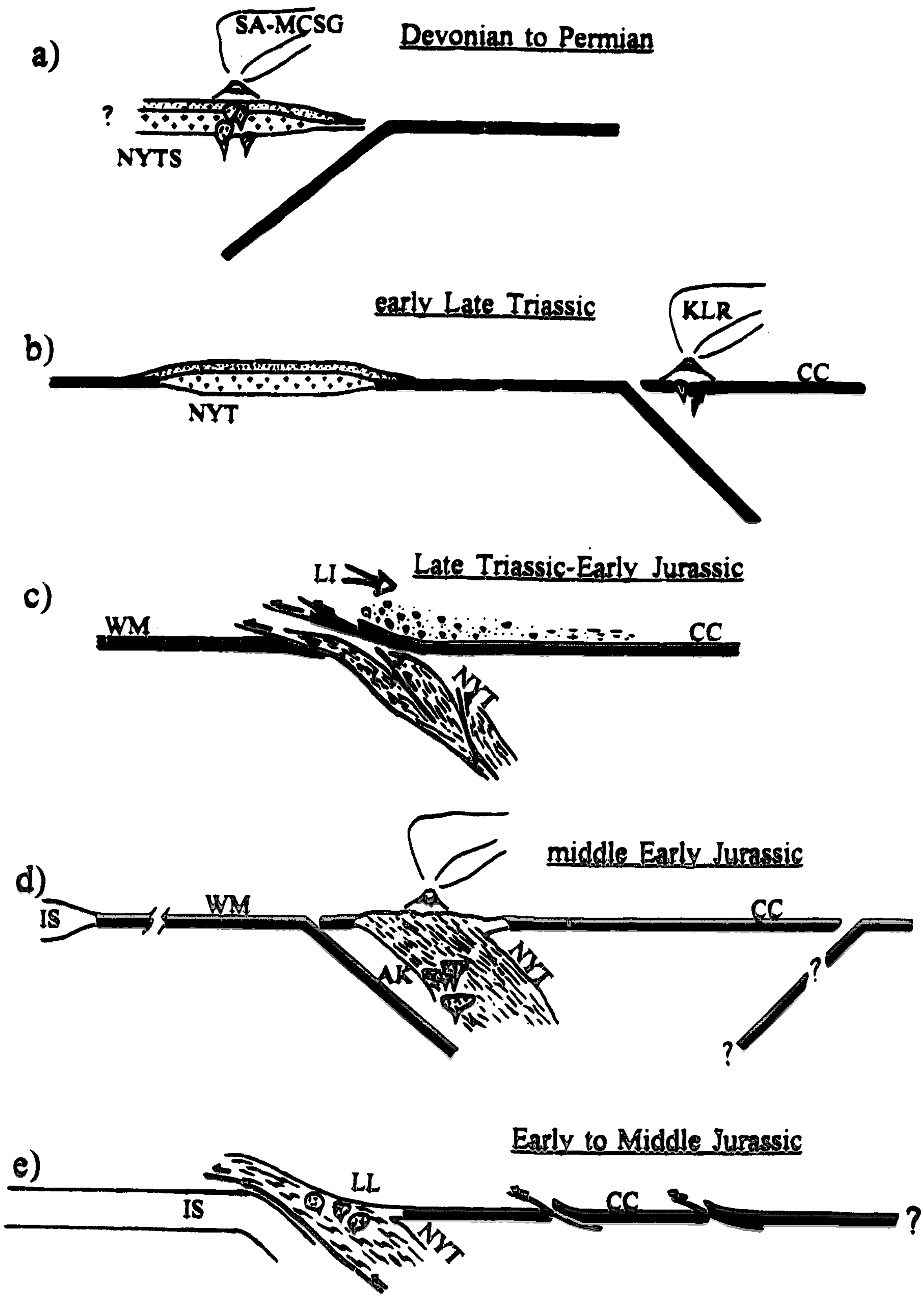
a)
SA-MCSG
Devonian to Permian
?
NYTS
b)
early Late Triassic
KLR
CC
NYT
c)
LI
Late Triassic-Early Jurassic
WM
CC
NYT
d)
middle Early Jurassic
IS
WM
CC
AK
NYT
?
?
e)
Early to Middle Jurassic
LL
IS
CC
NYT
?

stratigraphic record of Late Triassic collision with a terrane of continental affinity, including: 1) the cessation arc volcanism of the Kutcho and Lewes River groups; 2) shearing of rocks of the Lewes River Group in the Tally-Ho shear zone along the west margin of Whitehorse Trough (Hart and Radloff, 1990); 3) the development of southwest verging folds which affect 218 Ma to 211 Ma blueschists (Paterson, 1974) but which are deformed by earliest Late Jurassic structures (Monger, 1977); and 4) the deposition of a thick blanket of molasse, including the Laberge Group and the Inklin formation. Collision with a terrane of continental affinity is suggested by the presence of clasts of quartzite and quartz mica schist in the molasse sequence (Hart and Radloff, 1990; Wheeler, 1960).

Subduction beneath the tectonically buried Nisling Assemblage began in the earliest Jurassic and was responsible for the development of the Klotassin Plutonic Suite (Figure 6.1d). Early Jurassic plutons and volcanic sequences, in particular the Hazelton Group, are present across the entire width of the Intermontane Belt consistent with the inward-dipping subduction beneath both sides of the belt (Marsden and Thorkelson, 1992).

The bulk of the plutons that constitute the Klotassin Suite occur along the southwest margin of Nisling Assemblage and Yukon-Tanana Terrane consistent with their development above crust subducting to the east (present day coordinates) beneath the ancient west coast of Nisling Assemblage. The White River Assemblage, which crops out west of Nisling Assemblage in southwest Yukon (Tempelman-Kluit, 1974) and which is included in Windy-McKinley Terrane (Wheeler and McFeely, 1991), may constitute a relic of the ocean subducted beneath Nisling Assemblage. The assemblage consists of marine Paleozoic rocks, including cherty argillite, chert, phyllite, and Devonian limestone, and mafic and ultramafic rocks of oceanic affinity (Tempelman-Kluit, 1974).

In this model post-Aishihik Batholith tectonism is attributed to the closure of the Windy-McKinley ocean closed by about 187 Ma. Buoyant crust, probably of the Insular Superterrane, entered the subduction zone colliding with and being thrust beneath Nisling Assemblage (Figure 6.1e). Nisling Assemblage and Aishihik Batholith were folded and rapidly uplifted. Yukon-Tanana Terrane was imbricated along regional scale thrust faults. Deep-seated intrusions of foliated hornblende granodiorite of the Klotassin Suite were succeeded by shallow-level emplacement of massive leucocratic pink quartz monzonite of the Long Lake Suite. Accretion of the more westerly Insular Superterrane may have begun in the Early Jurassic (van der Heyden, 1990; Currie, 1991), consistent with this interpretation.

The demise of the Windy-McKinley ocean coincided with intra- and inter-terrane contractional tectonism, and a cessation of Early Jurassic arc volcanism. Inboard and outboard subduction beneath Stikinia ceased (Marsden and Thorkelson, 1992). Cache Creek was thrust west over Stikinia along the King Salmon and Nahlin thrust faults. Internal imbrication of Cache Creek terrane also occurred at this time (Gabrielse, 1991) and molasse shed from the emergent terrane was deposited on Stikinia forming Bowser Basin.

This model explains the Late Triassic-Early Jurassic tectonic evolution of the Northern Cordillera in terms of two collisional events. Late Triassic tectonic burial of Nisling Assemblage resulted from the closure an ocean by subduction beneath Cache Creek Terrane. Subsequent closure of the Windy-McKinley ocean by subduction beneath Nisling Assemblage resulted in the Early Jurassic accretion of Insular Superterrane to the ancient outboard margin of Nisling Assemblage.

6.2 Conclusions

To elucidate the relationship between Stikinia and Nisling Assemblage, this study examined the contact between Aishihik Batholith, an intrusion previously considered to be part of Stikinia, and a metamorphosed package of quartzose clastic rocks, marble, amphibolite and orthogneiss, constituting Nisling Assemblage. The evidence presented here indicates that: 1) Aishihik Batholith crystallized at about 186 Ma and belongs to the Klotassin Plutonic Suite; and 2) that the batholith intrudes Nisling Assemblage.

These findings, together with other recent research in the northern Cordillera, indicate that there is a profound misunderstanding of northern Stikinia. The origin of this misunderstanding is twofold, and includes: 1) the assumption that the Klotassin Suite represents the plutonic root of Late Triassic volcanic rocks of the Lewes River Group (Tempelman-Kluit, 1979); and 2) an initial correlation of Nisling Assemblage with Stikinia (Tempelman-Kluit, 1979). Because Klotassin Suite appeared to intrude "Stikinia" (now Nisling Assemblage) and because the Klotassin Suite was thought to be related to the volcanic rocks of the Lewes River Group, the Lewes River Group was inferred to have been deposited on Stikinia. By 1981 Nisling Assemblage was considered as part of a terrane distinct from Stikinia (Tempelman-Kluit, 1981). This reinterpretation did not, however, result in a re-evaluation of the terrane affinity of the Lewes River arc. Indeed it was the continued inclusion of the Lewes River arc, including the Lewes River Group and the Klotassin Suite, in Stikinia which suggested that the Klotassin Suite was allochthonous with respect to Nisling Assemblage. Even the subsequent realization that the Klotassin

Suite was too young to represent the plutonic root of the Lewes River arc did not result in a re-assignment of the terrane affinity of the Lewes River Group. Thus on recent terrane maps (Wheeler and McFeely, 1991) the Lewes River succession is considered as part of Stikinia despite the fact that the two initial assumptions which led to its inclusion in Stikinia (Klotassin Suite related to Lewes River Group and Nisling Assemblage equivalent to Stikinia) had been discarded. The only remaining basis for the inclusion of the Lewes River Group in Stikinia is the lithological similarity of the Lewes River and Stuhini groups. However, the lithological similarity of two successions is not in itself sufficient evidence that they belong to the same terrane.

This confusion over what constitutes northern Stikinia has hindered the development of ideas concerning the tectonic evolution of the northern Cordillera. To address this problem I suggest that the current terrane nomenclature of the Cordillera be changed such that neither the Lewes River Group nor the Klotassin Suite are included in, or are used to define, Stikinia.

If the Lewes River Group and the Klotassin Suite are not part of Stikinia, what then is their terrane affinity? In Whitehorse Trough Lewes River Group strata unconformably overlie fragments of former oceanic crust thought to be correlative with nearby Cache Creek Terrane. This relationship suggests that the Whitehorse Trough, including the Lewes River Group, should be included in Cache Creek Terrane. In northern British Columbia Gabrielse (1991) has included Whitehorse Trough strata carried in the hangingwall of the King Salmon fault in the Cache Creek Terrane, consistent with this interpretation. The inclusion of Lewes River Group in Cache Creek Terrane is strong evidence in support of the suggestion that a volcanic arc developed on Cache Creek in the Late Triassic (Thorstad and Gabrielse, 1986). The Klotassin Suite should not be accorded terrane status. The suite post-dates tectonism related to the collision of Nisling Assemblage with another terrane, probably Cache Creek, and constitutes part of a pan-Intermontane magmatic-volcanic sequence.

Nisling Assemblage, Yukon-Tanana Terrane and Stikinia are inferred to have formed a Paleozoic microcontinent that fragmented in the Triassic. These correlations and suggested terrane relations await testing by further comparative mapping, geochronological, and geochemical studies of these tectonic assemblages.

REFERENCES

Baadsgaard, H., and Lerbekmo, J.F., 1983. Rb - Sr and U - Pb dating of bentonites. Can. J. Earth Sci., 20, p. 1282-1290.

Barbarin, B., 1988. Field evidence for successive mixing and mingling between the Piolard Diorite and the Saint-Julien-LaVetre Monzogranite (Nord-Forez, Massif Central, France). Can. J. Earth Sci., p. 49-59.

Bateman, P.C., Busacca, A.J., and Sawka, W.N., 1983. Cretaceous deformation in the western foothills of the Sierra Nevada, California. Bull. Geol. Soc. Amer., 94, p. 30-42.

Bateman, R., 1985. Aureole deformation by flattening around a diapir during in situ ballooning: the Cannibal Creek granite. J. Geol., 93, p. 293-310.

Bence, A.E., and Albee, A.L., 1968. Empirical correction factors of the electron microanalysis of silicates and oxides. J. Geol., 76, p. 382-403.

Berman, R.G., 1988. Internally-consistent thermodynamic data for minerals in the system NaO-KO-CaO-MgO-FeO-FeO-AlO-SiO-TiO-HO-CO. J. Petrol., 29, p. 445-522.

Berman, R.G., Brown, T.H., and Greenwood, H.J., 1987. GEOCALC: Software for calculation and display of P-T-X phase diagrams. Amer. Mineral., 72, p. 861 862.

Brew, D.A., and Morrell, R.P., 1983. Intrusive rocks and plutonic belts of southeastern Alaska, U.S.A. in Roddick, J.A. (ed.), Circum-Pacific Plutonic Terranes, Geol. Soc. America, Mem. 159, p. 171-193.

Brown, D.A., Logan, J.M., Gunning, M.H., Orchard, M.J., and Bamber, W.E., 1991. Can. J. Earth Sci., 28, p. 958-972.

Bultman, T.R., 1979. Geology and tectonic history of the Whitehorse Trough west of Atlin, British columbia. Yale University, unpublished Ph.D. thesis, 284 p.

Burg, J.-P., 1991. Syn-migmatization way-up criteria. J. Structural Geol., 13.

Burg, J.-P., and Philippot, P., 1991. Asymmetric compositional layering of syntectonic metamorphic veins as way-up criterion. Geology, 19, p. 1112-1115.

Charlesworth, H.A.K., Guidos, J., Gold, C., and Wynne, D., 1989. TRIPOD 3.0, a microcomputer program for storing, retrieving, displaying and analysing orientation, stratigraphic and positional data from drillholes, outcrops and seismic lines. University of Alberta, unpublished manual, 80 p.

Cockfield, W.E., 1927. Aishihik Lake District, Yukon. Geol. Surv. Can., Sum. Rept. 1926, p. 1-13, reprinted in Bostock, H.S., 1957, Selected field reports of the Geological Survey of Canada, 1898-1933. Geol. surv. Can., Mem. 284, p. 558-569.

Copeland, P., Hodges, K.V., Harrison, T.M., LeFort, P., and Pecher, A., 1988. Rapid Pliocene uplift associated with the Main Boundary thrust, central Nepal: Geol. Soc. America., Abstracts with Programs, 20, p. A321.

Currie, L.D., 1992. Jurassic accretion of Nisling Terrane along the western margin of Stikinia, Coast Mountains, northwestern British Columbia (abstract). in Southern Cordillera Transect Workshop (Report no. 24) and Cordilleran Tectonics Workshop, Program and Abstracts, p. 89.

Currie, L.D., 1991. Geology of the Tagish Lake area, northern Coast Mountains, northwestern British Columbia. in Geol. Surv. Canada, Paper 91-1A, Current Research, Part A, Cordillera and Pacific margin, p. 147-154.

Cushing, G., Foster, H.L., and Garrison, T.M., 1984. Mesozoic age of metamorphism and thrusting in the eastern part of east-central Alaska (abstract). Trans. AGU, 65, p. 290-291.

Dickie, J.R., and Hein, F.J., 1990. A Pliensbachian submarine slope and conglomeratic gully-fill succession: Richtofen to Conglomerate Formation Transition (Laberge Group), Brute Mountain, Yukon. in Yukon Geology, 3, Indian and Northern Affairs Canada, Yukon Region, Whitehorse. p.

Dickie, J.R., and Hein, F.J., 1988. Facies and depositional setting of Laberge Conglomerates (Jurassic), Whitehorse Trough. *in* Yukon Geology, 2, Exploration and Geological services division, Yukon, Indian and Northern Affairs Canada, p. 26-32.

Dusel-Bacon, C., and Foster, H.L., 1990. New thermobarometric evidence for high pressure, medium temperature metamorphism of two subterranes of the Yukon Tanana composite terrane (YTT) in easternmost Alaska (Abstract). Geol. Assoc. Can. Program with Abstracts, 15, p. A35.

Eisbacher, G.H., 1976. Sedimentology of the Dezadeash flysch and its implications for strike-slip faulting along the Denali fault, Yukon Territory and Alaska. Can. J. Earth Sci., 13, p. 1495-1513.

Erdmer, P.E., 1991. Metamorphic terrane east of Denali fault between Kluane Lake and Kusawa Lake, Yukon Territory. in Current Research, Part E, Geol. Surv. Can. Pap 90-1E, p. 107-111.

Erdmer, P.E., 1990. Studies of the Kluane and Nisling assemblages in Kluane and Dezadeash map areas, Yukon. in Current Research, Part E, Geol. Surv. Can. Pap 90-1E, p. 107-111.

Erdmer, P.E., and 21 others, 1989. Lithoprobe transect proposal, unpublished, 25 p.

Evenchick, C.A., 1991. Geometry, evolution, and tectonic framework of the Skeena Fold Belt, north-central British Columbia. Tectonics, 10, p. 527-546.

Farrar, E., Clark, A.H., Archibald, D.A., and Way, D.C., 1988. Potassium-Argon age of granitoid plutonic rocks, southwest Yukon territory, Canada. Isochron/West, 51, p. 19-23.

Ferry, J.M., and Spear, F.S., 1978. Experimental calibration of the partitioning of Fe and Mg between biotite and garnet. Contributions to Mineralogy and Petrology, 66, p. 113-114.

Fuhrman, M.L., and Lindsley, D.H., 1988. Ternary-feldspar modeling and thermometry. Amer. Mineral., 73, p. 201-215.

Gabrielse, H., 1991. Late Paleozoic and Mesozoic terrane interactions in north-central British Columbia, Can. J. Earth Sci., 28, p. 947-957.

Gabrielse, H., and Reesor, J.E., 1974. The nature and setting of granitic plutonism in the central and eastern parts of the Canadian Cordillera. Pacific Geology, 8, p. 109-138.

Ganguly, J., and Saxena, S.K., 1984. Mixing properties of aluminosilicate garnets: Constraints from natural and experimental data, and applications to geothermobarometry. American Mineralogist, 69, p. 88-97.

Gapais, D., and Barbarin, B., 1986. Quartz fabric transition in a cooling syntectonic granite (Hermitage Massif, France). Tectonophysics, 125, p. 357-370.

Gehrels, G.E., McClelland, W.C., Samson, S.D., Patchett, P.J., and Jackson, J.L., 1990. Ancient continental margin assemblage in the Coast Mountains, southeast Alaska and northwest Canada. Geology, 18, p. 208-211.

Gehrels, G.E., McClelland, W.C., Jackson, J.L., Samson, S.D., and Patchett, J., 1989. Nisling terrane, a Proterozoic - Lower Paleozoic (?) continental margin assemblage, in and adjacent to the northern Coast Mountains Batholith. *in* Program and Abstracts, 1989 Cordilleran Tectonics Workshop, p. 2.

Ghent, E.K., Robbins, D.B., and Stout, M.Z., 1979. Geothermometry, geobarometry and fluid compositions of metamorphosed calc-silicates and pelites, Mica Creek, British Columbia. American Mineralogist, 64, p. 874-885.

Gordey, S.L. 1973. Petrology and structural relations of volcanic and basement rocks on the west side of Aishihik Lake Yukon Territory. Unpublished B.Sc. thesis, University of British Columbia, 69 p.

Hansen, V.L., Yukon-Tanana Terrane: a partial acquittal. Geology, 18, p. 365-369.

Hansen, V.L., Mortensen, J.K., and Armstrong, R.L., 1989. Pre-Jurassic ductile deformation and synchronous metamorphism of the Yukon-Tanana Terrane: geochronologic constraints from the Teslin suture zone, Yukon. Can. J. Earth Sci., 26, p. 2224-2235.

Harland, W.B., Armstrong, R.L., Cox, A.V., Craig, L.E., Smith, A.G., and Smith, D.G., 1990. A geologic time scale 1989. Cambridge University Press, Cambridge, 263 p.

Hart, C.J.R., and Radloff, J.K., 1990. Geology of Whitehorse, Alligator Lake, Fenwick Creek, Carcross and part of Robinson map areas (105D/11, 6, 3, 2, and 7). Indian and Northern Affairs Canada, Open File 1990-4, 113 p.

Heaman, L., and Parrish, R., 1991. U-Pb geochronology of accessory minerals. in Heaman, L., and Ludden, J.N. (eds.), G.A.C. short course handbook on applications of radiogenic isotope systems to problems in geology, p. 59-102.

Hodges, K.V., and Spear, F.S., 1982. Geothermometry, geobarometry and the Al_2SiO_5 triple point at Mt. Moosilauke, New Hampshire. Amer. Min., 67, p. 1118-1134.

Hutchison, W.W., 1970. Metamorphic framework and plutonic styles in the Prince Rupert region of the central Coast Mountains. Can. J. Earth Sci., 7, 376-405.

Jackson, J.L., Gehrels, G.E., Patchett, P.J., and Mihalynuk, M.G., 1991. Stratigraphic and isotopic link between the northern Stikine terrane and an ancient continental margin assemblage, Canadian Cordillera. Geology, 19, p. 1177-1180.

Kindle, E.D., 1952. Dezadeash map-area, Yukon Territory. Geol. Surv. Canada. Mem., 364, 68 p.

Krogh, T.E., 1982. Improved accuracy of U-Pb zircon ages by the creation of more concordant systems using an air abrasion technique. Geochim. Cosmochim. Acta, 46, p. 631-649.

Lanphere, M.A., 1978. Displacement history of the Denali fault system, Alaska and Canada. Can. J. Earth Sci., 15, p. 817-822.

Le Couteur, P.C., and Tempelman-Kluit, D.J., 1976. Rb/Sr ages and a profile of initial 87Sr/86Sr ratios for plutonic rocks across the Yukon Crystalline terrane. Can. J. Earth Sci., 13, p. 319-330.

Lynch, G.V., Pride, C., and Watson, P.I, 1983. Petrology and geochemistry of the Pattison Alaskite pluton. *in* Yukon Exploration and Geology 1982, Dept. Indian North. Affairs, Whitehorse, Yukon, p. 38-49.

Ludwig, K.R., 1980. Calculation of uncertainties of U-Pb isotope data. Earth Planet. Sci. Lett., 46, p. 212-220.

Marsden, H., and Thorkelson, D.J., 1992. Geology of the Hazelton volcanic belt in British Columbia: implications for the early to middle Jurassic evolution of Stikinia. Tectonics, in press.

McClelland, W.C., Anovitz, L.M., and Gehrels, G.E., 1991. Thermobarometric constraints on the structural evolution of the Coast Mountains batholith, central southeastern Alaska. Can. J. Earth Sci., 28, p. 912-928.

Mihalynuk, M.G., and Rouse, J.N., 1987. Preliminary geology of the Tutshi Lake area, northwestern British Columbia (104M/15). *in* British Columbia Ministry of Energy, Mines and Petroleum Resources, Geological Fieldwork, Pap. 1988-1, p. 217-231.

Monger, J.W.H., 1989. Overview of Cordilleran Geology. in Ricketts, B.D. (ed.), Western Canada Sedimentary Basin: a case history. Can. Soc. Petrol. Geol., Calgary, p. 9-32.

Monger, J.W.H., 1977. Upper Paleozoic rocks of northwestern British Columbia. in Report of activities, part A. Geol. Surv. Can. Pap., 77-1A, p. 255-261.

Monger, J.W.H., 1975. Upper Paleozoic rocks of the Atlin Terrane, northwestern B.C. and southcentral Yukon. Geol. Surv. Canada., Pap. 74-47, 63 p.

Monger, J.W.H., 1974. Paleozoic rocks of the Atlin terrane, northwestern British Columbia and south-central Yukon. Geol. Surv. Can. Pap., 74-47, 63 p.

Monger, J.W.H., and Berg, H.C., 1987. Lithotectonic terrane map of western Canada and southeastern Alaska. U.S. Geol. Surv. Misc. Field Stud. map, MF 1874-B.

Monger, J.W.H., and Church, B.N., 1977. Revised stratigraphy of the Takla Group, north-central British Columbia. Can. J. Earth Sci., 14, p. 318-326.

Monger, J.W.H., Price, R.A., and Tempelman-Kluit, D.J., 1982. Tectonic accretion and the origin of the two major metamorphic and plutonic welts in the Canadian Cordillera. Geology, 10, p. 70-75.

Morin, J.A., 1981. Geology and Mineralization of the Hopkins lake area, 115 H 2, 3, 6, 7. *in* Geology and Exploration, 1979-80., Dept. Indian Northern Affairs, Whitehorse, Yukon, p. 98-104.

Mortensen, J.K., 1992. Pre-mid-Mesozoic tectonic evolution of the Yukon-Tanana Terrane, Yukon and Alaska. Tectonics, 11, 4, p. 836-853.

Mortensen, J.K., 1990. Geology and U-Pb geochronology of the Klondike District, west-central Yukon Territory. Can. J. Earth Sci., 27, p. 903-914.

Mortensen, J.K., and Jilson, G.A., 1985. Evolution of the Yukon-Tanana terrane: Evidence from southeastern Yukon Territory. Geology, 13, p. 806-810.

Muller, J.E., 1967. Kluane Lake map area, Yukon Territory (115G, 115F(E1/2)). Geol. Surv. Can. Mem., 340, 137 p.

Nicholls, J., and Stout, M.Z., 1988. Picritic melts in Kilauea: Evidence from the 1967-1968 Halemaumau and Hilaka eruptions. J. Petrology, 29, p. 1031-1057.

Nokleberg, W.J., Jones, D.L., and Silberling, N.J., 1985. Origin and tectonic evolution of the Maclaren and Wrangellia terranes, eastern Alaska Range, Alaska. G.S.A. Bull., 96, p. 1251-1270.

Page, R.W., and Bell, T.H., 1986. Isotopic and structural responses of granite to successive deformation and metamorphism. J. Geol., 94, p. 365-379.

Parrish, R.R., Roddick, J.C., Loveridge, W.D., and Sullivan, R.W., 1987. Uranium lead analytical techniques at the geochronology laboratory, Geological Survey of Canada. Geol. Surv. Can. Pap., 87-2, p. 3-7.

Paterson, I.A., 1974. Geology of the Cache Cr. Group and Mesozoic rocks at the north end of the Stuart Lake Belt, central British Columbia. Geol. Surv. Canada Pap., 74-1B, p. 31-42.

Paterson, S.R., Vernon, R.H., and Tobisch, O.T., 1989. A review of criteria for the identification of magmatic and tectonic foliations in granitoids. J. Structural Geol., 11, p. 349-363.

Roddick, J.C., 1987. Generalized numerical error analysis with applications to geochronology and thermodynamics. Geochim. Cosmochim. Acta, 51, p. 2129-2135.

Roddick, J.A., and Hutchison, W.W., 1974. Setting of the Coast Plutonic Complex, British Columbia. Pacific Geology, 8, p. 91-108.

Samson, S.D., McClelland, W.C., Patchett, P.J., Gehrels, G.E., and Anderson, R.G., 1989. Evidence from Nd isotopes for mantle contributions to Phanerozoic crustal genesis in the Canadian Cordillera. Nature, 337, p. 705-709.

Souther, J.G., 1971. Geology and mineral deposits of Tulsequah map area, British Columbia (104K). Geol. Surv. Can. Mem., 362, 84 p.

Spear, F.S., and Cheney, J.T., 1989. A petrogenetic grid for pelitic schists in the system SiO_2-Al_2O_3-FeO-MgO-K_2O-H_2O. Contrib. Min. Pet., 1989.

Stanley, W.D., Labson, V.F., Nokleberg, W.J., Csejtey, B. Jr., and Fisher, M.A., 1990. The Denali fault system and Alaska Range of Alaska: Evidence for underplated Mesozoic flysch from magnetotelluric surveys. G.S.A. Bull., 102, p. 160-173.

Steiger, R.H., and Jager, E., 1977. Subcommission on geochronology: Conventions on the use of decay constants in geo- and cosmochronology. Earth Planet. Sci. Lett., 36, p. 359-362.

Sylvester, A.G., Oertel, G., Nelson, C.A., and Christie, J.M., 1978. Papoose Flat pluton: a granite blister in the Inyo Mountains, easter California. Bull. geol. Soc. Amer., 89, p. 1205-1219.

Tempelman-Kluit, D.J., 1981. Geology and mineral deposits of southern Yukon. *in* Yukon Geology and Exploration 1979-80. Dept. Indian Northern Affairs, Whitehorse, Yukon, p. 7-31.

Tempelman-Kluit, D.J., 1979. Transported cataclasite, ophiolite and granodiorite in Yukon: Evidence of arc-continent collision. Geol. Surv. Can., Pap. 79-14, 27 p.

Tempelman-Kluit, D.J., 1977b. Quiet Lake (105F) and Finlayson Lake (105G) map-areas, Yukon. Geol. Surv. Canada, Open File 486.

Tempelman-Kluit, D.J., 1976. The Yukon Crystalline Terrane: Enigma in the Canadian Cordillera. Geol. Soc. America Bull., 87, p. 1343-1357.

Tempelman-Kluit, D.J., 1974. Reconnaissance geology of Aishihik Lake, Snag and part of Stewart River map-areas, west-central Yukon Territory. Geol. Surv. Can., Pap. 73-14, 93 p.

Tempelman-Kluit, D.J., and Wanless, R.K., 1980. Zircon ages for the Pelly Gneiss and Klotassin granodiorite in western Yukon; Can. J. Earth Sci., 17, p. 297-306.

Tempelman-Kluit, D.J., and Wanless, R.K., 1975. Potassium - argon age determinations of metamorphic and plutonic rocks in the Yukon Crystalline terrane. Can. J. Earth Sci., 12, p. 1895-1909.

Thorstad, L.E., and Gabrielse, H., 1986. The Upper Triassic Kutcho Formation, Cassiar Mountains, north-central British Columbia. Geol. Surv. Can. Pap., 86 16, 53 p.

Tipper, H.W., and Richards, T.A., 1976. Jurassic stratigraphy and history of north central British Columbia. Geol. Surv. Can. Bull., 270, 58 p.

van der Heyden, P., 1990. Preliminary U-Pb dates and field observations from the eastern Coast Belt near 52°N, British Columbia. in Current Research, Part A, Geol. Surv. Can. Pap., 91-1A, p. 79-84.

van der Molen, I., and Peterson, M.S., 1979. Experimental deformation of partly melted granite. Contrib. Min. Pet., 70, p. 299-318.

Wang, C.-H., and Burnett, W.C., 1990. Holocene mean uplift rates across an active plate-collision boundary in Taiwan. Science, 248, p. 204-206.

Way, D.C., 1977. A reconnaissance study of granitoid plutonism in southwestern Yukon Territory. Queen's University, M.Sc. thesis, Kingston, Ontario, 177 p.

Werner, L.J., 1978. Metamorphic Terrane, Northern Coast Mountains west of Atlin Lake, British Columbia. *in* Current Research, Part A, Geol. Surv. Canada, Pap. 78-1A, p. 69-70.

Werner, L.J., 1977. Metamorphic Terrane, Northern Coast Mountains west of Atlin Lake, British Columbia. *in* Report of Activities, Part A, Geol. Surv. Canada, Pap. 77-1A, p. 267-269.

Wheeler, J.O., 1961. Whitehorse map-area, Yukon Territory (105D). Geological Survey of Canada, Memoir 312, 156 p.

Wheeler, J.O., and McFeely, P., 1991. Tectonic Assemblage map of the Canadian Cordillera and adjacent parts of the United States of America. in Gabrielse, H. and Yorath, C.J. (editors), Geology of Canada no. 4: Geology of the Cordilleran Orogen in Canada.

Woodsworth, G.J., Anderson, R.G., and Armstrong, R.L., 1991. Plutonic Regimes in the Canadian Cordillera. in Gabrielse, H. and Yorath, C.J. (editors), Geology of Canada no. 4: Geology of the Cordilleran Orogen in Canada, p. 491 - 532.

Zen, E., 1989. Plumbing the depths of batholiths. Amer. J. Sci., 289, p. 1137-1157.

Zen, E., and Hammarstrom, J.M., 1984. Magmatic epidote and its petrologic significance. Geology, 12, p. 515-518.

APPENDIX 2.1

Locations of all samples

SAMPLE no.	id	EASTING (m) UTM grid zone - 8V	NORTHING (m)	LONGITUDE	LATITUDE	ELEV (masl)	UNIT
1	85-1	379436	6825036	61°32'30.6"N	137°16'05.1"W	944	eJab
2	85-2	379100	6825072	61°32'31.3"N	137°16'27.9"W	917	eJab
3	85-3	379569	6823716	61°31'48.1"N	137°15'53.0"W	915	eJab
4	85-4	380038	6822564	61°31'11.4"N	137°15'18.6"W	915	eJab
5	85-5	393282	6806972	61°23'01.8"N	136°59'50.7"W	1015	Tfp
6	85-6	394842	6806912	61°23'01.4"N	136°58'05.5"W	1264	eJab
7	85-7	395301	6806042	61°22'33.8"N	136°57'32.8"W	1264	eJab
8	85-8	395930	6805978	61°22'32.3"N	136°56'50.4"W	1219	eJab
9	85-9	395953	6806322	61°22'43.4"N	136°56'49.5"W	1234	PPm
10	85-10	395349	6805542	61°22'17.7"N	136°57'28.6"W	1203	PPo
11	85-11	395168	6805458	61°22'14.8"N	136°57'40.6"W	1188	PPo
12	85-12	395168	6805458	61°22'14.8"N	136°57'40.6"W	1219	Tfp
13	85-13	393551	6788195	61°12'55.6"N	136°58'54.2"W	917	PPms
14	85-14	393438	6788454	61°13'03.9"N	136°59'02.3"W	917	PPms
15	85-15	393364	6789172	61°13'27.0"N	136°59'08.7"W	917	PPms
16	85-16	393418	6789694	61°13'43.9"N	136°59'06.1"W	917	PPm
17	85-17	393364	6791063	61°14'28.1"N	136°59'12.5"W	917	PPms

18	86-1	392550	6785500	61°11'27.6"N	136°59'55.7"W	930	Tfp
19	86-2	391830	6784551	61°10'56.2"N	137°00'41.9"W	1097	PPms
20	86-3	397506	6798053	61°18'17.8"N	136°54'48.6"W	1295	PPm
21	86-4	391081	6786401	61°11'55.2"N	137°01'35.9"W	1204	PPa
22	86-5	378007	6834112	61°37'22.0"N	137°18'03.5"W	1036	cJab
23	86-6	378643	6829061	61°34'39.6"N	137°17'08.3"W	960	Tv
24	86-7	373692	6831411	61°35'49.8"N	137°22'49.5"W	1128	cJab
25	86-8	374107	6832935	61°36'39.5"N	137°22'25.1"W	1234	Tv
26	86-9	376300	6826831	61°33'25.0"N	137°19'41.6"W	914	cJab
27	86-10	386810	6818988	61°29'23.3"N	137°07'32.8"W	1006	cJab
28	86-11	387152	6819524	61°29'41.0"N	137°07'10.9"W	1090	cJab
29	86-12	387152	6819524	61°29'41.0"N	137°07'10.9"W	1090	cJab
29	86-13	384239	6819627	61°29'41.2"N	137°10'27.9"W	930	cJab
30	86-14	385597	6817779	61°28'43.0"N	137°08'52.0"W	983	cJab
31	86-15	385633	6817856	61°28'45.5"N	137°08'49.8"W	1006	cJab
32	86-16	391175	6813180	61°26'20.2"N	137°02'25.6"W	1059	PPms
33	86-17	390560	6813110	61°26'17.3"N	137°03'06.9"W	1052	PPms
34	86-18	377722	6827974	61°34'03.5"N	137°18'08.1"W	922	Tv
35	86-19	376703	6827838	61°33'57.9"N	137°19'16.8"W	914	cJab
36	86-20	377292	6825440	61°32'41.2"N	137°18'31.1"W	922	cJab
37	86-21	378902	6822562	61°31'10.1"N	137°16'35.4"W	960	cJab
38	86-22	378902	6822562	61°31'10.1"N	137°16'35.4"W	960	cJab
39	86-23	378827	6822608	61°31'11.5"N	137°16'40.6"W	960	Tfp
40	86-24	378843	6822707	61°31'14.7"N	137°16'39.7"W	975	PPo
41	86-25	378697	6823490	61°31'39.8"N	137°16'51.5"W	945	cJab
42	86-26	378377	6823409	61°31'36.8"N	137°17'12.9"W	983	Tfp
43	86-27	378262	6823220	61°31'30.6"N	137°17'20.2"W	937	cJab
44	86-28	378094	6823184	61°31'29.2"N	137°17'31.5"W	945	cJab
45	86-29	377931	6822721	61°31'14.1"N	137°17'41.4"W	922	Tfp
46	86-30	378434	6822862	61°31'19.2"N	137°17'07.8"W	968	PPms

47	86-31	378622	6822602	61°31'11.0"N	137°16'54.4"W	960	PPo
48	86-32	379471	6823332	61°31'35.6"N	137°15'58.7"W	975	cJab
49	86-33	380614	6822791	61°31'19.4"N	137°14'40.2"W	960	cJab
50	86-34	380025	6822256	61°31'01.5"N	137°15'18.8"W	922	cJab
51	86-35	379926	6822318	61°31'03.3"N	137°15'25.6"W	922	cJab
52	86-36	383487	6818782	61°29'13.1"N	137°11'16.8"W	922	PPms
53	86-37	378615	6824631	61°32'16.6"N	137°16'59.7"W	917	Tfp
54	86-38	383448	6818811	61°29'14.0"N	137°11'19.5"W	922	PPms
55	86-39	383448	6818811	61°29'14.0"N	137°11'19.5"W	922	PPms
56	86-40	383545	6818646	61°29'08.7"N	137°11'12.6"W	922	PPo
57	86-41	383545	6818646	61°29'08.7"N	137°11'12.6"W	922	PPo
58	86-42	393963	6805012	61°21'59.2"N	136°59'00.8"W	1059	PPm
59	86-43	394594	6806180	61°22'37.5"N	136°58'20.7"W	1181	PPms
60	86-44	394626	6806943	61°23'02.2"N	136°58'20.1"W	1234	cJab
61	86-45	395396	6805570	61°22'18.6"N	136°57'25.5"W	1311	cJab
62	86-46	397438	6804735	61°21'53.6"N	136°55'06.4"W	1311	Q
63	86-47	397523	6804425	61°21'43.7"N	136°55'00.1"W	1471	cJab
64	86-48	398075	6804303	61°21'40.2"N	136°54'22.7"W	1562	PPo
65	86-49	404482	6851517	61°47'11.2"N	136°48'39.9"W	1341	cJll
66	86-50	402894	6851929	61°47'23.0"N	136°50'29.0"W	1402	cJll
67	86-51	410390	6848748	61°45'46.9"N	136°41'51.9"W	1364	cJab
68	86-52	398314	6849368	61°45'56.0"N	136°55'36.3"W	1402	Q
69	86-53	398460	6849473	61°45'59.5"N	136°55'26.6"W	1402	Q
70	86-54	400617	6848820	61°45'40.5"N	136°52'58.2"W	1425	Q
71	86-55	397926	6846919	61°44'36.5"N	136°55'57.8"W	1250	cJll
72	86-56	399272	6845466	61°43'50.9"N	136°54'23.2"W	1433	Q
73	86-57	399623	6845349	61°43'47.5"N	136°53'59.1"W	1425	PPo
74	86-58	399516	6845355	61°43'47.5"N	136°54'06.4"W	1440	PPo
75	86-59	342000	6856550	61°48'39.0"N	137°59'55.1"W	1181	cJll
76	86-60	393500	6857250	61°50'05.9"N	137°01'21.2"W	1227	PPa

77	86-61	397922	6855329	61°49'08.2"N	136°56'15.1"W	1219	PPms
78	86-62	399263	6853023	61°47'55.0"N	136°54'38.9"W	1521	cJll
79	86-63	397855	6852328	61°47'31.2"N	136°56'13.6"W	1288	PPm
80	86-64	397363	6851898	61°47'16.8"N	136°56'46.3"W	1314	PPa
81	86-65	397363	6851898	61°47'16.8"N	136°56'46.3"W	1314	PPa
82	86-66	398670	6842153	61°42'03.3"N	136°54'57.5"W	1417	cJab
83	86-67	398511	6842060	61°42'00.2"N	136°55'08.2"W	1394	cJab
84	86-68	385507	6819989	61°29'54.2"N	137°09'03.0"W	1005	cJab
85	86-69	376167	6835456	61°38'03.3"N	137°20'11.6"W	1005	cJab
86	86-74	384052	6818033	61°28'49.5"N	137°10'36.9"W	914	PPo
87	86-75	391650	6784348	61°10'49.5"N	137°00'53.6"W	1219	PPms
88	86-76	391410	6784425	61°10'51.7"N	137°01'09.8"W	1249	PPms
89	86-78	393959	6809569	61°24'26.4"N	136°59'10.4"W	1082	cJab
90	86-79	392783	6786205	61°11'50.6"N	136°[illegible]'41.6"W	922	KTrr
91	86-80	379949	6822362	61°31'04.8"N	137°15'24.1"W	915	cJab
92	86-82	376329	6826868	61°33'26.2"N	137°19'39.8"W	914	cJab
93	86-83	397926	6803613	61°21'17.8"N	136°54'31.3"W	1539	Tfp
94	86-84	397775	6803837	61°21'24.9"N	136°54'41.9"W	1532	PPa
95	86-85	397459	6804255	61°21'38.1"N	136°55'04.0"W	1433	cJab
96	87-1	393339	6787829	61°12'43.6"N	136°59'07.6"W	975	Q
97	87-2	393385	6787692	61°12'39.2"N	136°59'04.3"W	983	PPms
98	87-3	393530	6787465	61°12'32.0"N	136°58'54.1"W	1006	Tfp
99	87-4	393812	6787450	61°12'31.8"N	136°58'35.2"W	1021	KTrr
100	87-5	393941	6787519	61°12'34.2"N	136°58'26.7"W	1021	PPms
101	87-6	394196	6788340	61°13'00.9"N	136°58'11.3"W	975	Tfp
102	87-7	393481	6788688	61°13'11.5"N	136°58'59.9"W	983	PPm
103	87-8	393481	6788688	61°13'11.5"N	136°58'59.9"W	983	PPm
104	87-9	393511	6788810	61°13'15.4"N	136°58'58.1"W	975	PPms

105	87-10	395327	6792516	61°15'16.9"N	136°57'03.9"W	991	PPms
106	87-11	394693	6792384	61°15'12.0"N	136°57'46.1"W	1006	Q
107	87-12	394693	6792384	61°15'12.0"N	136°57'46.1"W	1006	Q
108	87-13	395261	6793073	61°15'34.8"N	136°57'09.4"W	1006	Q
109	87-14	397661	6791312	61°14'40.2"N	136°54'25.0"W	1067	PPa
110	87-15	397987	6791083	61°14'33.1"N	136°54'02.7"W	1219	PPa
111	87-16	397987	6791083	61°14'33.1"N	136°54'02.7"W	1219	PPa
112	87-17	397987	6791083	61°14'33.1"N	136°54'02.7"W	1219	Tfp
113	87-18	398437	6791264	61°14'39.4"N	136°53'32.9"W	1234	PPm
114	87-19	399128	6793184	61°15'42.1"N	136°52'50.3"W	1387	Q
115	87-20	399043	6793505	61°15'52.4"N	136°52'56.6"W	1394	KTrr
116	87-21	398300	6792000	61°15'03.1"N	136°53'43.5"W	1181	PPms
117	87-22	397140	6793906	61°16'03.5"N	136°55'05.0"W	1052	PPm
118	87-23	397592	6794468	61°16'22.1"N	136°54'35.8"W	1189	PPms
119	87-24	397369	6795560	61°16'57.2"N	136°54'52.9"W	1303	PPm
120	87-25	397354	6796374	61°17'23.4"N	136°54'55.5"W	1372	KTrr
121	87-26	397188	6797678	61°18'05.4"N	136°55'09.3"W	1341	PPm
122	87-27	393282	6789389	61°13'33.9"N	136°59'14.6"W	922	PPms
123	87-28	393289	6789335	61°13'32.2"N	136°59'14.1"W	922	PPms
124	87-29	393357	6789023	61°13'22.2"N	136°59'08.9"W	922	PPm
125	87-30	393280	6790736	61°14'17.4"N	136°59'17.5"W	922	PPms
126	87-31	393280	6790668	61°14'15.2"N	136°59'17.4"W	922	PPm
127	87-32	393317	6790561	61°14'11.8"N	136°59'14.7"W	922	Tfp
128	87-33	392927	6790068	61°13'55.5"N	136°59'39.8"W	922	PPa
129	87-34	393002	6789869	61°13'49.1"N	136°59'34.4"W	922	PPms
130	87-35	394855	6795485	61°16'52.3"N	136°57'41.5"W	1234	Tfp
131	87-37	393439	6796226	61°17'14.9"N	136°59'18.1"W	1158	Q
132	87-38	393563	6796375	61°17'19.8"N	136°59'10.0"W	1158	PPa
133	87-39	394802	6795493	61°16'52.5"N	136°57'45.1"W	1219	PPm
134	87-40	388278	6765137	61°00'25.6"N	137°03'58.5"W	762	KTrr

135	87-42	392422	6773358	61°04'55.3"N	136°59'39.5"W	914	KTrr
136	87-43	394569	6804046	61°21'28.6"N	136°58'18.1"W	1120	PPo
137	87-44	395106	6804739	61°21'51.5"N	136°57'43.3"W	1204	PPo
138	87-45	395452	6805442	61°22'14.5"N	136°57'21.5"W	1273	PPo
139	87-46	395328	6805530	61°22'17.2"N	136°57'30.0"W	1295	PPms
140	87-47	395359	6805508	61°22'16.6"N	136°57'27.9"W	1295	PPms
141	87-48	394750	6807000	61°23'04.2"N	136°58'11.9"W	1280	eJab
142	87-49	394750	6807000	61°23'04.2"N	136°58'11.9"W	1280	eJab
143	87-50	394902	6804413	61°21'40.8"N	136°57'56.4"W	1196	PPms
144	87-51	395104	6805639	61°22'20.5"N	136°57'45.3"W	1219	PPms
145	87-52	391289	6793934	61°15'58.7"N	137°01'37.6"W	1029	Q
146	87-53	391859	6793898	61°15'58.1"N	137°00'59.3"W	1036	PPms
147	87-54	392877	6794601	61°16'21.8"N	136°59'52.4"W	1151	Q
148	87-55	393007	6795100	61°16'38.1"N	136°59'44.7"W	1196	PPms
149	87-56	392951	6795322	61°16'45.2"N	136°59'49.0"W	1196	PPa
150	87-57	392140	6794625	61°16'21.9"N	137°00'41.9"W	1097	PPms
151	87-58	390970	6795435	61°16'46.9"N	137°02'02.1"W	945	PPa
152	87-59	391465	6795536	61°16'50.6"N	137°01'29.1"W	975	PPm
153	87-60	391662	6795458	61°16'48.3"N	137°01'15.7"W	1006	Q
154	87-61	392257	6795688	61°16'56.3"N	137°00'36.3"W	1128	Tfp
155	87-62	392688	6796253	61°17'15.0"N	137°00'08.5"W	1219	Q
156	87-63	391787	6796528	61°17'23.0"N	137°01'09.6"W	1143	PPm
157	87-64	391178	6796421	61°17'18.9"N	137°01'50.2"W	1021	PPms
158	87-65	391147	6796368	61°17'17.2"N	137°01'52.2"W	1029	PPms
159	87-66	390315	6799690	61°19'03.7"N	137°02'55.0"W	991	Q
160	87-67	390789	6799245	61°18'49.8"N	137°02'22.3"W	1021	PPm
161	87-68	391580	6799457	61°18'57.4"N	137°01'29.6"W	1166	PPms
162	87-69	391112	6800403	61°19'27.5"N	137°02'03.0"W	1082	PPm
163	87-70	389889	6800302	61°19'23.0"N	137°03'25.0"W	968	KTrr
164	87-71	392313	6785057	61°11'13.0"N	137°00'10.7"W	945	Tfp

165	87-72	392319	6784989	61°11'10.8"N	137°00'10.1"W	945	PPm
166	87-73	392347	6784874	61°11'07.2"N	137°00'08.0"W	975	PPms
167	87-74	392377	6784539	61°10'56.4"N	137°00'05.3"W	1067	PPms
168	87-75	392064	6784166	61°10'44.0"N	137°00'25.5"W	1143	PPm
169	87-76	391442	6784530	61°10'55.1"N	137°01'07.8"W	1257	PPms
170	87-77	391207	6784915	61°11'07.3"N	137°01'24.4"W	1250	PPm
171	87-78	391395	6785139	61°11'14.8"N	137°01'12.2"W	1189	PPms
172	87-79	385963	6817767	61°28'43.0"N	137°08'27.3"W	975	cJab
173	87-80	385538	6817623	61°28'37.9"N	137°08'55.7"W	975	PPms
174	87-81	400118	6795707	61°17'04.5"N	136°51'48.7"W	1554	KTrr
175	87-82	392945	6778026	61°07'26.6"N	136°59'14.1"W	1066	KTrr
176	87-83	393292	6775798	61°06'14.9"N	136°58'46.4"W	1036	KTrr
177	87-84	396952	6803014	61°20'57.5"N	136°55'35.7"W	1280	PPo
178	87-85	397552	6803092	61°21'00.6"N	136°54'55.5"W	1334	PPo
179	87-86	397639	6803254	61°21'05.9"N	136°54'49.9"W	1417	PPo
180	87-88	398029	6804301	61°21'40.1"N	136°54'25.8"W	1570	PPo
181	87-90	432727	6842178	61°42'31.1"N	136°16'20.2"W	822	cJll
182	87-91	432727	6842178	61°42'31.1"N	136°16'20.2"W	822	TJgk
183	87-92	432693	6841067	61°41'55.2"N	136°16'21.0"W	777	cJll
184	87-93	431369	6839011	61°40'47.9"N	136°17'48.3"W	899	TJgk
185	87-94	431110	6838463	61°40'30.0"N	136°18'05.2"W	822	TJgk
186	87-95	430516	6838628	61°40'35.0"N	136°18'45.8"W	777	TJgk
187	87-96	430087	6838801	61°40'40.3"N	136°19'15.2"W	792	TJgk
188	87-97	429696	6839350	61°40'57.8"N	136°19'42.5"W	853	cJll
189	87-98	431223	6835865	61°39'06.2"N	136°17'54.0"W	1319	cJll
190	87-99	426970	6831220	61°36'33.3"N	136°22'36.2"W	1374	cJll
191	87-100	393243	6845769	61°43'54.8"N	137°01'14.3"W	1394	PPa
192	87-101	393548	6845557	61°43'48.0"N	137°00'53.1"W	1364	PPi
193	87-102	393670	6845497	61°43'46.5"N	137°00'44.7"W	1341	PPa
194	87-103	393670	6845497	61°43'46.5"N	137°00'44.7"W	1341	PPa

195	87-104	395537	6844285	61°43'09.2"N	136°58'35.1"W	1349	PPms
196	87-105	395979	6844199	61°43'06.8"N	136°58'04.8"W	1173	PPm
197	87-106	396123	6844216	61°43'07.5"N	136°57'55.0"W	1143	PPm
198	87-107	397900	6841489	61°41'41.1"N	136°55'48.6"W	1371	eJab
199	87-108	399144	6842358	61°42'10.4"N	136°54'25.7"W	1371	eJab
200	87-109	400545	6845058	61°43'38.9"N	136°52'55.7"W	1371	eJab
201	87-110	400955	6849576	61°46'05.2"N	136°52'36.7"W	1432	eJll
202	87-111	403746	6851632	61°47'14.2"N	136°49'30.3"W	1463	eJll
203	87-112	406922	6852929	61°47'58.9"N	136°45'56.1"W	1310	eJll
204	87-113	406597	6863509	61°53'40.4"N	136°46'38.0"W	1676	eJll
205	87-114	368565	6827037	61°33'22.4"N	137°28'25.7"W	1212	PPa
206	87-115	368772	6826275	61°32'58.0"N	137°28'09.7"W	1227	PPm
207	87-116	368892	6826153	61°32'54.3"N	137°28'01.3"W	1234	PPa
208	87-117	368836	6825728	61°32'40.5"N	137°28'04.0"W	1219	Q
209	87-118	368873	6825674	61°32'38.8"N	137°28'01.4"W	1219	Q
210	87-119	368560	6824234	61°31'51.9"N	137°28'18.8"W	1371	PPms
211	87-120	368749	6824338	61°31'55.5"N	137°28'06.3"W	1311	Ttp
212	87-121	368320	6824014	61°31'44.5"N	137°28'34.5"W	1402	PPms
213	87-122	366500	6824930	61°32'11.8"N	137°30'40.0"W	1420	PPms

APPENDIX 2.2 - SAMPLE DESCRIPTIONS

Sample no.	field id[a]	Description
1	85-1	unit[b]: eJab name: foliated to gneissic hornblende biotite granodiorite maj.[c]: qt, $pl_{(30)}$ min.: hbl, bi, ks, op, chl, ep, cc, sc acc.: tt
2	85-2	unit: eJab name: foliated hornblende granodiorite maj.: hbl, $pl_{(33)}$, qt min.: bi, ks, op, chl, ep, cc, sc acc.: al, ep, ap, tt, zi
3	85-3	unit: eJab name: leucocratic, foliated quartz monzonite maj.: $pl_{(25)}$, ks min.: hlb, bi, qt, op, chl, cc, ep, sc acc.: al, ep
4	85-4	unit: eJab name: foliated hornblende granodiorite maj.: hbl, pl, qt min.: ks, sc, op acc.:
5	85-5	unit: Tfp name: massive, dark green, ultramafic maj.: pl, ol, py min.: tr, op acc.:
6	85-6	unit: eJab name: foliated biotite hornblende quartz diorite maj.: hbl, $plag_{(40)}$ min.: bi, qt, op, sc, ep acc.: tt

7 85-7 unit: eJab
name: foliated biotite hornblende quartz diorite
maj.: qt, $pl_{(35)}$
min.: hbl, bi, op, sc, ep
acc.: tt

8 85-8 unit: eJab
name: foliated biotite granodiorite
maj.: $pl_{(25)}$, qt
min.: ks, bi, op, chl, ep, sc, cc
acc.: al, ep

9 85-9 unit: PPm
name: coarsely crystalline banded fetid tremolite diopside marble
maj.: cc, di
min.: tr, ep, qt, fs, sc, op
acc.: tt

10 85-10 unit: PPo
name: biotite augan granodiorite orthogneiss
maj.: qt, $pl_{(30)}$, ks
min.: bi, chl, sc, cc, gt, op
acc.: zi

11 85-11 unit: PPo
name: bioitite hornblende granodiorite orthogneiss
maj.: qt, pl, ks
min.: hbl, bi, chl, op
acc.: zi, ap

12 85-12 unit: Tfp
name: chloritized feldspar horblende porphyry
maj.: fs, qt, hbl
min.: chl, op
acc.: zi, tt, ap

13 85-13 unit: PPms
name: mica schist
maj.: qt, $bi_{1,2}$, $mu_{1,2}$, $pl_{(35)}$
min.: chl, sc, op
acc.: zi, to, ap

14 85-14 unit: PPms

name: andalusite staurolite mica schist
maj.: qt, $bi_{1,2}$, $mu_{1,2}$, fs
min.: ad_2, st, op, chl, sc
acc.: ap

15 85-15 unit: PPms
name: quartzose sillimanite mica schist
maj.: qt
min.: $bi_{1,2}$, $mu_{1,2}$, sil_4, fs, op, chl, sc
acc.: rt

16 85-16 unit: PPm
name: chloritized diopside marble
maj.: cc
min.: di, chl, op
acc.:

17 85-17 unit: PPms
name: andalusite cordierite staurolite sillimanite mica schist
maj.: qt
min.: fs, bi_2, mu_2, op, gt, st, sil_4, ad_2, cd_2, sc
acc.: tt, zi

18 86-1 unit: KTrr
name: quartz porphyritic biotite hornblende granodiorite
maj.: qt, fs
min.: bi, hbl, op, sc
acc.:

19 86-2 unit: PPms
name: sillimanite andalusite mica schist
maj.: qt, bi
min.: mu, fs, op, ad_4, sil_4
acc.:

20 86-3 unit: PPm
name: garnet diopside magnetite skarn
maj.: gt, di, mt
min.:
acc.:

21 86-4 unit: PPa

name: chloritized amphibolite breccia hosted in leucocratic pegmatite
maj.: hbl, chl, fs
min.: qt, bi, op, sc, ep
acc.: ap, tt

22 86-5 unit: eJab
name: weakly foliated hornblende granodiorite
maj.: hbl, fs, qz
min.: bi, op, chl
acc.: tt

23 86-6 unit: Tertiary volcanics
name: brown weathering, dark olive brown finely crystalline volcanics
maj.: hbl, fs
min.:
acc.:

24 86-7 unit: eJab
name: foliated and altered hornblende granodiorite
maj.: hbl, qt, fs
min.: chl, ep, sc, op
acc.: ap, tt

25 86-8 unit: Tfp
name: finely crystalline, leucocratic, brown weathering, vesicular, flow banded, rhyolitic volcanic
maj.: qt, fs
min.: op, sc, ep
acc.:

26 86-9 unit: eJab
name: K-feldspar megacrystic, foliated hornblende granodiorite
maj.: pl, qt, hbl
min.: ks, op, chl, sc, ep
acc.: tt, ap

27 86-10 unit: eJab
name: coarsely crystalline, pink and white micaceous pegmatite
maj.: ks, $pl_{(30)}$, qt
min.: mu, chl
acc.:

28 86-11 unit: eJab
name: sheared hornblende biotite granodiorite

maj.: bi, qt, fs
min.: hbl, fs, op, ep, sc, chl
acc.: ap, zi, ep, al, tt

29 86-12 unit: eJab
name: mafic hornblende biotite granodiorite
maj.: bi, qt, fs
min.: hbl, op, chl, sc
acc.: tt, ap, , ep, al

29 86-13 unit: eJab
name: chloritized foliated biotite hornblende granodiorite
maj.: hbl, qt, fs
min.: chl, bi, sc, op
acc.: tt, ap, ep, al

30 86-14 unit: eJab
name: leucocratic coarsely crystalline micaceouspegmatite
maj.: qt, fs
min.: bi, chl, sc, ep, sp, op
acc.:

31 86-15 unit: eJab
name: heavily altered foliated hornblende granodiorite
maj.: qt, fs, bi
min.: chl, cc, ep, sc
acc.:

32 86-16 unit: PPo
name: biotite granite orthogneiss
maj.: qt, $pl_{(30)}$
min.: bi, ks, op
acc.: al, tt, to

33 86-17 unit: PPo
name: biotite granite orthogneiss
maj.: qt, fs
min.: bi, op
acc.: al, ap

34 86-18 unit: Tfp
name: dark green, amygdoloidal feldspar porphyry
maj.: hbl, pl
min.: chl, qt

acc.:

35 86-19 unit: eJab
name: fissile, foliated chloritized biotite granodiorite
maj.: bi, pl, qt
min.: ks, chl, cc
acc.:

36 86-20 unit: ?
name: pink weathering, medium grained, equicrystalline hornblende granite
maj.: ks, qt, pl
min.: hbl
acc.:

37 86-21 unit: eJab
name: well foliated hornblende granodiorite
maj.: hbl, fs, qt
min.: bi, op, chl
acc.:

38 86-22 unit: eJab
name: hornblende biotite foliated to gneissic granodiorite
maj.: hbl, qt, fs
min.: bi, op, chl, sc
acc.: al, ep, zi, ap, tt

39 86-23 unit: Tfp
name: leucocratic, finely crystalline, siliceous dyke
maj.: qt, fs
min.: op, cc, sc, chl
acc.:

40 86-24 unit: PPo
name: fine grained quartzo-feldspathic biotite schist / biotite granite orthogneiss
maj.: bi, qt, fs
min.:
acc.: ap

41 86-25 unit: eJab
name: gneissic hornblende granodiorite
maj.: bhl, qt, fs
min.: bi, op, chl, sc, cc, ep

acc.: tt, ap, al, ep

42 86-26 unit: Tfp
name: fractured and altered diabase dyke
maj.:
min.:
acc.:

43 86-27 unit: eJab
name: finely crystalline mafic, biotite microdiorite enclave
maj.: bi, fs
min.: qt, op, sc, ep, chl
acc.: al, ep, tt, ap, zi

44 86-28 unit: eJab
name: blastomylonitic micaceous quartz hornblende schist
maj.: qt, hbl, fs
min.: bi, cc, sc, chl
acc.: tt, ap

45 86-29 unit: Tfp
name: dark green weathering, phenocrystic, diabase dyke
maj.: hbl, pl, op
min.: cc
acc.:

46 86-30 unit: PPo
name: biotite hornblende granite orthogneiss
maj.: qt, $pl_{(30)}$, ks, hbl
min.: bi, op, sc
acc.: al, ep, ap, tt

47 86-31 unit: PPo
name: hornblende granodiorite orthogneiss
maj.: hb, fs
min.: qt, bi, op, ep, cc, chl, sc
acc.: ap

48 86-32 unit: eJab
name: amphibolitic quartz diorite gneiss
maj.: hbl, fs
min.: qt, bi, chl, sc, cc
acc.: al, ep, tt, ap, zi

49 86-33 unit: eJab
name: gneissic, mafic, hornblende granodiorite with folded leucocratic aplite veins
maj.: hbl, qt, fs
min.: bi, op, sc, chl, cc
acc.: tt, ap, al, ep

50 86-34 unit: eJab
name: migmatic hornblende orthogneiss
maj.: hbl, qt, fs
min.: bi, op, ep, chl
acc.: tt, ap, al, ep

51 86-35 unit: eJab
name: banded green and red calc-silicate (inclusion)
maj.: ga, ep, qt
min.: di, fs, cc, sc
acc.:

52 86-36 unit: PPo
name: blastomylonitic feldspar augan gneiss
maj.: qt, fs
min.: bi, op, gt, mu, sc
acc.: ap

53 86-37 unit: Tfp
name: fractured and heavily jointed diabase dyke
maj.: pl
min.: chl, hbl
acc.:

54 86-38 unit: PPo
name: blastomylonitic feldspar augan gneiss
maj.: qt, $pl_{(36)}$, ks
min.: bi, op, chl, sc
acc.: al, tt

55 86-39 unit: PPo
name: blastomylonitic feldspar augan gneiss
maj.: qt, fs
min.: bi, op, gt, mu
acc.:

56 86-40 unit: PPo

name: altered hornblende granodiorite orthogneiss
maj.: hbl, fs, ep, qt
min.: bi, op, chl
acc.: ap

57 86-41 unit: PPo
name: hornblende granodiorite orthogneiss
maj.: hbl, fs, qt
min.: bi, ep, cc, chl, sc
acc.: zi, ap

58 86-42 unit: PPms
name: migmatitic sillimanite garnet mica schist
maj.: qt, bi_2
min.: $sil_{2,4}$, $pl_{(32)}$, op, gt, mu, ep, chl, sc
acc.: tt, to, ap

59 86-43 unit: PPo
name: garnetiferous hornblende granodiorite orthogneiss
maj.: fs, hbl, qt
min.: bi, gt
acc.:

60 86-44 unit: eJab
name: glassy, siliceous, finely laminated mylonite
maj.: qt, ks, pl
min.: bi, mu, sc, chl, ep
acc.:

61 86-45 unit: eJab
name: brown, feldspathic garnetiferous micaceous gneiss
maj.: $pl_{(28)}$, qt, ks
min.: bi, op, gt, cc, chl, sc
acc.:

62 86-46 unit: PPqtz
name: finely banded orthoquartzite
maj.: qt
min.: fs, op, ap, sc
acc.:

63 86-47 unit: eJab
name: heavily altered, megacrystic granodiorite
maj.: qt, fs

min.: sc, mu, op, ep
acc.: ap

64 86-48 unit: PPo
name: finely crystalline hornblende biotite granite orthogneiss
maj.: qt, gs, hb, bi
min.: op, ch, sc
acc.:

65 86-49 unit: ejll
name: orange weathering, finely crystalline, equigranular quartz monzonite
maj.: ks, pl, qt
min.: sc
acc.:

66 86-50 unit: eJll
name: equigranular, medium grained, well foliated, biotite quartz monzonite
maj.: pl, ks, qt
min.: bi, chl, sc, op
acc.:

67 86-51 unit: eJll
name: equigranular, orange weathering, pink quartz monzonite
maj.: fs, qt
min.: sc
acc.:

68 86-52 unit: PPms
name: micaceous quartzite
maj.: qt
min.: bi, $pl_{(28)}$, ks, op, mu, chl, sc
acc.: zi, to, ap

69 86-53 unit: PPms
name: sillimanite mica schist
maj.: bi, mu, qt
min.: qt, fs, gt, op, sil_2, sc
acc.: zi, ap

70 86-54 unit: PPms
name: quartzose garnet sillimanite mica schist
maj.: qt, bi

min.: mu, fs, op, sil, sc
acc.:

71 86-55 unit: eJll
name: highly altered pink weathering, miarolitic, finely crystalline leucocratic quartz monzonite
maj.: fs, qt
min.: sc, op
acc.:

72 86-56 unit: PPa
name: banded hornblende amphibolite
maj.: hbl
min.: bi, fs, qt, chl
acc.: tt, ap

73 86-57 unit: PPa
name: leucocratic hornblende biotite gneiss
maj.: qt, fs
min.: hbl, bi, gt, ep, chl
acc.: tt, zi ap

74 86-58 unit: PPa
name: leucocratic hornblende biotite gneiss
maj.: qt, fs
min.: hbl, bi, ep, sc
acc.: zi, ap, al

75 86-59 unit: eJll
name: orange weathering, finely crystalline, well foliated biotite quartz monzonite
maj.: qt, $pl_{(>10)}$, ks
min.: bi, op, chl, sc
acc.: zi

76 86-60 unit: PPa
name: weakly foliated hornblende amphibolite
maj.: hbl, $pl_{(54)}$
min.: ks, op, sc
acc.: ap

77 86-61 unit: PPms
name: crenulated sillimanite mica schist
maj.: bi_2, qt, mu_2

min.: fs, op, sil_2
acc.: to

78 86-62 unit: eJll
name: massive, orange weathering, quartz monzonite
maj.: fs, qt
min.:
acc.:

79 86-63 unit: PPm
name: diopside marble / skarn
maj.: di
min.: cc, tr, op
acc.:

80 86-64 unit: PPa
name: leucocratic, finely crystalline, quartz porphyritic meta-tuff
maj.: qt, fs
min.: hbl, ep, cc
acc.: ap

81 86-65 unit: PPa
name: augite hornblende amphibolite
maj.: hbl, ag
min.: chl
acc.: tt, ap

82 86-66 unit: eJab
name: leucocratic white to pink hornblende granodiorite
maj.: qt, fs
min.: hbl, sc, op
acc.:

83 86-67 unit: eJab
name: gneissic biotite hornblende granodiorite
maj.: qt, fs, hbl
min.: bi, op, chl, sc, cc
acc.: tt, ap, ep, al

84 86-68 unit: eJab
name: foliated biotite hornblende quartz diorite to granodiorite
maj.: hbl, fs, qt
min.: bi, op, chl, sc
acc.: zi, tt, ap

85 86-69 unit: eJab
name: weathered and chloritized foliated biotite hornblende granodiorite
maj.: hbl, fs, qt
min.: bi, op, chl, cc, sc
acc.: zi, tt, ap

86 86-74 unit: PPo
name: two mica banded augan granite orthogneiss
maj.: qt, fs
min.: bi, mu, gt, sc
acc.:

87 86-75 unit: PPms
name: sillimanite garnet mica schist
maj.: $bi_{1,2}$, $mu_{1,2}$, qt, $pl_{(33)}$
min.: ks, gt, op, $sil_{2,4}$, chl, sc
acc.:

88 86-76 unit: PPms
name: quartzose garnet biotite schist
maj.: qt, fs
min.: bi, op, gt, chl, sc
acc.: zi, ap

89 86-78 unit: eJab
name: leucocratic hornblende granodiorite
maj.: hbl, fs, qt
min.: op
acc.: zi, tt, ap

90 86-79 unit: KTrr
name: massive to mildly foliated mafic hornblende quartz diorite
maj.: hbl, fs, qt
min.: op, bi
acc.: zi, tt, ap

91 86-80 unit: eJab
name: migmatitic hornblende granodiorite with mafic hornblendite enclaves
maj.: hbl, fs, qt
min.: op, chl, sc
acc.: zi, tt, ap

92 86-82 unit: eJab
name: foliated K-spar megacrystic hornblende granodiorite
maj.: hbl, fs, qt
min.: op, chl, sc, ep
acc.: zi, tt, ap

93 86-83 unit: Tfp
name: flesh colored, feldspar and quartz porphyry
maj.: ks, qt
min.: sc
acc.:

94 86-84 unit: PPa
name: mafic biotite hornblende amphibolite
maj.: hbl, bi
min.: pl, op, ep, chl, sc
acc.: tt

95 86-85 unit: eJab
name: feldspathic augan gneiss
maj.: fs, qt,
min.: bi, op, gt
acc.:

96 87-1 unit: PPms
name: micaceous garnetiferous grey quartz gneiss
maj.: qt
min.: bi, fs, gt, op, chl
acc.: zi, ap

97 87-2 unit: PPms
name: migmatitic garnet biotite schist
maj.: qt, fs, $bi_{1,2}$
min.: gt, chl, sc
acc.: ap, al

98 87-3 unit: Tfp
name: finely crystalline biotite feldspar porphyry
maj.: fs
min.: bi, qt, op
acc.:

99 87-4 unit: KTrr?
name: coarsely crystalline hornblende feldspar porphyry
maj.: hbl, pl
min.:
acc.:

100 87-5 unit: PPms
name: andalusite biotite schist
maj.: $bi_{2,3}$, $pl_{(28)}$, qt
min.: op, ad_2, ks, chl, sc
acc.:

101 87-6 unit: Tfp
name: finely crystalline asicular hornblende porphyry
maj.: hbl, fs
min.: bi, op, qt, op
acc.: tt

102 87-7 unit: PPms
name: sillimanite (?) mica schist
maj.: qt, fs, $bi_{1,2}$
min.: $mu_{1,2}$, sil_4, chl, sc
acc.: zi, to, ap, tt

103 87-8 unit: PPa
name: hornblende amphibolite gneiss
maj.: hbl
min.: bi, pl, qt, ep, cc, chl, sc
acc.: tt

104 87-9 unit: PPms
name: migmatitic mica schist
maj.: qt, fl
min.: $bi_{1,2}$, $mu_{1,2}$, chl, sc
acc.: zi, to

105 87-10 unit: PPms
name: quartzose sillimanite garnet mica schist
maj.: qt, mu, bi
min.: fs, op, gt, $sil_{2,4}$, chl, sc
acc.: zi, to, ap

106 87-11 unit: PPms

name: quartzose kyanite garnet mica schist
maj.: qt, bi, mu
min.: fl, op, gt, ky, ch, sc
acc.:

107 87-12 unit: PPa
name: garnetiferous diopside calc-silicate
maj.: cc, di
min.: gt, ep, tr, chl
acc.: tt

108 87-13 unit: PPa
name: hornblende amphibolite gneiss
maj.: hbl
min.: pl, bi, qt, op, py, chl, sc
acc.: tt, zi, ap

109 87-14 unit: PPa
name: hornblende amphibolite gneiss
maj.: hbl
min.: bi, fs, qt, op, chl, sc
acc.: al, ap

110 87-15 unit: PPa
name: blastomylonitic hornblende amphibolite
maj.: hbl
min.: bi, fs, qt, op, ep, cc, chl, sc
acc.: ap

111 87-16 unit: PPa
name: hornblende amphibolite with biotite schist laminae
maj.: qt, fs, bi, hbl
min.: op, ep, sc
acc.: tt, zi, ap

112 87-17 unit: Tfp
name: hornblende feldspar porphyry
maj.: fs, hbl
min.: cc, chl, ep
acc.:

113 87-18 unit: PPm
name: banded fetid tremolite marble
maj.: cc

min.: tr, qt, fs, op, chl, sc
acc.: tt

114 87-19 unit: PPms
name: micaceous grey sillimanite quartz gneiss
maj.: qt, fs
min.: $bi_{2,4}$, $mu_{2,4}$, sil_{4}, chl, sc
acc.:

115 87-20 unit: Tfp?
name: coarsely crystalline hornblende gabbro
maj.: hbl, py, pl
min.: op
acc.:

116 87-21 unit: PPms
name: quartzose garnet mica schist
maj.: qt
min.: bi, fs, op, gt, mu, chl, sc
acc.: tt, zi

117 87-22 unit: PPm
name: tremolite diopside calc-silicate
maj.: di, tr, qt
min.: cc, fs, sc
acc.: tt

118 87-23 unit: PPms
name: tourmaline mica schist
maj.: $bi_{1,2}$, qt
min.: $pl_{(46)}$, ks, op, $mu_{1,2}$, chl, sc
acc.: zi, to, ap

119 87-24 unit: PPm
name: banded garnet diopside skarn
maj.: gt, di, qt, fs
min.: tr, chl sc,
acc.: tt

120 87-25 unit: KTrr
name: biotite granodiorite
maj.: bi, qt, fs
min.:
acc.:

121 87-26 unit: PPm
name: garnet tremolite diopside calc-silicate
maj.: di
min.: phl, fs, qt, gt, tr, chl, sc
acc.: tt

122 87-27 unit: PPms
name: biotite schist
maj.: $bi_{1,2,4}$
min.: qt, fs, gt, $cd_{2?}$, chl, sc, op
acc.: zi, ap

123 87-28 unit: PPms
name: andalusite mica schist
maj.: qt, bi
min.: $pl_{(34)}$, ks, op, mu, $ad_{2?}$, sil_4, chl, sc
acc.: zi, ap

124 87-29 unit: PPm
name: coarsely crystalline banded diopside marble
maj.: cc
min.: phl, qt, tr, di, chl, sc
acc.:

125 87-30 unit: PPms
name: mica schist
maj.: $bi_{1,2}$, $mu_{1,2}$, qt
min.: $pl_{(32)}$, ks, op, sc
acc.: zi, to, ap

126 87-31 unit: PPm
name: tremolite diopside calc-silicate
maj.: qt, tr, di
min.: fs, ep, cc, chl, sc
acc.: tt

127 87-32 unit: Tfp
name: hornblende porphyry
maj.: hbl, fs
min.:
acc.:

128 87-33 unit: PPa

name: fine grained hornblende amphibolite
maj.: hbl, fs
min.: bi, qt, chl, sc
acc.: ap

129 87-34 unit: PPms
name: kyanite mica schist
maj.: bi, qt, fs
min.: $pl_{(34)}$, ks, mu, st, ky, cd_{2}, sc
acc.: rt

130 87-35 unit: Tfp
name: quartz feldspar porphyry
maj.: fs, qt
min.:
acc.:

131 87-37 unit: PPms
name: crenulated mica schist
maj.: qt, $mu_{2,3}$
min.: bi_{2}, fs, op, chl, sc
acc.: tt

132 87-38 unit: PPa
name: banded hornblende amphibolite
maj.: hbl
min.: bi, pl, qt, op, ep, chl, sc
acc.: tt

133 87-39 unit: PPm
name: altered diopside marble
maj.: cc
min.: qt, di, sc, chl
acc.:

134 87-40 unit: KTrr
name: finely crystalline hornblende biotite granodiorite
maj.: bi, $pl_{(12)}$, qt
min.: hbl, ks, op, sc
acc.: zi, tt, ap

135 87-42 unit: KTrr
name: nebulitic biotite granite with minor mafic biotite rich enclaves

maj.: bi, fs, qt
min.: sc
acc.: zi, tt, ap

136 87-43 unit: PPo
name: biotite muscovite graniteorthogneiss
maj.: qt, fs
min.: mu, bi, op, sc, chl, cc
acc.: ap, zi

137 87-44 unit: PPo
name: leucocratic two mica granite orthogneiss
maj.: qt, fs
min.: bi, mu, op, sc
acc.:

138 87-45 unit: PPo
name: chloritized biotite feldspar orthogneiss
maj.: qt, fs
min.: bi, chl, op, chl
acc.:

139 87-46 unit: PPms
name: garnet amphibolite schist
maj.: hbl, qt, fs
min.: op, gt, chl, sc
acc.: tt, zi, ap

140 87-47 unit: PPms
name: mica schist with thin amphibolite laminae
maj.: qt, fs, bi
min.: hbl, op, gt, mu
acc.:

141 87-48 unit: eJab
name: heavily altered finely crystalline, biotite hornblende granodiorite
maj.: hbl, qt, fs
min.: bi, chl, sc, ep, cc
acc.:

142 87-49 unit: eJab
name: gneissic, finely crystalline, biotite hornblende granodiorite
maj.: hbl, qt, fsp

min.: bi, op, sc, sch
acc.: ap, al, ep

143 87-50 unit: PPa
name: calc-silicate gneiss
maj.: di, cc, qt
min.: bi, bhl, op, fs, sc, chl, ep
acc.: tt, ap, zi

144 87-51 unit: PPms
name: sillimanite garnet mica schist
maj.: bi, fs, qt
min.: mu, op, gt, $sil_{2,4}$, chl
acc.: zi, to

145 87-52 unit: PPms
name: garnet mica schist
maj.: bi, qt
min.: fs, op, mu, gt
acc.: zi, to, ap

146 87-53 unit: PPms
name: kyanite garnet mica schist
maj.: $bi_{1,2,3}$, qt, $mu_{1,2,3}$
min.: fs, op, gt, ky, chl
acc.: zi, to, ap

147 87-54 unit: PPms
name: interfoliated garnet mica schist and amphibolite
maj.: qt, bi, hbl, fs
min.: op, gt, ep, chl, sc
acc.: tt, zi, ap

148 87-55 unit: PPms
name: garnet biotite schist
maj.: bi, qt, gt
min.: fs, op, chl, sc
acc.: zi, to

149 87-56 unit: PPa
name: banded amphibolite gneiss
maj.: hbl, qt
min.: fs, bi, op, ep, chl, sc
acc.: tt, ap

150 87-57 unit: PPms
name: garnet mica schist
maj.: qt, fs
min.: bi, gt, mu, op, ep, chl, sc
acc.: zi, ap

151 87-58 unit: PPa
name: dark green garnetiferous calc-silicate skarn
maj.: ga, di
min.: qt, op, fs, sc, ep, cc
acc.: tt

152 87-59 unit: PPm
name: coarsely crystalline banded grey and white marble
maj.: cc
min.: qt, op, di(?), sc
acc.:

153 87-60 unit:
name: PPms
maj.: micaceous quartzite
min.: qt
acc.: fs, mu, chl

154 87-61 unit: Tfp
name: chloritized hornblende porphyry
maj.: hbl, pl
min.: chl, op
acc.:

155 87-62 unit: PPms
name: garnet mica quartzite
maj.: qt
min.: bi, fs, op, mu, gt, chl, sc
acc.: zi, to, ap

156 87-63 unit: PPm
name: gneissic diopside hornblende marble - calc silicate
maj.: hbl, qt, di
min.: ph, ep, cc, chl, sc
acc.: tt, zi, ap

157 87-64 unit: PPms

name: micaceous quartzite
maj.: qt, mu
min.: bi, fs, op
acc.: zi

158 87-65 unit: PPms
name: andalusite mica schist
maj.: qt, fs, $mu_{2,3}$, bi_2
min.: op, $ad_{2?}$, ep, sc
acc.: zi, to

159 87-66 unit: PPms
name: garnet mica schist
maj.: qt, $mu_{1,2}$
min.: $bi_{1,2}$, fs, op, gt, chl, sc
acc.: zi, to, ap

160 87-67 unit: PPm
name: interfoliated hornblende amphibolite and marble
maj.: hbl, cc
min.: qt, fs, chl, sc
acc.:

161 87-68 unit: PPms
name: quartzose sillimanite garnet mica schist
maj.: qt
min.: bi, $pl_{(34)}$, ks, op, mu, gt, sil_2, chl, sc
acc.: zi, to, ap

162 87-69 unit: PPm
name: coarsely crystalline banded white and grey tremolite marble
maj.: cc
min.: qt, tr, ph
acc.: tt

163 87-70 unit: KTrr
name: hornblende granodiorite with mafic enclaves
maj.: hbl, fs, qt
min.: op, chl, sc
acc.: zi, tt, ap

164 87-71 unit: Tfp
name: hornblende feldspar porphyry
maj.: hbl, fs

min.: chl, ep, op
acc.:

165 87-72 unit: PPm
name: coarsely crystalline banded green and white tremolite diopside marble
maj.: cc
min.: fs, qt, tr, di, sc
acc.: tt

166 87-73 unit: PPms
name: andalusite staurolite kyanite sillimanite garnet mica schist
maj.: qt, $mu_{2,4}$
min.: $bi_{2,4}$, fs, op, gt, st, ky, $ad_{2,4}$, sil_4, chl, sc
acc.: zi, to

167 87-74 unit: PPms
name: andalusite staurolite garnet mica schist
maj.: qt, fs, mu
min.: bi, op, gt, st, $ad_{2,4}$, chl, sc
acc.:

168 87-75 unit: PPms
name: crenulated sericitized porphyroblastic mica schist
maj.: qt, fs, mu
min.: bi, chl, sc
acc.: to, ap

169 87-76 unit: PPms
name: sericitized andalusite mica schist
maj.: qt
min.: bi, fs, mu, $sil?_4$, ad, chl, sc
acc.: tt, zi, to

170 87-77 unit: PPm
name: coarsely crystalline banded garnet tremolite diopside marble
maj.: cc
min.: qt, fs, gt, tr, di, chl, sc
acc.: tt

171 87-78 unit: PPms
name: andalusite staurolite sillimanite garnet mica schist
maj.: qt, mu
min.: bi, fs, op, gt, st, $ad_{2,4}$, sil_4, chl, sc

acc.: tt, zi, to, ap

172 87-79 unit: eJab
name: amphibolite schist
maj.: hbl, qt, fs
min.: bi, op, sc, chl
acc.: al, ep, ap, tt

173 87-80 unit: PPms
name: mica schist
maj.: qt,
min.: pl$_{(38)}$, ks, bi, mu, wp, gt, chl, sc
acc.:

174 87-81 unit: KTrr
name: biotite hornblende quartz diorite
maj.: pl
min.: hbl, bi, qt
acc.: zi, ap, chl, sc

175 87-82 unit: KTrr
name: hornblende granodiorite
maj.: hbl, fs, qt
min.: op, bi
acc.: zi, tt, ap

176 87-83 unit: KTrr
name: hornblende granodiorite
maj.: hbl, fs, qt
min.: op, bi
acc.: zi, tt, ap

177 87-84 unit: PPa
name: massive hornblende amphibolite
maj.: hbl, fs
min.: qt, op, ep, chl, sc
acc.:

178 87-85 unit: PPms
name: sillimanite garnet mica schist
maj.: qt, fs
min.: bi, mu, gt, op, sil$_2$, chl, sc
acc.:

179 87-86 unit: PPm
name: banded calcite marble and garnet diopside hornblende calc silicate
maj.: cc, hbl
min.: fs, qt, gt, ep, cc, tr, di, chl, sc
acc.:

180 87-88 unit: PPa
name: sericitized feldspar amphibolite gneiss
maj.: hbl, fs, sc
min.: qt, bi, chl
acc.:

181 87-90 unit: eJll
name: pink orange weathering, coarsely crystalline granite
maj.: qt, ks
min.: pl, ep, cc, sc
acc.:

182 87-91 unit: Trgk?
name: dark green micaceous feldspar porphyry
maj.: pl, qt
min.: hbl, bi
acc.:

183 87-92 unit: eJll
name: orange weathering massive K-spar megacrystic biotite monzonite
maj.: fs
min.: bi, qt, op, sc
acc.: zi, tt, ap

184 87-93 unit: Trgk
name: augite porphyritic volcanic breccia
maj.: ag, pl
min.: hbl, ep
acc.:

185 87-94 unit: Trgk
name: hornblende feldspar andesite breccia
maj.: ag, pl
min.: hbl, chl, op
acc.:

186 87-95 unit: Trgk
name: heavily altered dark green andesite
maj.: pl, ag
min.: hbl, ep
acc.:

187 87-96 unit: Trgk
name: pl, ag
maj.: hbl
min.:
acc.:

188 87-97 unit: eJIl
name: orange weathering massive K-spar megacrystic biotite quartz monzonite
maj.: fs, qt
min.: bi, op, sc
acc.: zi, tt, ap

189 87-98 unit: Trgk
name: dark green andesite
maj.: pl, ag
min.: hbl
acc.:

190 87-99 unit: Trgk
name: dark green andesite
maj.: pl, ag
min.: hbl
acc.:

191 87-100 unit: PPa
name: biotite amphibolite gneiss
maj.: hbl, fs, qt
min.: bi, cc, sc
acc.: tt, ap

192 87-101 unit:
name: finely crystalline white to grey biotite hornblende granite
maj.: qt, pl, ks
min.: bi, hbl, op, chl
acc.: ap

193 87-102 unit: PPa

name: garnet biotite hornblende amphibolite
maj.: hbl, fs
min.: qt, bi, op, gt, chl, sc
acc.:

194 87-103 unit: PPa
name: feldspar augan hornblende amphibolite
maj.: hlb, fs
min.: qt, op, chl, sc
acc.:

195 87-104 unit: PPms
name: sillimanite garnet mica schist
maj.: qt, mu
min.: bi, fs, op, sil$_4$, chl, sc
acc.: tt, zi to

196 87-105 unit: PPm
name: brown weathering diopside marble breccia
maj.: cc
min.: di, op, ep, chl
acc.:

197 87-106 unit: PPm
name: diopside marble
maj.: cc, di
min.: ph, fs, qt, op, ep, tr, sc
acc.: tt, ap

198 87-107 unit: eJab
name: foliated to gneissic biotite hornblende granodiorite to hornblende quartz diorite
maj.: hbl, fs, qt
min.: bi, op, chl, sc
acc.: zi, tt, ap,

199 87-108 unit: eJab
name: foliated to gneissic biotite hornblende granodiorite to hornblende quartz diorite
maj.: hbl, fs, qt
min.: bi, op, sc
acc.: zi, tt, ap,

200 87-109 unit: eJab

name: foliated to gneissic biotite hornblende granodiorite to hornblende quartz diorite
maj.: hbl, fs, qt
min.: bi, op, chl, sc, cc
acc.: zi, tt, ap,

201 87-110 unit: eJll
name: orange weathering massive feldspar porphyritic quartz monzonite
maj.: $pl_{(9)}$, ks, qt
min.: op, bi, sc
acc.: zi, tt, ap

202 87-111 unit: eJll
name: orange weathering massive feldspar porphyritic quartz monzonite
maj.: fs, qt
min.: op, sc
acc.: zi, tt, ap

203 87-112 unit: eJll
name: orange weathering massive feldspar porphyritic quartz monzonite
maj.: fs, qt
min.: op, bi, sc
acc.: zi, tt, ap

204 87-113 unit: eJll
name: orange weathering massive feldspar porphyritic quartz monzonite
maj.: fs, qt
min.: op, bi, sc
acc.: zi, tt, ap

205 87-114 unit: PPa
name: leucocratic micaceous augan mylonite
maj.: qt, fs
min.: bi, mu, op, chl, sc
acc.:

206 87-115 unit: PPm
name: mylonitized calcite marble
maj.: cc
min.: qt

acc.:

207 87-116 unit: PPa
name: biotite hornblende blastomylonite
maj.: hbl, fs, qt
min.: bi, op, ep, cc, chl, sc
acc.: tt, ap

208 87-117 unit: PPms
name: brown graphitic quartzite
maj.: qt
min.: $bi_{1,2}$, fs, op
acc.:

209 87-118 unit: PPms
name: micaceous brown graphitic quartzite
maj.: qt
min.: bi, fs, qp, mu, chl, sc
acc.:

210 87-119 unit: PPms
name: sericitized and altered mica schist
maj.: qt, sc
min.: bi, fs, chl
acc.: to

211 87-120 unit: Tfp
name: flesh colored quartz feldspar porphyry
maj.: qt, fs
min.: sc
acc.:

212 87-121 unit: PPms
name: quartzose staurolite mica schist
maj.: qt
min.: bi, fs, op, st, chl, sc
acc.:

213 87-122 unit: PPms
name: crenulated sillimanite staurolite kyanite garnet mica schist
maj.: bi, mu, qt
min.: fs, op, gt, st, sil_4, ky, chl, sc
acc.: zi, to

a - sample id refers to the number that was assigned to a sample when it was collected in the field. The id indicates the year the sample was collected, followed by a sequential number (e.g. 86-33 - the 33rd sample collected in 1986)

b - unit monikers are the same as those used on all maps and are defined in the text.

c - maj., min., acc.; major, minor, and accessory mineral constituents, respectively, of a sample.

APPENDIX 3.1
Geochronological Methods

Whole rock samples of between 15 and 30 kg were collected for the extraction of zircon and titanite separates. Sample locations are shown in Figure 3.1. Sample preparation followed Baadsgaard and Lerbeckmo (1983). Standard mineral separation techniques, including the use of a Wilfley table, a Frantz magnetic separator, and heavy liquids (ethylene-tetrabromide and methylene-iodide), were used to prepare zircon and titanite separates. Zircon separates were then acid washed, first by boiling in 7 N HNO_3 at 350 °C for 1 to 2 hours, and secondly by boiling in 12 N HCl at 275 °C for one hour. Finally, zircon separates were boiled in twice distilled 6 N HCl at 300 °C for one hour. Zircon separates processed at the GSC geochronology laboratory in Ottawa were strongly abraded prior to analysis (Krogh, 1982) to minimize the effects of Pb - loss related to surface weathering.

Samples analyzed at the University of Alberta were decomposed by heating in a Teflon bomb with an HF and HNO_3 solution (approximately 12:1 ratio) for 3 to 6 days at a temperature of 170 °C. The resulting solution was evaporated and the precipitate dissolved in 1 ml of 6 N HNO_3. To determine Pb and U concentrations a mixed ^{208}Pb - ^{235}U spike was added to the samples. In four of the samples (samples 2 - 5; Table 3.1; Appendix 3.2) Pb was separated out of solution by co-precipitation with Pb-free $Ba(NO_3)_2$ and was purified using a Dowex 1-X8 anion exchange resin in chloride form. Pb from the remaining samples was purified using an anion exchange column in chloride form. U from all samples was separated from solution using a cation exchange column in nitrate form. The Pb and U eluates were then evaporated. For mass spectrometric analysis, the Pb precipitate was taken up in phosphoric acid and was loaded on a silica gel substrate on single Re filaments. The U precipitate was taken up in nitric acid and loaded directly onto the side filament of a double Re filament. Pb and U were analyzed by conventional mass spectrometry using either a Micromass 30 or VG - 354 mass spectrometer. A Pb blank of less than 1.0 ng and a U blank of less than 0.4 ng was determined using repeated blank measurements. Accurate error analysis for bulk zircon separates, which are characterized by high and variable Pb blanks, is difficult, especially for $^{207}Pb/^{206}Pb$. The values used here are provided by replicate analyses (n=11) of concordant Campanian zircon from a bentonite horizon (Baadsgaard and Lerbeckmo, 1983); at the one sigma level (1σ) they are: $^{206}Pb/^{238}U$ - .61%; $^{207}Pb/^{235}U$ - 1.00%; $^{207}Pb/^{206}Pb$- 2.34%.

Zircon fractions A to E of the Nisling Assemblage orthogneiss, D to G of the Aishihik Batholith, and A to G of the pink quartz monzonite suite were analyzed at the GSC Geochronology Laboratory in Ottawa. Two titanite separates (fractions I and J, sample 86 - 82, Aishihik Batholith) were also analyzed at the GSC laboratory. Preparation techniques and analytical procedures have been described in Parrish et al. (1987). Measured blank levels were 0.016 to 0.043 ng for Pb, and less than 1 pg for U. Isotopic measurements were done on a Finnegan MAT 261 solid source mass spectrometer equipped with a fully adjustable multiple collector, electron multiplier, and operating software modified to permit simultaneous measurement of all five Pb masses.

All ages were calculated using the constants recommended by Steiger and Jager (1977). A numerical error propagation technique was used to calculate errors associated with individual analyses (Roddick, 1987). Discordia line fitting and calculation of concordia intercept ages and associated errors employed a modified York-II regression model (Parrish et al., 1987), and the algorithm of Ludwig (1980). All errors are quoted at the 2σ level. Age assignments follow Harland *et al.* (1989)

APPENDIX 3.2

Locations of samples collected for geochronological study

SAMPLE no.	id	EASTING (m)	NORTHING (m)	LONGITUDE	LATITUDE	ELEV (masl)	UNIT
		UTM grid zone - 8V					
Nisling Assemblage two mica orthogneiss							
1)	86-74	384052	6818033	61°28'49.5"N	137°10'36.9"W	914	PPo
Aishihik Batholith - Foliated hornblende granodiorite							
2)	86-82	376329	6826868	61°33'26.2"N	137°19'39.8"W	914	eJab
Long Lake Suite - Pink Quartz Monzonite							
3)	87-92	432693	6841067	61°41'55.2"N	136°16'21.0"W	777	eJll
Ruby Range Batholith							
4)	86-79	392783	6786205	61°11'50.6"N	136°59'41.6"W	922	KTrr
5)	87-40	388278	6765137	61°00'25.6"N	137°03'58.5"W	762	KTrr
6)	87-42	392422	6773358	61°04'55.3"N	136°59'39.5"W	914	KTrr
7)	87-70	389889	6800302	61°19'23.0"N	137°03'25.0"W	968	KTrr
8)	87-82	392945	6778026	61°07'26.6"N	136°59'14.1"W	1066	KTrr
9)	87-83	393292	6775798	61°06'14.9"N	136°58'46.4"W	1036	KTrr

APPENDIX 3.3

Geochronologic samples - mineral assemblages

Sample		Description
no.	field id[a]	

Nisling Assemblage two mica orthogneiss

1) 86-74
unit[b]: PPog
name: two mica banded augan granite orthogneiss
maj.[c]: qt, fs
min.: bi, mu, gt, sc
acc.: zi, tt

Aishihik Batholith - foliated hornblende granodiorite

2) 86-82
unit: eJab
name: foliated K-spar megacrystic hornblende granodiorite
maj.: hbl, fs, qt
min.: op, chl, sc, ep
acc.: zi, tt, ap

Long Lake Suite - pink quartz monzonite

3) 87-92
unit: eJll
name: orange weathering massive K-spar megacrystic biotite monzonite
maj.: fs
min.: bi, qt, op, sc
acc.: zi, tt, ap

Ruby Range Batholith

4) 86-79
unit: KTrr
name: massive to mildly foliated mafic hornblende quartz diorite
maj.: hbl, fs, qt
min.: op, bi
acc.: zi, tt, ap

5)	87-40	unit: KTrr name: finely crystalline hornblende biotite granodiorite maj.: bi, fs, qt min.: hbl, op, sc acc.: zi, tt, ap
6)	87-42	unit: KTrr name: nebulitic biotite granite with minor mafic biotite rich enclaves maj.: bi, fs, qt min.: sc acc.: zi, tt, ap
7)	87-70	unit: KTrr name: hornblende granodiorite with mafic enclaves maj.: hbl, fs, qt min.: op, chl, sc acc.: zi, tt, ap
8)	87-82	unit: KTrr name: hornblende granodiorite maj.: hbl, fs, qt min.: op, bi acc.: zi, tt, ap
9)	87-83	unit: KTrr name: hornblende granodiorite maj.: hbl, fs, qt min.: op, bi acc.: zi, tt, ap

---

a - sample id refers to the number that was assigned to a sample when it was collected in the field. The id indicates the year the sample was collected, followed by a sequential number (e.g. 86-33 - the 33rd sample collected in 1986)

b - unit monikers are the same as those used on all maps and are defined in the text.

c - maj., min., acc.; major, minor, and accessory mineral constituents, respectively, of a sample.

APPENDIX 4.1

TRIPOD

TRIPOD (Charlesworth *et al.*, 1988) is a computer program designed for the analysis and display of drillhole, outcrop and seismic data from deformed sedimentary terrains. TRIPOD has three main functions. These are:
i) to create databases using structural, stratigraphic and positional data from drillholes, outcrops and seismic sections, entered at the keyboard or imported as data files. Drillhole data can include deviation, intersection and dip-meter readings. Outcrop data can include coordinates, the exposed stratigraphic horizon, and the orientation of up to ten kinds of planar and linear structures (per outcrop).
ii) to retrieve data from a database according to geographic position, stratigraphic horizon, structural unit, structural type, etc.
iii) to display and analyze retrieved data. Orientations can be used, for example, to prepare contoured pi diagrams and rose diagrams and to calculate orientation parameters. Data can be displayed on maps. They can also be used to establish domains in which folding can be considered cylindrical, and to construct plots showing drillhole, outcrop and seismic data projected parallel to fold axes onto planes of any orientation and position. These plots can then be used to draw cross-sections. Data can be rotated before being processed which enables composite plots from areas with several cylindrically folded domains to be produced.

To use TRIPOD you begin with a Database Manager which enables you to create and edit a database and select which database is to be used. A Job Selector enables you to choose the way in which you want to display or analyze data. During a "worksession" you specify, by means of a Job Utility, what data are to be retrieved and how they are to be displayed and analyzed. The way you operate this Utility can be stored in a worksession record. The Worksession Manager enables you to create, copy and delete such records. A more complete description of the TRIPOD program is presented in Charlesworth *et al.* (1988).

APPENDIX 5.1

Locations of Nisling Assemblage samples

SAMPLE no.	id	EASTING (m) UTM grid zone - 8V	NORTHING (m)	LONGITUDE	LATITUDE	ELEV (masl)	UNIT
1	85-9	395953	6806322	61°22'43.4"N	136°56'49.5"W	1234	Ppm
2	85-10	395349	6805542	61°22'17.7"N	136°57'28.6"W	1203	Ppo
3	85-11	395168	6805458	61°22'14.8"N	136°57'40.6"W	1188	Ppo
4	85-13	393551	6788195	61°12'55.6"N	136°58'54.2"W	917	Ppms
5	85-14	393438	6788454	61°13'03.9"N	136°59'02.3"W	917	Ppms
6	85-15	393364	6789172	61°13'27.0"N	136°59'08.7"W	917	Ppms
7	85-16	393418	6789694	61°13'43.9"N	136°59'06.1"W	917	Ppm
8	85-17	393364	6791063	61°14'28.1"N	136°59'12.5"W	917	Ppms
9	86-2	391830	6784551	61°10'56.2"N	137°00'41.9"W	1097	Ppms
10	86-3	397506	6798053	61°18'17.8"N	136°54'48.6"W	1295	Ppm
11	86-4	391081	6786401	61°11'55.2"N	137°01'35.9"W	1204	Ppha
12	86-16	391175	6813180	61°26'20.2"N	137°02'25.6"W	1059	Ppo
13	86-17	390560	6813110	61°26'17.3"N	137°03'06.9"W	1052	Ppo
14	86-24	378843	6822707	61°31'14.7"N	137°16'39.7"W	975	Ppo
15	86-30	378434	6822862	61°31'19.2"N	137°17'07.8"W	968	Ppo
16	86-31	378622	6822602	61°31'11.0"N	137°16'54.4"W	960	Ppo
17	86-36	383487	6818782	61°29'13.1"N	137°11'16.8"W	922	Ppo

18	86-38	383448	6818811	61°29'14.0"N	137°11'19.5"W	922	Ppo
19	86-39	383448	6818811	61°29'14.0"N	137°11'19.5"W	922	Ppo
20	86-40	383545	6818646	61°29'08.7"N	137°11'12.6"W	922	Ppo
21	86-41	383545	6818646	61°29'08.7"N	137°11'12.6"W	922	Ppo
22	86-42	393963	6805012	61°21'59.2"N	136°59'00.8"W	1059	Ppms
23	86-43	394594	6806180	61°22'37.5"N	136°58'20.7"W	1181	Ppo
24	86-46	397438	6804735	61°21'53.6"N	136°55'06.4"W	1311	Ppqtz
25	86-48	398075	6804303	61°21'40.2"N	136°54'22.7"W	1562	Ppo
26	86-52	398314	6849368	61°45'56.0"N	136°55'36.3"W	1402	Ppms
27	86-53	398460	6849473	61°45'59.5"N	136°55'26.6"W	1402	Ppms
28	86-54	400617	6848820	61°45'40.5"N	136°52'58.2"W	1425	Ppms
29	86-56	399272	6845466	61°43'50.9"N	136°54'23.2"W	1433	Ppa
30	86-57	399623	6845349	61°43'47.5"N	136°53'59.1"W	1425	Ppa
31	86-58	399516	6845355	61°43'47.5"N	136°54'06.4"W	1440	Ppa
32	86-60	393500	6857250	61°50'05.9"N	137°01'21.2"W	1227	Ppa
33	86-61	397922	6855329	61°49'08.2"N	136°56'15.1"W	1219	Ppms
34	86-63	397855	6852328	61°47'31.2"N	136°56'13.6"W	1288	Ppm
35	86-64	397363	6851898	61°47'16.8"N	136°56'46.3"W	1314	Ppa
36	86-65	397363	6851898	61°47'16.8"N	136°56'46.3"W	1314	Ppa
37	86-74	384052	6818033	61°28'49.5"N	137°10'36.9"W	914	Ppo
38	86-75	391650	6784348	61°10'49.5"N	137°00'53.6"W	1219	Ppms
39	86-76	391410	6784425	61°10'51.7"N	137°01'09.8"W	1249	Ppms
40	86-84	397775	6803837	61°21'24.9"N	136°54'41.9"W	1532	Ppa
41	87-1	393339	6787829	61°12'43.6"N	136°59'07.6"W	975	Ppms
42	87-2	393385	6787692	61°12'39.2"N	136°59'04.3"W	983	Ppms
43	87-5	393941	6787519	61°12'34.2"N	136°58'26.7"W	1021	Ppms
44	87-7	393481	6788688	61°13'11.5"N	136°58'59.9"W	983	Ppms
45	87-8	393481	6788688	61°13'11.5"N	136°58'59.9"W	983	Ppa

46	87-9	393511	6788810	61°13'15.4"N	136°58'58.1"W	975	Ppms
47	87-10	395327	6792516	61°15'16.9"N	136°57'03.9"W	991	Ppms
48	87-11	394693	6792384	61°15'12.0"N	136°57'46.1"W	1006	Ppms
49	87-12	394693	6792384	61°15'12.0"N	136°57'46.1"W	1006	Ppm
50	87-13	395261	6793073	61°15'34.8"N	136°57'09.4"W	1006	Ppa
51	87-14	397661	6791312	61°14'40.2"N	136°54'25.0"W	1067	Ppa
52	87-15	397987	6791083	61°14'33.1"N	136°54'02.7"W	1219	Ppa
53	87-16	397987	6791083	61°14'33.1"N	136°54'02.7"W	1219	Ppa
54	87-18	398437	6791264	61°14'39.4"N	136°53'32.9"W	1234	Ppm
55	87-19	399128	6793184	61°15'42.1"N	136°52'50.3"W	1387	Ppms
56	87-21	398300	6792000	61°15'03.1"N	136°53'43.5"W	1181	Ppms
57	87-22	397140	6793906	61°16'03.5"N	136°55'05.0"W	1052	Ppm
58	87-23	397592	6794468	61°16'22.1"N	136°54'35.8"W	1189	Ppms
59	87-24	397369	6795560	61°16'57.2"N	136°54'52.9"W	1303	Ppm
60	87-26	397188	6797678	61°18'05.4"N	136°55'09.3"W	1341	Ppm
61	87-27	393282	6789389	61°13'33.9"N	136°59'14.6"W	922	Ppms
62	87-28	393289	6789335	61°13'32.2"N	136°59'14.1"W	922	Ppms
63	87-29	393357	6789023	61°13'22.2"N	136°59'08.9"W	922	Ppm
64	87-30	393280	6790736	61°14'17.4"N	136°59'17.5"W	922	Ppms
65	87-31	393280	6790668	61°14'15.2"N	136°59'17.4"W	922	Ppm
66	87-33	392927	6790068	61°13'55.5"N	136°59'39.8"W	922	Ppa
67	87-34	393002	6789869	61°13'49.1"N	136°59'34.4"W	922	Ppms
68	87-37	393439	6796226	61°17'14.9"N	136°59'18.1"W	1158	Ppms
69	87-38	393563	6796375	61°17'19.8"N	136°59'10.0"W	1158	Ppa
70	87-39	394802	6795493	61°16'52.5"N	136°57'45.1"W	1219	Ppm
71	87-43	394569	6804046	72°26'19.7"N	138°07'54.4"W	1120	PPo
72	87-44	395106	6804739	61°21'51.5"N	136°57'43.3"W	1204	Ppo
73	87-45	395452	6805442	61°22'14.5"N	136°57'21.5"W	1273	Ppo
74	87-46	395328	6805530	61°22'17.2"N	136°57'30.0"W	1295	Ppms
75	87-47	395359	6805508	61°22'16.6"N	136°57'27.9"W	1295	Ppms

76	87-50	394902	6804413	72°28'18.5"N	138°07'39.3"W	1196	PPms
77	87-51	395104	6805639	61°22'20.5"N	136°57'45.3"W	1219	Ppms
78	87-52	391289	6793934	61°15'58.7"N	137°01'37.6"W	1029	Ppms
79	87-53	391859	6793898	61°15'58.1"N	137°00'59.3"W	1036	Ppms
80	87-54	392877	6794601	61°16'21.8"N	136°59'52.4"W	1151	Ppms
81	87-55	393007	6795100	61°16'38.1"N	136°59'44.7"W	1196	Ppms
82	87-56	392951	6795322	61°16'45.2"N	136°59'49.0"W	1196	Ppa
83	87-57	392140	6794625	61°16'21.9"N	137°00'41.9"W	109[illegible]	Ppms
84	87-58	390970	6795435	61°16'46.9"N	137°02'02.1"W	94[illegible]	Ppms
85	87-59	391465	6795536	61°16'50.6"N	137°01'29.1"W	975	Ppm
86	87-60	391662	6795458	61°16'48.3"N	137°01'15.7"W	1006	Ppms
87	87-62	392688	6796253	61°17'15.0"N	137°00'08.5"W	1219	Ppms
88	87-63	391787	6796528	61°17'23.0"N	137°01'09.6"W	1143	Ppm
89	87-64	391178	6796421	61°17'18.9"N	137°01'50.2"W	1021	Ppms
90	87-65	391147	6796368	61°17'17.2"N	137°01'52.2"W	1029	Ppms
91	87-66	390315	6799690	61°19'03.7"N	137°02'55.0"W	991	Ppms
92	87-67	390789	6799245	61°18'49.8"N	137°02'22.3"W	1021	Ppm
93	87-68	391580	6799457	61°18'57.4"N	137°01'29.6"W	1166	Ppms
94	87-69	391112	6800403	61°19'27.5"N	137°02'03.0"W	1082	Ppm
95	87-72	392319	6784989	61°11'10.8"N	137°00'10.1"W	945	Ppm
96	87-73	392347	6784874	61°11'07.2"N	137°00'08.0"W	975	Ppms
97	87-74	392377	6784539	61°10'56.4"N	137°00'05.3"W	1067	Ppms
98	87-75	392064	6784166	61°10'44.0"N	137°00'25.5"W	1143	Ppms
99	87-76	391442	6784530	61°10'55.1"N	137°01'07.8"W	1257	Ppms
100	87-77	391207	6784915	61°11'07.3"N	137°01'24.4"W	1250	Ppm
101	87-78	391395	6785139	61°11'14.8"N	137°01'12.2"W	1189	Ppms
102	87-80	385538	6817623	61°28'37.9"N	137°08'55.7"W	975	Ppms
103	87-84	396952	6803014	61°20'57.5"N	136°55'35.7"W	1280	Ppa
104	87-85	397552	6803092	61°21'00.6"N	136°54'55.5"W	1334	Ppms
105	87-86	397639	6803254	61°21'05.9"N	136°54'49.9"W	1417	Ppm

106	87-88	398029	6804301	61°21'40.1"N	136°54'25.8"W	1570	Ppa
107	87-100	393243	6845769	61°43'54.8"N	137°01'14.3"W	1394	Ppa
108	87-102	393670	6845497	61°43'46.5"N	137°00'44.7"W	1341	Ppa
109	87-103	393670	6845497	61°43'46.5"N	137°00'44.7"W	1341	Ppa
110	87-104	395537	6844285	61°43'09.2"N	136°58'35.1"W	1349	Ppms
111	87-105	395979	6844199	61°43'06.8"N	136°58'04.8"W	1173	Ppm
112	87-106	396123	6844216	61°43'07.5"N	136°57'55.0"W	1143	Ppm
113	87-114	368565	6827037	61°33'22.4"N	137°28'25.7"W	1212	Ppa
114	87-115	368772	6826275	61°32'58.0"N	137°28'09.7"W	1227	Ppm
115	87-116	368892	6826153	61°32'54.3"N	137°28'01.3"W	1234	Ppa
116	87-117	368836	6825728	61°32'40.5"N	137°28'04.0"W	1219	Ppqtz
117	87-118	368873	6825674	61°32'38.3"N	137°28'01.4"W	1219	Ppqtz
118	87-119	368560	6824234	61°31'51.9"N	137°28'18.8"W	1371	Ppms
119	87-121	368320	6824014	61°31'44.5"N	137°28'34.5"W	1402	Ppms
120	87-122	366500	6824930	61°32'11.8"N	137°30'40.0"W	1420	Ppms

APPENDIX 5.2
NISLING ASSEMBLAGE SAMPLES: MINERAL ASSEMBLAGES

Sample no.	Sample field id[a]	Description
1	85-9	unit[b]: PPm name: coarsely crystalline banded fetid tremolite diopside marble maj.[c]: cc, di min.: tr, ep, qt, fs, sc, op acc.: tt
2	85-10	unit: PPog name: biotite augan granite orthogneiss maj.: qt, pl, ks min.: bi, chl, sc, cc, ga, op acc.: zi
3	85-11	unit: PPog name: bioitite hornblende granite orthogneiss maj.: qt, pl, ks min.: hbl, bi, chl, op acc.: zi, ap
4	85-13	unit: PPms name: mica schist maj.: qt, $bi_{1,2}$, $mu_{1,2}$, fs min.: chl, sc, op acc.: zi, to, ap
5	85-14	unit: PPms name: andalusite staurolite mica schist maj.: qt, $bi_{1,2}$, $mu_{1,2}$, fs min.: and_2, st, op, chl, sc acc.: ap
6	85-15	unit: PPms name: quartzose sillimanite mica schist maj.: qt min.: $bi_{1,2}$, $mu_{1,2}$, sil_4, fs, op, chl, sc

acc.: rt

7 85-16
unit: PPm
name: chloritized diopside marble
maj.: cc
min.: di, chl, op
acc.:

8 85-17
unit: PPms
name: andalusite cordierite staurolite sillimanite mica schist
maj.: qt
min.: fs, bi_2, mu_2, op, ga, st, si_4, ad_2, cd_2, sc
acc.: tt, zi

9 86-2
unit: PPms
name: sillimanite andalusite mica schist
maj.: qt, bi
min.: mu, fs, op, ad_4, sil_4
acc.:

10 86-3
unit: PPm
name: garnet diopside magnetite skarn
maj.: ga, di, mt
min.:
acc.:

11 86-4
unit: PPa
name: chloritized amphibolite breccia hosted in leucocratic pegmatite
maj.: hbl, chl, qt, fs
min.:
acc.:

12 86-16
unit: PPog
name: biotite granite orthogneiss
maj.: qt, fs
min.: bi, op
acc.: al, tt, to

13 86-17
unit: PPog
name: biotite granite orthogneiss
maj.: qt, fs
min.: bi, op
acc.: al, ap

14	86-24	unit: PPog(?) or PPbs name: fine grained quartzo-feldspathic biotite schist / biotite granite orthogneiss maj.: bi, qt, fs min.: acc.: ap
15	86-30	unit: PPog name: biotite hornblende granite orthogneiss maj.: qt, fs min.: bi, hb, op, sc acc.: al, ap
16	86-31	unit: PPog name: hornblende granodiorite orthogneiss maj.: hb, fs min.: qt, bi, op, ep, cc, chl, sc acc.: ap
17	86-36	unit: PPog name: blastomylonitic feldspar augan gneiss maj.: qt, fs min.: bi, op, gt, mu, sc acc.: ap
18	86-38	unit: PPog name: blastomylonitic feldspar augan gneiss maj.: qt, fs min.: bi, op acc.: al
19	86-39	unit: PPog name: blastomylonitic feldspar augan gneiss maj.: qt, fs min.: bi, op, gt, mu acc.:
20	86-40	unit: PPog name: altered hornblende granodiorite orthogneiss maj.: hbl, fs, ep, qt min.: bi, op, chl acc.: ap

21 86-41 unit: PPog
name: hornblende granodiorite orthogneiss
maj.: hbl, fs, qt
min.: bi, ep, cc, chl, sc
acc.: zi, ap

22 86-42 unit: PPms
name: migmatitic sillimanite garnet mica schist
maj.: qt, bi_2
min.: $sil_{2,4}$, fs, op, gt, mu, ep, chl, sc
acc.: tt, to, ap

23 86-43 unit: PPog
name: garnetiferous hornblende granodiorite orthogneiss
maj.: fs, hbl, qt
min.: bi, gt
acc.:

24 86-46 unit: PPqtz
name: finely banded orthoquartzite
maj.: qt
min.: fs, op, ap, sc
acc.:

25 86-48 unit: PPog
name: finely crystalline hornblende biotite granite orthogneiss
maj.: qt, gs, hb, bi
min.: op, ch, sc
acc.:

26 86-52 unit: PPms
name: micaceous quartzite
maj.: qt
min.: bi, fs, op, mu, chl, sc
acc.: zi, to, ap

27 86-53 unit: PPms
name: sillimanite mica schist
maj.: bi, mu, qt
min.: qt, fs, ga, op, sil_2, sc
acc.: zi, ap

28 86-54 unit: PPms
name: quartzose garnet mica schist

maj.: qt, bi
min.: mu, fs, op, sil, sc
acc.:

29 86-56 unit: PPa
name: banded hornblende amphibolite
maj.: hbl
min.: bi, fs, qt, chl
acc.: tt, ap

30 86-57 unit: PPa
name: leucocratic hornblende biotite gneiss
maj.: qt, fs
min.: hbl, bi, gt, ep, chl
acc.: tt, zi ap

31 86-58 unit: PPa
name: leucocratic hornblende biotite gneiss
maj.: qt, fs
min.: hbl, bi, ep, sc
acc.: zi, ap, al

32 86-60 unit: PPa
name: weakly foliated hornblende amphibolite
maj.: hbl, pl
min.: ks, op, sc
acc.: ap

33 86-61 unit: PPms
name: crenulated sillimanite mica schist
maj.: bi_2, qt, mu_2
min.: fs, op, sil_2
acc.: to

34 86-63 unit: PPm
name: diopside marble / skarn
maj.: di
min.: cc, tr, op
acc.: sp

35 86-64 unit: PPa
name: leucocratic, finely crystalline, quartz porphyritic meta-tuff?
maj.: qt, fs

min.: hbl, ep, cc
acc.: ap

36 86-65 unit: PPa
name: augite hornblende amphibolite
maj.: hbl, ag
min.: chl
acc.: tt, ap

37 86-74 unit: PPog
name: two mica banded augan granite orthogneiss
maj.: qt, fs
min.: bi, mu, gt, sc
acc.:

38 86-75 unit: PPms
name: sillimanite garnet mica schist
maj.: $bi_{1,2}$, $mu_{1,2}$, qt, fs
min.: gt, op, $sil_{2,4}$, chl, sc
acc.:

39 86-76 unit: PPms
name: quartzose garnet biotite schist
maj.: qt, fs
min.: bi, op, ga, chl, sc
acc.: zi, ap

40 86-84 unit: PPa
name: mafic biotite hornblende amphibolite
maj.: hbl, bi
min.: pl, op, ep, chl, sc
acc.: tt

41 87-1 unit: PPms
name: micaceous garnetiferous grey quartz gneiss
maj.: qt
min.: bi, fs, ga, op, chl
acc.: zi, ap

42 87-2 unit: PPms
name: migmatitic garnet biotite schist
maj.: qt, fs, $bi_{1,2}$
min.: ga, chl, sc
acc.: ap, al

43 87-5 unit: PPms
name: andalusite biotite schist
maj.: $bi_{2,3}$, fs, qt
min.: op, ad_2, chl, sc
acc.:

44 87-7 unit: PPms
name: sillimanite (?) mica schist
maj.: qt, fs, $bi_{1,2}$
min.: $mu_{1,2}$, sil_4, chl, sc
acc.: zi, to, ap, tt

45 87-8 unit: PPa
name: hornblende amphibolite gneiss
maj.: hbl
min.: bi, pl, qt, ep, cc, chl, sc
acc.: tt

46 87-9 unit: PPms
name: migmatitic mica schist
maj.: qt, fl
min.: $bi_{1,2}$, $mu_{1,2}$, chl, sc
acc.: zi, to

47 87-10 unit: PPms
name: quartzose sillimanite garnet mica schist
maj.: qt, mu, bi
min.: fs, op, ga, $sil_{2,4}$, chl, sc
acc.: zi, to, ap

48 87-11 unit: PPms
name: quartzose kyanite garnet mica schist
maj.: qt, bi, mu
min.: fl, op, ga, ky, ch, sc
acc.:

49 87-12 unit: PPm
name: garnetiferous diopside calc-silicate
maj.: cc, di
min.: gt, ep, tr, chl
acc.: tt

50 87-13 unit: PPa

name: hornblende amphibolite gneiss
maj.: hbl
min.: pl, bi, qt, op, py, chl, sc
acc.: tt, zi, ap

51 87-14 unit: PPa
name: hornblende amphibolite gneiss
maj.: hbl
min.: bi, fs, qt, op, chl, sc
acc.: al, ap

52 87-15 unit: PPa
name: blastomylonitic hornblende amphibolite
maj.: hbl
min.: bi, fs, qt, op, ep, cc, chl, sc
acc.: ap

53 87-16 unit: PPa
name: hornblende amphibolite with biotite schist laminae
maj.: qt, fs, bi, hbl
min.: op, ep, sc
acc.: tt, zi, ap

54 87-18 unit: PPm
name: banded fetid tremolite marble
maj.: cc
min.: tr, qt, fs, op, chl, sc
acc.: tt

55 87-19 unit: PPms
name: micaceous grey sillimanite quartz gneiss
maj.: qt, fs
min.: $bi_{2,4}$, $mu_{2,4}$, sil_4, chl, sc
acc.:

56 87-21 unit: PPms
name: quartzose garnet mica schist
maj.: qt
min.: bi, fs, op, ga, mu, chl, sc
acc.: tt, zi

57 87-22 unit: PPm
name: tremolite diopside calc-silicate
maj.: di, tr, qt

min.: cc, fs, sc
acc.: tt

58 87-23 unit: PPms
name: tourmaline mica schist
maj.: $bi_{1,2}$, qt, fs
min.: op, $mu_{1,2}$, chl, sc
acc.: zi, to, ap

59 87-24 unit: PPm
name: banded garnet diopside skarn
maj.: ga, di, qt, fs
min.: tr, chl sc,
acc.: tt

60 87-26 unit: PPm
name: garnet tremolite diopside calc-silicate
maj.: di
min.: phl, fs, qt, ga, tr, chl, sc
acc.: tt

61 87-27 unit: PPms
name: biotite schist
maj.: $bi_{1,2,4}$
min.: qt, fs, gt, $cd_{2?}$, chl, sc, op
acc.: zi, ap

62 87-28 unit: PPms
name: andalusite mica schist
maj.: qt, bi
min.: fs, op, mu, $ad_{2?}$, sil_4, chl, sc
acc.: zi, ap

63 87-29 unit: PPm
name: coarsely crystalline banded diopside marble
maj.: cc
min.: phl, qt, tr, di, chl, sc
acc.:

64 87-30 unit: PPms
name: mica schist
maj.: $bi_{1,2}$, $mu_{1,2}$, qt
min.: fs, op, sc
acc.: zi, to, ap

65 87-31 unit: PPm
name: tremolite diopside calc-silicate
maj.: qt, tr, di
min.: fs, ep, cc, chl, sc
acc.: tt

66 87-33 unit: PPa
name: fine grained hornblende amphibolite
maj.: hbl, fs
min.: bi, qt, chl, sc
acc.: ap

67 87-34 unit: PPms
name: kyanite mica schist
maj.: bi, qt, fs
min.: mu, st, ky, $cd_{2,3}$, sc
acc.: rt

68 87-37 unit: PPms
name: crenulated mica schist
maj.: qt, $mu_{2,3}$
min.: bi_2, fs, op, chl, sc
acc.: tt

69 87-38 unit: PPa
name: banded hornblende amphibolite
maj.: hbl
min.: bi, pl, qt, op, ep, chl, sc
acc.: tt

70 87-39 unit: PPm
name: altered diopside marble
maj.: cc
min.: qt, di, sc, chl
acc.:

71 87-43 unit: PPo
name: biotite muscovite graniteorthogneiss
maj.: qt, fs
min.: mu, bi, op, sc, chl, cc
acc.: ap, zi

72 87-44 unit: PPog

name: leucocratic two mica granite orthogneiss
maj.: qt, fs
min.: bi, mu, op, sc
acc.:

73 87-45 unit: PPog
name: chloritized biotite feldspar orthogneiss
maj.: qt, fs
min.: bi, chl, op, chl
acc.:

74 87-46 unit: PPms
name: garnet mica schist
maj.: bi, qt, fs
min.: mu, op, ga, chl, sc
acc.: tt, zi, ap

75 87-47 unit: PPms
name: mica schist with thin amphibolite laminae
maj.: qt, fs, bi
min.: hbl, op, gt, mu
acc.:

76 87-50 unit: PPa
name: calc-silicate gneiss
maj.: di, cc, qt
min.: bi, bhl, op, fs, sc, chl, ep
acc.: tt, ap, zi

77 87-51 unit: PPms
name: sillimanite garnet mica schist
maj.: bi, fs, qt
min.: mu, op, gt, $sil_{2,4}$, chl
acc.: zi, to

78 87-52 unit: PPms
name: garnet mica schist
maj.: bi, qt
min.: fs, op, mu, ga
acc.: zi, to, ap

79 87-53 unit: PPms
name: kyanite garnet mica schist
maj.: $bi_{1,2,3}$, qt, $mu_{1,2,3}$

min.: fs, op, ga, ky, chl
acc.: zi, to, ap

80 87-54 unit: PPms
name: interfoliated garnet mica schist and amphibolite
maj.: qt, bi, hbl, fs
min.: op, ga, ep, chl, sc
acc.: tt, zi, ap

81 87-55 unit: PPms
name: garnet biotite schist
maj.: bi, qt, ga
min.: fs, op, chl, sc
acc.: zi, to

82 87-56 unit: PPa
name: banded amphibolite gneiss
maj.: hbl, qt
min.: fs, bi, op, ep, chl, sc
acc.: tt, ap

83 87-57 unit: PPms
name: garnet mica schist
maj.: qt, fs
min.: bi, gt, mu, op, ep, chl, sc
acc.: zi, ap

84 87-58 unit: PPms
name: mica schist
maj.: bi, qt, fs
min.: mu, op, chl, sc
acc.:

85 87-59 unit: PPm
name: coarsely crystalline banded grey and white marble
maj.: cc
min.: qt, op, di(?), sc
acc.:

86 87-60 unit: PPms
name: micaceous quartzite
maj.: qt
min.: fs, mu, chl
acc.:

87 87-62 unit: PPms
name: garnet mica quartzite
maj.: qt
min.: bi, fs, op, mu, gt, chl, sc
acc.: zi, to, ap

88 87-63 unit: PPm
name: gneissic diopside hornblende marble - calc silicate
maj.: hbl, qt, di
min.: ph, ep, cc, chl, sc
acc.: tt, zi, ap

89 87-64 unit: PPms
name: micaceous quartzite
maj.: qt, mu
min.: bi, fs, op
acc.: zi

90 87-65 unit: PPms
name: andalusite mica schist
maj.: qt, fs, $mu_{2,3}$, bi_2
min.: op, $ad_{2?}$, ep, sc
acc.: zi, to

91 87-66 unit: PPms
name: garnet mica schist
maj.: qt, $mu_{1,2}$
min.: $bi_{1,2}$, fs, op, gt, chl, sc
acc.: zi, to, ap

92 87-67 unit: PPm
name: interfoliated hornblende amphibolite and marble
maj.: hbl, cc
min.: qt, fs, chl, sc
acc.:

93 87-68 unit: PPms
name: quartzose sillimanite garnet mica schist
maj.: qt
min.: bi, fs, op, mu, ga, sil_2, chl, sc
acc.: zi, to, ap

94 87-69 unit: PPm

name: coarsely crystalline banded white and grey tremolite marble
maj.: cc
min.: qt, tr, ph
acc.: tt

95 87-72 unit: PPm
name: coarsely crystalline banded green and white tremolite diopside marble
maj.: cc
min.: fs, qt, tr, di, sc
acc.: tt

96 87-73 unit: PPms
name: andalusite staurolite kyanite sillimanite garnet mica schist
maj.: qt, $mu_{2,4}$
min.: $bi_{2,4}$, fs, op, ga, st, ky, $ad_{2,4}$, sil_{4}, chl, sc
acc.: zi, to

97 87-74 unit: PPms
name: andalusite staurolite garnet mica schist
maj.: qt, fs, mu
min.: bi, op, ga, st, $ad_{2,4}$, chl, sc
acc.:

98 87-75 unit: PPms
name: crenulated sericitized porphyroblastic mica schist
maj.: qt, fs, mu
min.: bi, chl, sc
acc.: to, ap

99 87-76 unit: PPms
name: sericitized andalusite mica schist
maj.: qt
min.: bi, fs, mu, $sil?_{4}$, ad, chl, sc
acc.: tt, zi, to

100 87-77 unit: PPm
name: coarsely crystalline banded garnet tremolite diopside marble
maj.: cc
min.: qt, fs, gt, tr, di, chl, sc
acc.: tt

101	87-78	unit: PPms name: andalusite staurolite sillimanite garnet mica schist maj.: qt, mu min.: bi, fs, op, ga, st, $ad_{2,4}$, sil_4, chl, sc acc.: tt, zi, to, ap
102	87-80	unit: PPms name: mica schist maj.: qt, fs min.: bi, mu, wp, gt, chl, sc acc.:
103	87-84	unit: PPa name: massive hornblende amphibolite maj.: hbl, fs min.: qt, op, ep, chl, sc acc.:
104	87-85	unit: PPms name: sillimanite garnet mica schist maj.: qt, fs min.: bi, mu, ga, op, sil_2, chl, sc acc.:
105	87-86	unit: PPm name: banded calcite marble and garnet diopside hornblende calc-silicate maj.: cc, hbl min.: fs, qt, ga, ep, cc, tr, di, chl, sc acc.:
106	87-88	unit: PPa name: sericitized feldspar amphibolite gneiss maj.: hbl, fs, sc min.: qt, bi, chl acc.:
107	87-100	unit: PPa name: biotite amphibolite gneiss maj.: hbl, fs, qt min.: bi, cc, sc acc.: tt, ap
108	87-102	unit: PPa

name: garnet biotite hornblende amphibolite
maj.: hbl, fs
min.: qt, bi, op, ga, chl, sc
acc.:

109 87-103 unit: PPa
name: feldspar augan hornblende amphibolite
maj.: hlb, fs
min.: qt, op, chl, sc
acc.:

110 87-104 unit: PPms
name: sillimanite garnet mica schist
maj.: qt, mu
min.: bi, fs, op, sil_4, chl, sc
acc.: tt, zi to

111 87-105 unit: PPm
name: brown weathering diopside marble breccia
maj.: cc
min.: di, op, ep, chl
acc.:

112 87-106 unit: PPm
name: diopside marble
maj.: cc, di
min.: ph, fs, qt, op, ep, tr, sc
acc.: tt, ap

113 87-114 unit: PPa
name: leucocratic micaceous augan mylonite
maj.: qt, fs
min.: bi, mu, op, chl, sc
acc.:

114 87-115 unit: PPm
name: mylonitized calcite marble
maj.: cc
min.: qt
acc.:

115 87-116 unit: PPa
name: biotite hornblende blastomylonite
maj.: hbl, fs, qt

		min.: bi, op, ep, cc, chl, sc acc.: tt, ap
116	87-117	unit: PPms name: brown graphitic quartzite maj.: qt min.: $bi_{1,2}$, fs, op acc.:
117	87-118	unit: PPms name: micaceous brown graphitic quartzite maj.: qt min.: bi, fs, qp, mu, chl, sc acc.:
118	87-119	unit: PPms name: sericitized and altered mica schist maj.: qt, sc min.: bi, fs, chl acc.: to
119	87-121	unit: PPms name: quartzose staurolite mica schist maj.: qt min.: bi, fs, op, st, chl, sc acc.:
120	87-122	unit: PPms name: crenulated sillimanite staurolite kyanite garnet mica schist maj.: bi, mu, qt min.: fs, op, ga, st, sil_4, ky, chl, sc acc.: zi, to

a - sample id refers to the number that was assigned to a sample when it was collected in the field. The id indicates the year the sample was collected, followed by a sequential number (e.g. 86-33 - the 33rd sample collected in 1986)
b - unit monikers are the same as those used on all maps and are defined in the text.
c - maj., min., acc.; major, minor, and accessory mineral constituents, respectively, of a sample.

APPENDIX 5.3
MICROPROBE DATA BASE

Garnet Analyses

sample no.	48	48	48	75	75	75	77	77	79
analysis	core	int	rim	core	int	rim	core	rim	core
SiO_2	37.22	36.89	37.64	37.24	37.17	37.07	37.30	37.62	37.40
Al_2O_3	19.74	20.14	19.91	20.89	20.68	20.33	20.26	20.80	20.48
FeO	35.29	36.08	35.28	32.22	31.52	30.23	30.90	33.46	35.39
MnO	0.44	0.14	0.93	4.66	7.09	8.98	5.70	2.22	0.20
MgO	1.43	1.93	2.14	3.49	2.57	1.99	1.47	2.45	2.82
CaO	6.42	5.12	4.95	1.93	1.86	1.75	5.41	5 00	4.82
Total	100.54	100.30	100.85	100.43	100.89	100.35	101.04	101.55	101.11
Cations per 12 oxygen									
Si	3.01	2.99	3.03	2.99	2.99	3.01	3.00	2.99	2.99
Al	1.88	1.95	1.89	1.96	1.95	1.95	1.92	1.94	1.92
Fe++	2.34	2.45	2.37	2.16	2.12	2.05	2.08	2.23	2.37
Mn	0.03	0.01	0.06	0.32	0.48	0.62	0.39	0.15	0.01
Mg	0.17	0.23	0.26	0.42	0.31	0.24	0.18	0.29	0.34
Ca	0.56	0.45	0.43	0.17	.16	0.15	0.47	0.43	0.41
Pyr	0.05	0.07	0.08	0.14	0.10	0.08	0.06	0.09	0.11
Alm	0.76	0.78	0.76	0.71	0.69	0.67	0.67	0.72	0.76
Sp	0.01	0.00	0.02	0.10	0.16	0.20	0.12	0.05	0.00
Gro	0.18	0.14	0.14	0.05	0.05	0.05	0.15	0.14	0.13

Garnet Analyses

sample no.	79	79	89	89	89	91	91	91	99	99
analysis	int	rim	core	int	rim	core	int	rim	core	rim
SiO_2		37.46	36.92	37.04	37.17	37.61	37.80	37.46	37.84	37.57
Al_2O_3		20.75	20.60	20.24	20.72	20.72	20.93	20.92	20.22	20.97
FeO		36.53	33.12	37.66	36.74	33.91	34.67	35.66	35.70	34.85
MnO		0.17	2.75	0.21	0.40	2.04	1.10	1.83	0.11	1.59
MgO		3.36	0.91	1.65	2.10	2.09	2.16	2.26	2.38	2.48
CaO		2.71	5.65	3.11	3.07	4.58	4.78	3.01	5.25	4.01
Total		100.98	99.95	99.91	100.20	100.95	101.44	101.14	101.50	101.47

Cations per 12 oxygen

Si		2.993	3.00	3.02	3.01	3.01	3.01	3.00	3.02	2.99
Al		1.95	1.97	1.94	1.97	1.95	1.96	1.97	1.90	1.96
Fe		2.44	2.25	2.57	2.48	2.2[illegible]	2.31	2.39	2.38	2.32
Mn		0.01	0.19	0.01	0.03	0.14	0.07	0.12	0.01	0.11
Mg		0.40	0.11	0.20	0.25	0.25	0.26	0.27	0.28	0.29
Ca		0.23	0.49	0.27	0.27	0.39	0.41	0.26	0.45	0.34
Pyr		0.13	0.04	0.07	0.08	0.08	0.08	0.09	0.09	0.10
Alm		0.79	0.74	0.84	0.82	0.74	0.76	0.79	0.76	0.76
Sp		0.00	0.06	0.00	0.01	0.05	0.02	0.04	0.00	0.03
Gro		0.08	0.16	0.09	0.09	0.13	0.13	0.08	0.14	0.11

Garnet Analyses

sample no.	102	102	108	108	120	120
analysis	core	rim	core	rim	core	rim
SiO_2	37.30	37.01	37.21	36.73	37.49	37.39
Al_2O_3	20.92	20.80	20.58	20.33	20.56	20.50
FeO	34.77	34.90	34.05	34.08	33.88	34.68
MnO	3.66	3.83	3.52	4.87	1.31	1.44
MgO	2.52	2.09	2.67	1.76	1.06	1.95
CaO	1.87	1.86	2.34	2.01	6.50	4.32
Total	101.04	100.49	100.37	99.78	100.80	100.28

Cations per 12 oxygen

Si	2.99	2.99	3.00	3.00	3.01	3.02
Al	1.97	1.98	1.96	1.96	1.97	1.95
Fe	2.33	2.36	2.30	2.33	2.27	2.34
Mn	0.25	0.26	0.24	0.34	0.08	0.10
Mg	0.30	0.25	0.32	0.21	0.13	0.23
Ca	0.16	0.16	0.20	0.18	0.56	0.37
Pyr	0.10	0.08	0.10	0.07	0.04	0.08
Alm	0.77	0.78	0.75	0.76	0.75	0.77
Sp	0.08	0.09	0.08	0.11	0.03	0.03
Gro	0.05	0.05	0.07	0.06	0.18	0.12

[illegible]iotite Analyses

sample no.	48	48	48	75	75	77	77	79	79	89
analysis	core	int	rim	core	rim	core	rim	core	rim	core
SiO_2	34.76	42.88	34.[illegible]6	35.45	35.37	35.99	35.27	34.37	35.23	34.04
TiO_2	2.08	0.95	2.02	2.91	2.84	1.71	0.84	1.75	0.94	2.43
Al_2O_3	19.63	30.61	19.55	19.87	20.34	20.37	20.83	18.89	19.40	18.97
FeO	21.87	7.32	22.38	20.41	20.20	18.65	19.33	22.22	22.35	22.88
MnO	0.04	0.05	0.06	0.28	0.43	0.20	0.26	0.03	0.01	0.04
MgO	8.21	2.87	8.00	8.01	7.89	10.20	10.07	9.81	9.45	6.98
CaO	0.01	0.04	0.02	0.00	0.16	0.00	0.01	0.18	0.17	0.00
Na_2O	0.17	0.04	0.14	0.10	0.13	0.21	0.06	0.28	0.19	0.14
K_2O	9.43	8.00	9.37	9.77	9.90	9.59	10.16	8.71	8.85	9.64
F	0.34	0.18	0.32	0.17	0.17	0.35	0.32	0.27	0.32	0.30
H_2O	3.28	6.79	3.38	2.78	2.42	2.43	2.66	3.26	2.88	4.32
Total	99.72	99.73	99.70	99.75	99.85	99.70	99.81	99.77	99.79	99.74
Total - F	99.58	99.65	99.57	99.68	99.78	99.55	99.68	99.66	99.66	99.61
Cations per 22 oxygen										
Si	5.31	6.01	5.29	5.34	5.31	5.36	5.30	5.26	5.35	5.31
Al^{iv}	2.69	1.989	2.71	2.66	2.69	2.65	2.71	2.75	2.65	2.69
Ti	0.24	0.10	0.23	0.33	0.32	0.19	0.10	0.20	0.11	0.29
Al	0.84	3.07	0.83	0.87	0.91	0.93	0.98	0.66	0.82	0.79
Fe_2	2.79	0.86	2.87	2.57	2.54	2.32	2.43	2.84	2.84	2.98
Mn	0.01	0.01	0.01	0.04	0.06	0.03	0.03	0.00	0.00	0.01
Mg	1.87	0.60	1.83	1.80	1.77	2.26	2.25	2.24	2.14	1.62
Ca	0.00	0.01	0.00	0.00	0.01	0.00	0.00	0.01	0.01	0.00
Na	0.05	0.01	0.04	0.03	0.04	0.06	0.02	0.08	0.01	0.42
K	1.84	1.43	1.83	1.88	1.90	1.82	1.95	1.70	1.71	1.92
F	0.16	0.08	0.16	0.08	0.08	0.17	0.15	0.13	0.15	0.15
OH	3.84	3.92	3.85	3.92	3.92	3.84	3.85	3.87	3.85	3.85
Phl	0.40	0.41	0.39	0.41	0.41	0.49	0.47	0.44	0.43	0.35
Ann	0.60	0.59	0.61	0.58	0.58	0.50	0.52	0.56	0.57	0.64
Mn	0.00	0.00	0.00	0.01	0.0[illegible]	0.01	0.01	0.00	0.00	0.01

Biotite Analyses

sample no.	89	91	91	99	99	102	102	108	108	120
analysis	rim	core	rim	core	rim	core	rim	core	rim	core
SiO_2	32.46	34.44	34.60	34.73	34.49	34.56	33.24	34.77	34.02	34.66
TiO_2	1.48	1.95	1.78	1.90	1.71	2.65	2.54	1.98	1.99	1.96
Al_2O_3	19.13	19.89	20.55	19.98	20.39	19.07	20.34	19.46	19.55	19.42
FeO	25.14	22.85	22.56	22.16	21.98	22.56	23.57	21.72	22.29	22.12
MnO	0.09	0.08	0.07	0.10	0.10	0.08	0.17	0.13	0.18	0.12
MgO	7.36	7.24	7.09	8.06	7.93	7.42	7.12	7.48	7.42	7.43
CaO	0.04	0.00	0.02	0.24	0.28	0.00	0.04	0.03	0.05	0.00
Na_2O	0.08	0.20	0.23	0.20	0.14	0.24	0.14	0.12	0.12	0.11
K_2O	9.14	9.06	8.94	9.26	9.02	9.21	8.02	9.36	8.97	9.60
F	0.34	0.25	0.25	0.32	0.37	0.29	0.39	0.37	0.36	0.40
H_2O	4.53	3.71	3.56	2.86	3.35	3.62	4.33	4.35	4.79	3.87
Total	99.79	99.67	99.65	99.81	99.76	99.70	99.70	99.77	99.74	99.69
Total - F	99.65	99.56	99.54	99.68	99.60	99.58	99.54	99.61	99.59	99.52
Cations per 22 oxygen										
Si	5.14	5.30	5.30	5.29	5.27	5.32	5.16	5.40	5.30	5.35
Al^{iv}	2.86	2.70	2.70	2.71	2.73	2.68	2.85	2.63	2.71	2.65
Ti	0.18	0.23	0.21	0.22	0.20	0.31	0.30	0.23	0.23	0.23
Al	0.71	0.91	1.01	0.88	0.95	0.78	0.87	0.91	0.88	0.88
Fe_2	3.33	2.94	2.89	2.82	2.81	2.90	3.03	2.81	2.90	2.86
Mn	0.01	0.01	0.01	0.01	0.01	0.01	0.02	0.02	0.02	0.02
Mg	1.74	1.66	1.62	1.83	1.81	1.70	1.65	1.72	1.72	1.71
Ca	0.01	0.00	0.00	0.01	0.02	0.0	0.01	0.01	0.01	0.00
Na	0.03	0.06	0.07	0.06	0.04	0.07	0.04	0.04	0.04	0.03
K	1.85	1.78	1.75	1.80	1.76	1.81	1.59	1.84	1.78	1.89
F	0.17	0.12	0.12	0.15	0.18	0.14	0.19	0.18	0.17	0.20
CH	3.83	3.88	3.88	3.85	3.82	3.86	3.81	3.82	3.82	3.81
Phl	0.34	0.36	0.36	0.39	0.39	0.37	0.35	0.38	0.37	0.37
Ann	0.66	0.64	0.64	0.61	0.61	0.63	0.64	0.62	0.63	0.62
Mn	0.00	0.00	0.00	0.00	0.00	0.00	0.01	0.00	0.00	0.01

Biotite Analyses

sample no.	120
analysis	rim
SiO_2	34.90
TiO_2	2.03
Al_2O_3	19.43
FeO	23.39
MnO	0.13
MgO	6.22
CaO	0.17
Na_2O	0.03
K_2O	8.83
F	0.31
H_2O	4.35
Total	99.79
Total - F	99.66
Cations per 22 oxygen	
Si	5.41
Al^{iv}	2.59
Ti	0.24
Al	0.96
Fe_2	3.03
Mn	0.02
Mg	1.44
Ca	0.01
Na	0.01
K	1.75
F	0.15
OH	3.85
Phl	0.32
Ann	0.67
Mn	0.01

Plagioclase Analyses

sample no.	48	48	75	75	77	77	91	91	99	102
analysis	core	rim	core	rim	core	rim	core	rim	core	core
SiO_2	59.72	59.43	61.25	63.23	63.64	62.44	59.57	59.63	61.54	60.49
Al_2O_3	25.23	25.83	24.26	22.96	22.75	23.90	24.87	25.04	23.96	24.81
FeO	0.12	0.17	0.04	0.12	0.12	0.20	0.28	0.22	0.21	0.11
CaO	6.87	7.12	6.06	4.95	3.94	5.01	6.55	6.49	5.66	6.31
Na_2O	7.70	7.67	8.07	8.52	9.20	8.69	7.75	7.82	8.48	7.98
K_2O	0.13	0.13	0.21	0.17	0.17	0.18	0.15	0.13	0.07	0.15
Total	99.77	100.35	99.89	99.95	99.82	100.42	99.17	99.33	99.92	99.85
Cations per 8 oxygen										
Si	2.67	2.64	2.72	2.80	2.82	2.76	2.68	2.68	2.74	2.70
Al	1.33	1.35	1.27	1.20	1.19	1.24	1.32	1.32	1.26	1.30
Fe	0.00	0.01	0.00	0.00	0.00	0.01	0.01	0.01	0.01	0.00
Ca	0.33	0.34	0.29	0.24	0.19	0.24	0.32	0.31	0.27	0.30
Na	0.67	0.66	0.70	0.73	0.79	0.74	0.68	0.68	0.73	0.69
K	0.01	0.01	0.01	0.01	0.01	0.01	0.01	0.01	0.00	0.01
An	0.33	0.34	0.29	0.24	0.19	0.24	0.31	0.31	0.27	0.30
Ab	0.66	0.65	0.70	0.75	0.80	0.75	0.68	0.68	0.73	0.69
Or	0.01	0.01	0.01	0.01	0.01	0.01	0.01	0.01	0.00	0.01

Plagioclase Analyses (cont.)

sample no.	102	108	120
analysis	rim	core	core
SiO_2	60.50	59.18	63.07
Al_2O_3	24.51	25.28	22.95
FeO	0.05	0.08	0.20
CaO	4.42	7.01	4.24
Na_2O	7.61	7.61	9.00
K_2O	1.28	0.14	0.10
Total	98.37	99.30	99.56
Cations per 8 Oxygen			
Si	2.73	2.66	2.80
Al	1.30	1.34	1.20
Fe	0.00	0.00	0.01
Ca	0.21	0.34	0.20
Na	0.57	0.66	0.78
K	0.07	0.01	0.01
An	0.22	0.33	0.20
Ab	0.70	0.66	0.79
Or	0.08	0.01	0.01

ENCLOSURE 2.1

canada/yukon economic
development agreement

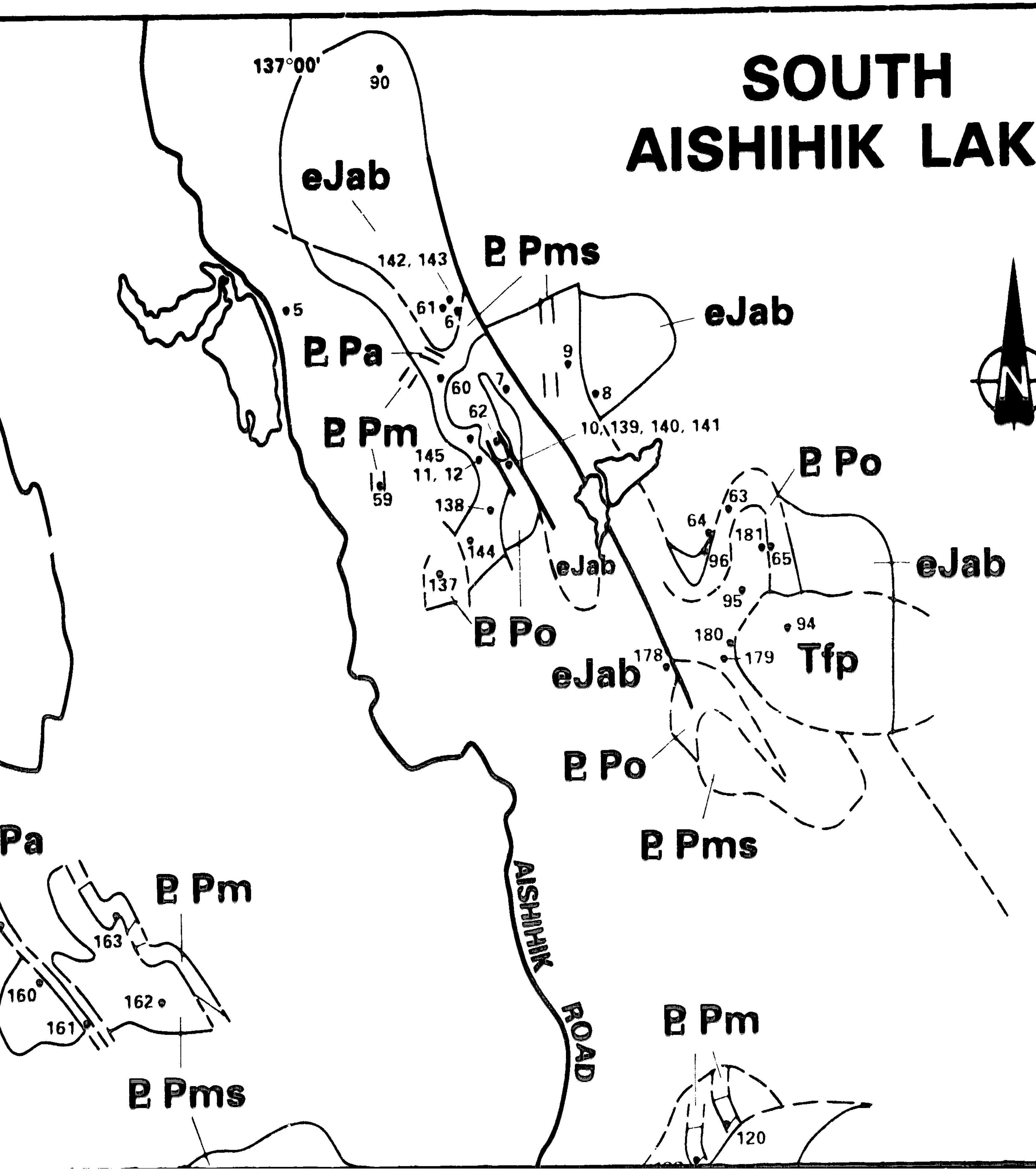

SOUTH
AISHIHIK LAK
137°00'
90
eJab
142, 143
P Pms
61
6
5
eJab
P Pa
9
60
7
8
62
P Pm
10, 139, 140, 141
145
11, 12
59
P Po
138
63
64
181
144
96
65
eJab
137
eJab
95
P Po
94
180
178
179
Tfp
eJab
P Po
P Pms
Pa
P Pm
AISHIHIK ROAD
163
160
162
161
P Pm
P Pms
120

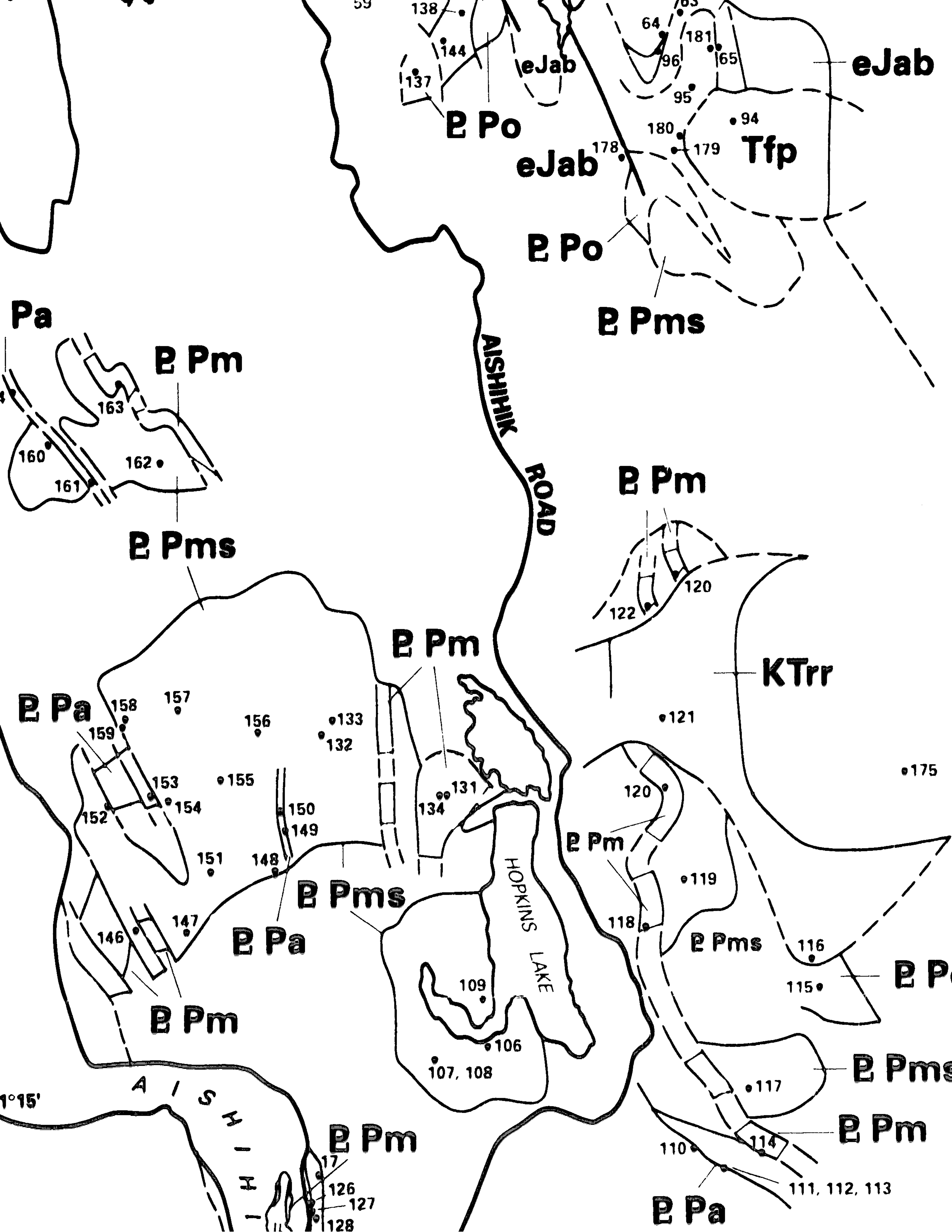

59
138
144
137
eJab
64
63
181
96
65
eJab
95
P Po
180
94
178
179
Tfp
eJab
P Po
P Pms
Pa
P Pm
163
160
162
161
AISHIHIK ROAD
P Pm
P Pms
120
122
P Pm
KTrr
P Pa
158
157
156
133
121
159
132
175
153
155
120
152
154
150
131
134
149
P Pm
HOPKINS LAKE
151
148
119
P Pms
118
146
147
P Pa
P Pms
116
P Pm
115
109
106
107, 108
P Pms
1°15'
A I S H I H I
117
P Pm
P Pm
17
114
110
126
127
128
111, 112, 113
P Pa

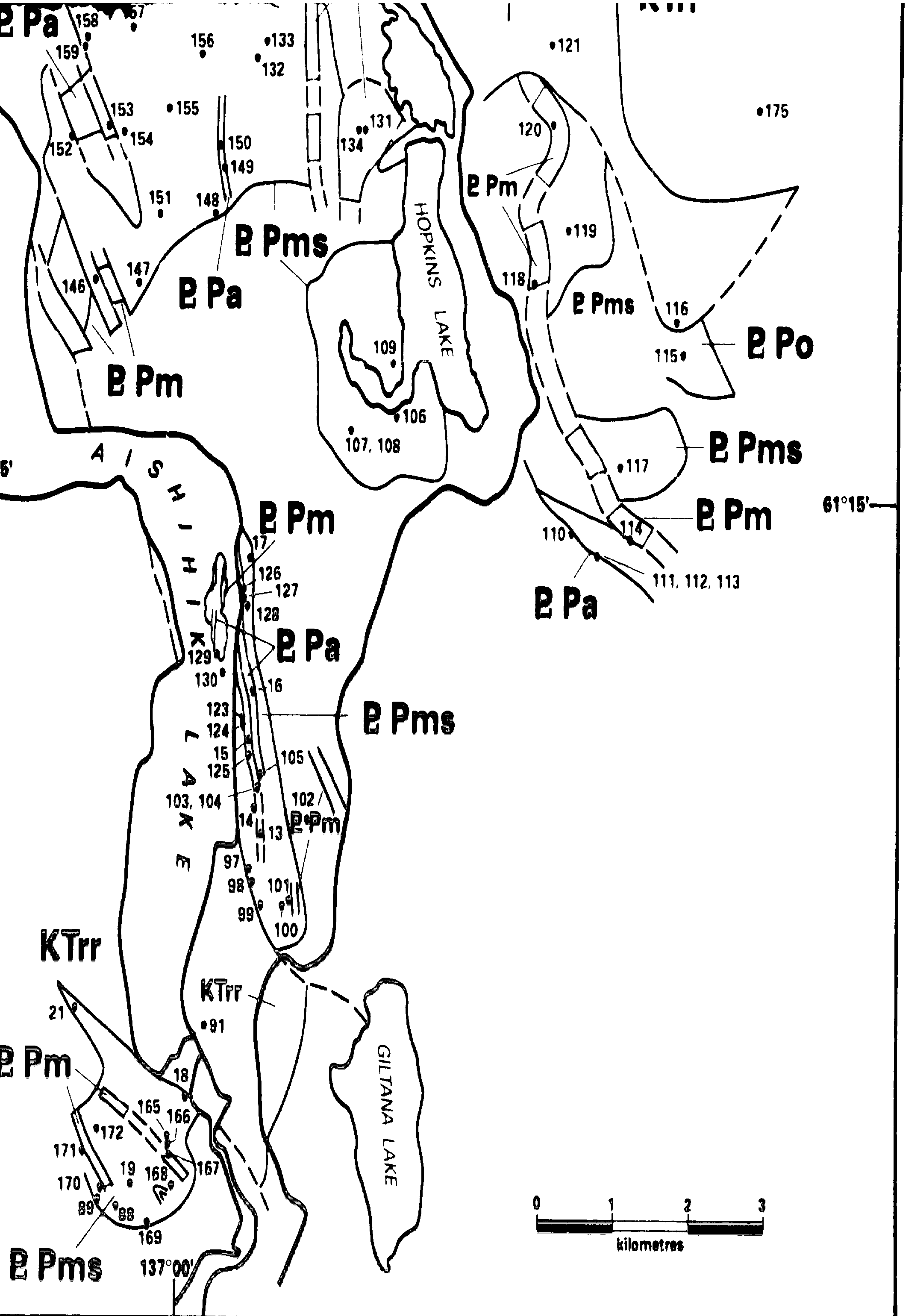

HOPKINS LAKE
AISHIHIK LAKE
GILTANA LAKE
Ꝑ Pa
Ꝑ Pm
Ꝑ Pms
Ꝑ Po
KTrr
61°15'
137°00'
0 1 2 3
kilometres

PW-610 J

UNABLE TO FILM MATERIAL ACCOMPANYING THIS THESIS (I.E. DISKETTE(S), SLIDES, MICROFICHE, ETC...).

PLEASE CONTACT THE UNIVERSITY LIBRARY.

INCAPABLE DE MICROFILMER LE MATERIEL QUI ACCOMPAGNE CETTE THESE (EX. DISQUETTES, DIAPOSITIVES, MICROFICHE (S), ETC...).

VEUILLEZ CONTACTER LA BIBLIOTHEQUE DE L'UNIVERSITE.

END

26-05-94

FIN